MINISTÉRIO DA EDUCAÇÃO

UNIVERSIDADE FEDERAL DO RIO GRANDE

PROGRAMA DE PÓS-GRADUAÇÃO EM CIÊNCIAS DA SAÚDE

Desenvolvimento e avaliação de modelos computacionais da bomba de efluxo Rv1258c e de uma membrana de PIM2 de *Mycobacterium tuberculosis* como alvo de antimicrobianos

João Luís Rheingantz Scaini

Rio Grande, 2020

MINISTÉRIO DA EDUCAÇÃO

UNIVERSIDADE FEDERAL DO RIO GRANDE

PROGRAMA DE PÓS-GRADUAÇÃO EM CIÊNCIAS DA SAÚDE

Desenvolvimento e avaliação de modelos computacionais da bomba de efluxo Rv1258c e de uma membrana de PIM2 de *Mycobacterium tuberculosis* como alvo de antimicrobianos

João Luís Rheingantz Scaini

Tese apresentada ao Programa de Pós-Graduação em Ciências da Saúde da Universidade Federal do Rio Grande, como requisito parcial à obtenção do título de Doutor em Ciências da Saúde.

Orientadora: Profa. Dra. Karina dos Santos Machado

Coorientador: Prof. Dr. Pedro Eduardo Almeida da Silva

Ficha Catalográfica

S278d Scaini, João Luís Rheingantz.
Desenvolvimento e avaliação de modelos computacionais da bomba de efluxo Rv1258c e de uma membrana de PIM2 de *Mycobacterium tuberculosis* como alvo de antimicrobianos / João Luís Rheingantz Scaini. – 2020.
169 f.

Tese (doutorado) – Universidade Federal do Rio Grande – FURG, Programa de Pós-Graduação em Ciências da Saúde, Rio Grande/RS, 2020.
Orientadora: Dra. Karina dos Santos Machado.
Coorientador: Dr. Pedro Eduardo Almeida da Silva.

1. Bioinformática Estrutural 2. Bomba de Efluxo Tap 3. Membrana de *Mycobacterium tuberculosis* 4. Modelo Estrutural 5. Estudo Racional de Antimicrobianos I. Machado, Karina dos Santos II. Silva, Pedro Eduardo Almeida da III. Título.

CDU 611.018.18

Catalogação na Fonte: Bibliotecário José Paulo dos Santos CRB 10/2344

Rio Grande, 2020

João Luís Rheingantz Scaini

Tese apresentada ao Programa de Pós-Graduação em Ciências da Saúde da Universidade Federal do Rio Grande, como requisito parcial à obtenção do título de Doutor em Ciências da Saúde.

Desenvolvimento e avaliação de modelos computacionais da bomba de efluxo Rv1258c e de uma membrana de PIM2 de *Mycobacterium tuberculosis* como alvo de antimicrobianos

Banca Examinadora

Profa. Dra. Daniela Fernandes Ramos – FURG

Prof. Dr. Leonardo Henrique França de Lima - Universidade Federal de São João del-Rei (UFSJ)

Prof. Dr. Hermes Luís Neubauer de Amorim - In Silico Solutions LTDA

Profa. Dra. Ivy Bastos Ramis (Suplente) – FURG

Orientadora: Profa. Dra. Karina dos Santos Machado

Coorientador: Prof. Dr. Pedro Eduardo Almeida da Silva

Agradecimentos / Epígrafe

Agradeço a todos que me auxiliaram de algum jeito durante esta caminhada.

A todos colegas e professores do CombiLab e do NUPEMM.

À Karina e ao Pedro pela orientação e por todo o apoio.

Aos meus amigos, por todos os momentos que passamos juntos (mesmo à distância).

Aos meus pais e irmã, por todo o suporte emocional.

Um agradecimento especial à Karen, por ser uma parceira de verdade, com quem sempre posso contar, e que me faz ter vontade de ser a melhor versão de mim mesmo.

"*É importante retirar sabedoria de lugares diferentes. Se retirá-la de um só lugar, ela se torna rígida e estagnada. Entender os outros ajuda a nos tornarmos completos.*"

Tio Iroh - Avatar, a Lenda de Aang

Sumário

Resumo

Tap é uma importante bomba de efluxo associada à resistência a múltiplos fármacos em *Myocbacterium tuberculosis*. O desenvolvimento de inibidores de efluxo (IEs) para Tap possivelmente aumentaria a eficácia dos antimicrobianos de segunda linha e reduziria a duração do tratamento atual. A bomba de efluxo Tap fica localizada na membrana plasmática, que faz parte de um complexo envelope celular, que tem importante papel da resistência intrínseca a antimicrobianos. O fosfatidil-mio-inositol dimanosídeo (PIM2) é um componente essencial do envelope celular e o lipídio mais predominante na membrana plasmática de *M. tuberculosis*. Dessa forma, o objetivo deste trabalho foi desenvolver modelos atomísticos computacionais das estruturas de uma membrana de PIM2 e da bomba de efluxo Tap de *M. tuberculosis*, como alvos no estudo racional de antimicrobianos. Um modelo estrutural de Tap permite estudo racional de IEs, enquanto um modelo para a membrana de PIM2 aumenta a acurácia do modelo de bombas de efluxo, além de permitir o estudo de fármacos que interagem com o envelope celular de *M. tuberculosis*. Desenvolvemos um modelo molecular de Tap, ao longo de um extenso estudo de modelagem molecular, que mostrou possível inibição competitiva entre IEs e antibióticos. Desenvolvemos e analisamos um modelo de membrana de PIM2 com simulações por Dinâmica Molecular, possibilitando aprimorar o modelo desta proteína. O modelo de membrana de PIM2 também foi usado para estudar a interação da membrana do *M. tuberculosis* com um candidato ao reposicionamento de fármacos, a mefloquina, por meio de simulações por Dinâmica Molecular, sendo que os resultados concordaram com as análises espectroscópicas. Esta tese gerou artigos que descrevem o desenvolvimento destes dois importantes modelos estruturais, da bomba de efluxo Tap e da PIM2, para o estudo racional de fármacos.

Palavras-Chave: Bioinformática estrutural; Bomba de efluxo Tap; Membrana de *Mycobacterium tuberculosis*; Modelo estrutural; Estudo racional de antimicrobianos.

Abstract

Tap is an important efflux pump associated with multidrug resistance in *Myocbacterium tuberculosis*. The development of efflux inhibitors for Tap could raise the effectiveness of second line drugs and reduce the duration of the current treatment. Tap efflux pumps are located in the plasma membrane, which is part of a complex cell envelope, which plays an important role in intrinsic resistance to antimicrobials. Phosphatidyl-myo-inositol dimannoside (PIM2) is an essential component of the cell envelope and the most predominant lipid in the plasma membrane of *M. tuberculosis*. Thus, the objective of this work was to develop atomistic computational models of the structures of a PIM2 membrane and the Tap efflux pump of *M. tuberculosis*, as targets in the rational study of antbiotics. A structural Tap model allows a rational study of EIs, while a model for the PIM2 membrane increases the accuracy of the efflux pump model, and also allows the rational study of drugs that interact with the *M. tuberculosis* cell envelope. We developed a molecular model of Tap, throughout an extensive molecular modelling study, that showed possible competitive inhibition between EIs and antibiotics. We developed and analyzed a Molecular Dynamics PIM2 membrane model, that showed reliability in its interaction with Tap, enhancing the Tap model. The PIM2 membrane model was also used to study the *M. tuberculosis* membrane interaction with a candidate for drug repurposing, mefloquine, throughout Molecular Dynamics, and the results agreed with the spectroscopic analyses. This thesis generated papers that describe the development of these two important structural models, the Tap efflux pump and the PIM2 membrane models, for the rational drugs study.

Keywords: Structural Bioinformatics; Tap Efflux Pump; *Mycobacterium tuberculosis* membrane; Structural model; Rational study of antibiotics.

Lista de figuras

Lista de abreviaturas e siglas

- ABC - Cassete de Ligação de adenosina trifosfato
- Ac2PIM2 – Diacil fosfatidil-mio-inositol dimanosídeo
- AG – Arabinogalactano
- ATP - Adenosina trifosfato
- BDQ - Bedaquilina
- CCCP - Carbonilcianeto m-clorofenil-hidrazona
- CL - Cardiolipina
- CPZ – Clorpromazina
- DOPC – dioleoylphosphatidylcholine
- DM - Dinâmica Molecular
- DPPC - dipalmitoylphosphatidylcholine
- DPPC – Dipalmitoilfosfatidilcolina
- ETB - Etambutol
- IE - Inibidor de Efluxo
- INH - Isoniazida
- LAM - Lipoarabinomanano
- LM - Lipomanano
- MATE - Extrusão de Compostos Tóxicos e de Múltiplas drogas
- MDR - Resistência a múltiplos fármacos
- ME - Membrana Externa
- MFS - Superfamília dos Grandes Facilitadores
- MI - Membrana Interna
- MmpL - Grandes Proteínas de Membrana de Micobactérias
- MmpS - Pequenas Proteínas de Dembrana de Micobactérias
- OFLO - Ofloxacina
- PAS - Ácido p-aminosalicílico
- PC - Parede celular

- PDB - Banco de dados de proteínas
- PE - Fosfatidiletanolamina
- PG - Peptidoglicano
- PI - Fosfatidil-mio-inositol
- PIM - Fosfatidil-mio-inositol manosídeo
- PIM2 - Fosfatidil-mio-inositol dimanosídeo
- PIM6 - Fosfatidil-mio-inositol hexamanosídeo
- POPE - 1-palmitoyl-2-oleoyl phosphatidylethanolamine
- POPG - palmitoyloleoylphosphatidylglycerol
- RIF - Rifampicina
- RND - Divisão de Resistencia e Nodulação
- SMR - Pequena família de resistência a múltiplos fármacos
- STR - Estreptomicina
- Tap - Bomba de efluxo de resistência a tetraciclina/aminoglicosídeos
- TB - Tuberculose
- TB-MDR - Tuberculose resistente a múltiplos fármacos
- TET - Tetraciclina
- VERA - Verapamil

1 Introdução

A tuberculose (TB) é uma doença infectocontagiosa cujo principal agente etiológico em seres humanos é o bacilo *Mycobacterium tuberculosis*. Foram estimados 10 milhões de casos novos de TB e 1,4 milhões de óbitos em 2019. Um dos desafios no combate à TB é a emergência da resistência a múltiplos fármacos (MDR) – causada por cepas resistentes a pelo menos isoniazida (INH) e rifampicina (RIF) - que estima-se ter tido 362 mil novos casos em 2019 (WORLD HEALTH ORGANIZATION, 2020). A principal forma de resistência de *M. tuberculosis* é a adquirida, porém a resistência intrínseca também se mostra importante (DA SILVA et al., 2011; GYGLI et al., 2017). *M. tuberculosis* apresenta dois principais mecanismos de resistência intrínsecos que reduzem a concentração de antimicrobianos na célula: um ativo sistema de efluxo e o envelope celular altamente impermeável (DE ROSSI; AÍNSA; RICCARDI, 2006; FAVROT; RONNING, 2012; GYGLI et al., 2017).

Bombas de efluxo em *M. tuberculosis* podem ser associadas à TB resistente a múltiplos fármacos (TB-MDR) (COELHO et al., 2015; LI et al., 2015) e até mesmo à resistência à bedaquilina (BDQ) (ALMEIDA et al., 2016; LI et al., 2018), que é um dos últimos antimicrobianos desenvolvidos para TB e recentemente introduzido no tratamento de pacientes com TB-MDR (ANDRIES et al., 2014; COHEN, 2013).

Além disso, o efluxo desempenha um papel importante na evolução para altos níveis de resistência em *M. tuberculosis* (COELHO et al., 2015; MACHADO et al., 2012; VIVEIROS et al., 2012), uma vez que confere baixos níveis de resistência, que podem resultar em uma maior exposição a concentrações subinibitórias de um antimicrobiano, e em consequência aumentar a probabilidade do desenvolvimento de outros mecanismos de resistência, como os de mutação pontual (MARTÍNEZ, 2017).

A bomba de efluxo de resistência a tetraciclina/aminoglicosídeo (Tap), Rv1258c (AÍNSA et al., 1998; DE ROSSI et al., 2002), é uma bomba de efluxo de *M. tuberculosis*

associada à TB-MDR (JIANG et al., 2008; SIDDIQI et al., 2004). O gene Tap apresentou maior expressão em amostras clínicas quando exposto a RIF (COELHO et al., 2015; JIANG et al., 2008; SIDDIQI et al., 2004), INH (COELHO et al., 2015; JIANG et al., 2008; MACHADO et al., 2012) e ofloxacina (OFLO) (SIDDIQI et al., 2004). Foi demonstrado que a deleção de Rv1258c do *M. bovis* BCG aumenta a suscetibilidade do organismo à INH e RIF (DE ROSSI; AÍNSA; RICCARDI, 2006). Esta bomba de efluxo também foi associada ao desenvolvimento de resistência a fluoroquinolonas de segunda linha e antibióticos aminoglicosídeos (MALINGA; STOLTZ; WALT, 2016).

Além da ação na resistência, as bombas de efluxo em *M. tuberculosis* também são associada à divisão celular (DHAMDHERE; ZGURSKAYA, 2010; LAU; ZGURSKAYA, 2005) e à virulência (CAMACHO et al., 1999), possivelmente por serem responsáveis pela secreção de componentes do envelope celular (CAMACHO et al., 2001). Foi mostrado que a inativação da Tap reprimiu genes da biossíntese da parede celular, em particular da formação do peptidoglicano (RAMÓN-GARCÍA et al., 2012).

Uma forma de superar e evitar a resistência relacionada ao mecanismo de efluxo é com a adição de Inibidores de Efluxo (IE) como adjuvantes no tratamento antimicrobiano (GUPTA et al., 2013; KAPP; MALAN; SAMPSON, 2017; MAHAMOUD et al., 2007; MARQUEZ, 2005). O uso de um IE com especificidade para a bomba de efluxo Tap poderia possibilitar: a introdução no tratamento da TB de antimicrobianos já disponíveis, porém não efetivos contra a TB, como espectinomicina ou tetraciclina (TET); a maior eficácia de antimocrobianos da segunda linha do tratamento de TB como PAS e estreptomicina (STR); a redução da duração do tratamento padrão, que por si só já é uma das causas de casos de resistência (RAMÓN-GARCÍA et al., 2012). O planejamento de IEs efetivos requer um entendimento da dinâmica funcional e dos mecanismos moleculares das mudanças conformacionais desse tipo de proteína (OPPERMAN; ST, 2015; OSWALD; TAM; POS, 2016; WANG et al., 2017). Desta

forma, o estudo racional de fármacos é uma forma rápida e precisa de descobrir IEs clinicamente (LIU; WRIGHT; HOP, 2014; WALMSLEY; MCKEEGAN; WALMSLEY, 2003; YE et al., 2014).

As bombas de efluxo de *M. tuberculosis* ficam localizadas na membrana plasmática, que faz parte de um complexo envelope celular que é responsável por proteção da bactéria em ambientes hostis, resistência mecânica, transporte de solutos e proteínas e adesão a receptores de hospedeiros, além de ter importante papel da resistência intrínseca a antimicrobianos (BRENNAN; GOREN, 1979; DAFFÉ; DRAPER, 1998; DULBERGER; RUBIN; BOUTTE, 2020; SARTAIN et al., 2011). Este envelope é composto pela membrana plasmática ou membrana interna (MI), o complexo peptidoglicano-arabinogalactano e a membrana externa (ME) que está covalentemente ligada ao arabinogalactano (BANSAL-MUTALIK; NIKAIDO, 2014). Lipídios exclusivos da espécie ou da micobactéria compõem esse envelope. A abundância e importância biológica desses lipídios refletem em extensos estudos para elucidar suas estruturas e funções (SARTAIN et al., 2011).

Os fosfatidil-mio-inositol manosídeos (PIMs) são glicolipídeos únicos abundantes nas MI e ME das micobactérias (GUERIN et al., 2010). Estes glicolipídeos também são precursores dos dois principais lipoglicanos micobacterianos, o lipomanano (LM) e o lipoarabinomanano (LAM) (SANCHO-VAELLO et al., 2017), que são formas multiglicosiladas de fosfatidil-mio-inositol dimanosídeos (PIM2) (CHATTERJEE et al., 1992; KHOO et al., 1995). Os PIMs, além de componentes essenciais do envelope celular micobacteriano, são fatores de virulência importantes em *M. tuberculosis* e podem modular interações patógeno-hospedeiro (SANCHO-VAELLO et al., 2017). Estruturalmente, os PIMs são constituídos por um grupo fosfatidil-mio-inositol (PI) contendo manosídeos esterificados no anel inositol (GUERIN et al., 2010). A classe mais abundante de PIMs em *M. tuberculosis* é PIM2, sendo a forma tetra acilada dos PIM2 – diacil fosfatidil-mio-inositol dimanosídeo

(Ac2PIM2) o lipídio mais abundante da MI, compondo até 42% de sua massa seca (BANSAL-MUTALIK; NIKAIDO, 2014).

A caracterização físico-química de uma membrana lipídica é de fundamental importância para entender seu papel em funções fisiológicas como o tráfego de vesículas, suas interações com proteínas (BOVIGNY et al., 2015). A Dinâmica Molecular (DM) é método de simulação computacional que se torna uma ferramenta poderosa para analisar as propriedades físicas e químicas de uma membrana, sua organização e dinâmica temporal em um nível de detalhe atomístico, que é atualmente indisponível diretamente em estudos espectroscópico (DESERNO et al., 2014; FRIGINI; LÓPEZ CASCALES; PORASSO, 2018; VENABLE; KRÄMER; PASTOR, 2019).

Um modelo de DM para uma membrana bacteriana permite analisar os efeitos na membrana de antimicrobianos que interajam com ela (BOAGS et al., 2017). Como é o caso da mefloquina (MFL), uma molécula que mostrou efeito antimicrobiano em *M. tuberculosis* (BERMUDEZ; MEEK, 2014; GONALVES et al., 2012; JAYAPRAKASH et al., 2006; RODRIGUES-JUNIOR et al., 2016), e que pode afetar a integridade de membranas procarióticas (BROWN; STANCATO; WOLFE, 1979). Um modelo assim também permite estudar as interações entre a membrana bacteriana e proteínas-transmembrana, como bombas de efluxo (MULLER et al., 2019). Adicionalmente, a simulação da inserção natural da bomba de efluxo em uma membrana bacteriana dá mais precisão ao estudo estrutural da bomba (CLOETE et al., 2018; SANDHU; AKHTER, 2017).

Esta tese está dividida da seguinte forma: a Seção 2 é a Revisão Bibliográfica, que detalha o estado da arte dos temas abordados; a Seção 3 é a de Objetivos, apontando os objetivos do trabalho; a Seção 4 é a de Material e Métodos, que explica de forma resumida a metodologia utilizada em cada artigo (as metodologias estão detalhadas nos artigos); e a Seção 5 é a Bibliografia, contendo toda a bibliografia

utilizada nas seções anteriores. Em seguida estão os três artigos: a Seção 6 é o Artigo I “Molecular modelling and competitive inhibition of a *Mycobacterium tuberculosis* multidrug-resistance efflux pump”, que já foi publicado na revista “Journal of Molecular Graphics and Modelling”; a Seção 7 é o Manuscrito II “A Molecular Dynamics study of PIM2 lipid bilayer membranes” pronto para a submissão para a revista “Biochimica et Biophysica Acta – Biomembranes”; a Seção 8 é o Manuscrito III “Mefloquine synergism with anti-tuberculosis drugs and correlation to membrane effects: biologic, spectroscopic and molecular dynamics simulations studies”, submetido para a revista “Bioorganic Chemistry”. A Seção 9 é a de Conclusões e a Seção 10 a de Considerações Finais e Perspectivas.

2 Revisão Bibliográfica

2.1 Tuberculose

A TB é uma doença infectocontagiosa cujo principal agente etiológico em seres humanos é o bacilo *Mycobacterium tuberculosis* (WORLD HEALTH ORGANIZATION, 2020). A doença é um importante problema na saúde pública pela sua alta taxa de morbimortalidade, tendo maior índice de mortalidade em pacientes HIV positivos (ÁLVARO-MECA et al., 2014; WORLD HEALTH ORGANIZATION, 2020).

Foram estimados 10 milhões de casos novos de TB e 1,4 milhões de óbitos em 2019 (WORLD HEALTH ORGANIZATION, 2020). A maioria dos infectados com o bacilo desenvolve a forma latente, que além de constituírem-se no maior reservatório de um patógeno em todo o mundo ainda coloca 10-15% destas pessoas em risco de desenvolver a doença em algum momento da vida. Estima-se que cerca de ¼ da população mundial esteja infectada com *M. tuberculosis* (HOUBEN; DODD, 2016).

A terapêutica antimicrobiana da TB é a principal estratégia para o controle da doença, pois além de promover a cura dos pacientes, rompe a cadeia de transmissão do bacilo. A estratégia terapêutica de primeira linha para TB tem duração de seis

meses, utilizando INH e RIF durante todo o tratamento com adição de pirazinamida e etambutol (ETB) nos dois primeiros meses (WORLD HEALTH ORGANIZATION, 2020). Esta longa duração do tratamento em que o paciente deve ingerir diariamente os antimicrobianos, somada à sua toxicidade e efeitos colaterais, contribui com que ocorra relapso no tratamento. A falha no tratamento representa um importante problema de saúde pública, pois um tratamento incompleto pode propiciar a seleção de cepas resistentes aos antimicrobianos (CLARK et al., 2013).

2.2 Resistência bacteriana aos antimicrobianos

A resistência bacteriana aos antimicrobianos é um crescente problema no cenário clínico (GYGLI et al., 2017; MARTINEZ, 2014). A exposição de compostos antimicrobianos em concentrações menores do que a concentração mínima inibitória favorece a seleção de cepas resistentes. Isto ocorre porque as bactérias resistentes irão sobreviver, fazendo com que o fenótipo de resistência vire predominante na população bacteriana (HOGAN; KOLTER, 2002; MARTINEZ, 2014).

Os mecanismos de resistência aos antimicrobianos ocorrem basicamente pela inativação do fármaco, pela modificação do alvo de ação e/ou por redução da concentração intracelular. Os mecanismos de resistência do primeiro tipo, causados por inativação do fármaco, incluem a produção de enzimas que o degradam ou modificam, como por exemplo: betalactamases e aminotransferases. A segunda categoria mencionada, por modificação do alvo de ação, envolve as mutações que alteram o sítio de ação do antimicrobiano. A terceira categoria de mecanismo de resistência consiste na redução da concentração intracelular como o efluxo e a diminuição da permeabilidade do envoltório celular. Tendo em vista que a eficácia de um antimicrobiano depende de sua capacidade de alcançar seu alvo, a diminuição da permeabilidade das paredes celulares e o efluxo são fatores efetivos no aumento da resistência aos antimicrobianos (HOGAN; KOLTER, 2002).

A resistência bacteriana aos antimicrobianos pode ser de natureza intrínseca ou adquirida. A resistência adquirida ocorre a partir da seleção das bactérias resistentes devido a da pressão seletiva causada pela exposição ao antimicrobiano em questão, enquanto a resistência intrínseca ocorre por mecanismos já presentes na bactéria (HOGAN; KOLTER, 2002; MARTINEZ, 2014). Bactérias têm mecanismos de resistência intrínsecos e complexos que frequentemente não são detectados em testes rotineiros de sensibilidade a antimicrobianos realizados em laboratórios clínicos (BURIAN et al., 2012; DA SILVA et al., 2011; GYGLI et al., 2017).

2.2.1 Resistência a antimicrobianos em *M. tuberculosis*

A emergência de cepas multidroga-resistentes (MDR) em *M. tuberculosis* é um obstáculo ao controle da TB. Em 2019, tiveram aproximadamente 362 mil novos casos de TB multirresistente (TB-MDR), como é chamada a TB causada por cepas resistentes a, pelo menos, INH e RIF (WORLD HEALTH ORGANIZATION, 2020).

A principal forma do desenvolvimento de resistência observada em isolados clínicos de *M. tuberculosis* é a mutação em genes que codificam os principais alvos de antimicrobianos ou em genes responsáveis pela ativação de pró-fármacos (DA SILVA et al., 2011; GYGLI et al., 2017). No entanto, o fenótipo de resistência aos antimicrobianos em *M. tuberculosis* e outros microrganismos é resultado de um cenário molecular mais complexo que mutações pontuais (BLACK et al., 2014).

Além da resistência adquirida, a resistência intrínseca se mostra importante em *M. tuberculosis* (DA SILVA et al., 2011; GYGLI et al., 2017). Micobactérias apresentam dois principais mecanismos de resistência intrínsecos que reduzem a concentração de antimicrobianos na célula: a parede celular altamente impermeável por ser rica em ácidos micólicos e um ativo sistema de efluxo (DE ROSSI; AÍNSA; RICCARDI, 2006; FAVROT; RONNING, 2012; GYGLI et al., 2017).

2.3 Mecanismo de Efluxo

O efluxo é a extrusão de compostos realizada por proteínas transportadoras, chamadas de bombas de efluxo, localizadas na membrana plasmática de todos os tipos de células (WALMSLEY; MCKEEGAN; WALMSLEY, 2003). Estas proteínas são importantes na resistência a antimicrobianos em diversos patógenos e a agentes quimioterápicos em células cancerígenas (WU; HSIEH; WU, 2011).

Uma das estratégias empregadas para prevenção e superação da resistência aos antimicrobianos é o desenvolvimento de compostos com capacidade de inativar o mecanismo de efluxo (GUPTA et al., 2013; MAHAMOUD et al., 2007). O racional desta estratégia é que estes IEs poderiam ser adicionados ao esquema terapêutico como adjuvantes que restaurariam ou potencializam a atividade de antimicrobianos frente a microrganismos cuja resistência aos antimicrobianos esteja relacionado, diretamente ou indiretamente, ao efluxo (MARQUEZ, 2005; RODRIGUES et al., 2013).

A MDR é um fenótipo que era antes considerado resultado exclusivo da combinação de vários genes de resistência, cada um codificando resistência a um antimicrobiano (NIKAIDO, 1998). Porém, esses fenótipos MDR também podem ser resultado da atividade de bombas de efluxo (PIDDOCK, 2006a).

O papel fisiológico das bombas de efluxo não é exclusivamente de conferir resistência a antimicrobianos, mas amplo espectro de funções da célula bacteriana como patogenicidade, virulência, formação de biofilme e *quorum sensing* (CHAN; CHUA, 2010; DA SILVA et al., 2011; HØIBY; CIOFU; BJARNSHOLT, 2010; PIDDOCK, 2006a, 2006b; SUN; DENG; YAN, 2014).

As bombas de efluxo constituem um diversificado grupo de transportadores, tanto quanto a especificidade do substrato transportado - específico a um antimicrobiano ou a múltiplos -, quanto do tipo de fonte de energia utilizada para o transporte - força próton-motriz, antiporte com sódio ou adenosina trifosfato (ATP)

(WALMSLEY; MCKEEGAN; WALMSLEY, 2003). As bombas de efluxo são divididas em cinco famílias (Figura 1) de acordo com sua especificidade para substratos e sua fonte de energia: Divisão de Resistencia e Nodulação (RND), Superfamília das Grandes Facilitadoras (MFS) e Pequena família de resistência a múltiplos fármacos (SMR), que utilizam a força próton-motriz para gerar energia, família de Extrusão de Compostos Tóxicos e de Múltiplas drogas (MATE) que realizam antiporte com sódio como fonte de energia e família de Cassete de Ligação de ATP (ABC) que utilizam ATP para obter sua energia (PIDDOCK, 2006b).

Figura 1: Representação das famílias de bomba de efluxo.

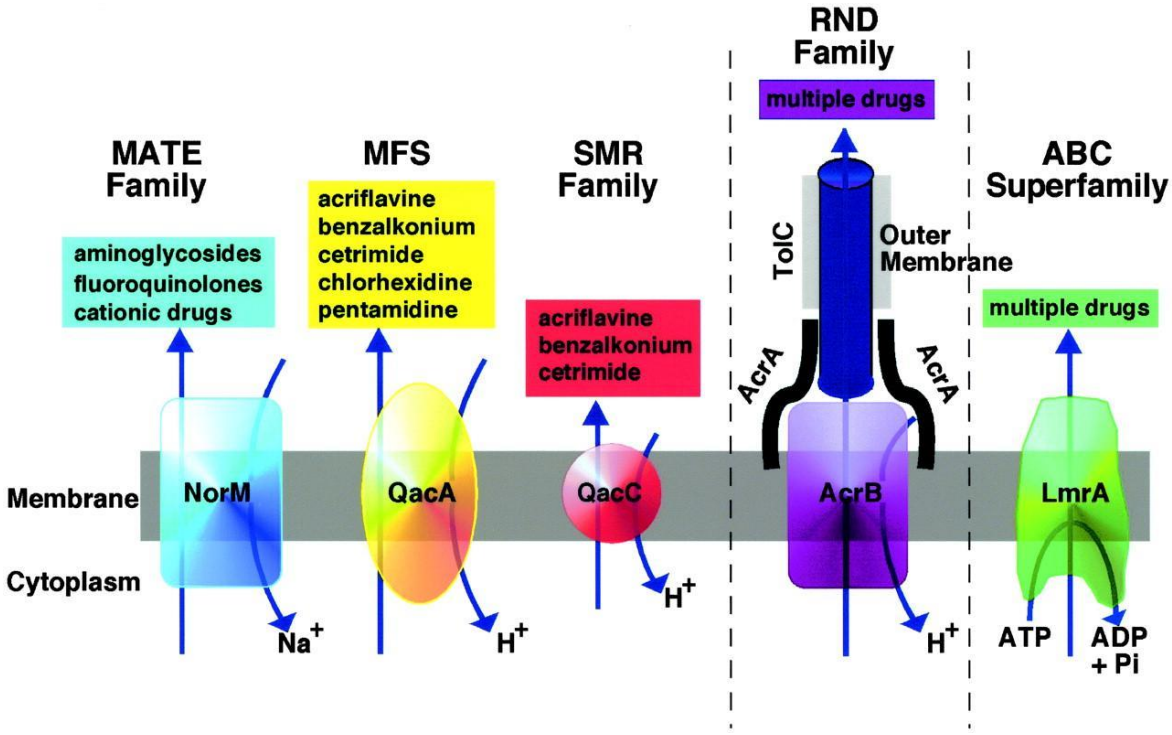

Famílias nas quais se classificam as proteínas de efluxo (PIDDOCK, 2006b).

2.3.1 Sistema de Efluxo em *Mycobacterium tuberculosis*

O número de bombas de efluxo em *M. tuberculosis* é um dos maiores entre as bactérias, considerando o tamanho de seu genoma (PAULSEN et al., 2001). A importância do efluxo na resistência de *M. tuberculosis* a antimicrobianos, parece estar associada ao processo evolutivo que envolve a resistência aos antimicrobianos, sendo uma etapa anterior as mutações que conferem resistência a altas concentrações e, eventualmente, participando em conjunto com estas mutações para determinar o nível de resistência. O efluxo confere baixos níveis de resistência, que pode resultar em uma maior exposição a concentrações subinibitórias de um antimicrobiano, e em consequência aumentar a probabilidade do desenvolvimento de outros mecanismos de resistência (MACHADO et al., 2012).

Além disso, em até 30% dos casos de resistência a INH e cerca de 5% dos casos de resistência a RIF, observada em isolados clínicos, a resistência não está relacionada com as mutações clássicas (LOUW et al., 2009). Isto permite inferir que, entre outros possíveis mecanismos de resistência, também por estar envolvido o efluxo (COELHO et al., 2015; DA SILVA et al., 2011; ESCRIBANO et al., 2007; SPIES et al., 2008).

Quanto a regulação da transcrição de genes de bombas de efluxo, diversos reguladores têm sido descritos em micobactérias (BOLLA et al., 2012; DA SILVA et al., 2011; RICHARD et al., 2018; VADIJA et al., 2018). O gene whiB7 é induzido por concentrações subinibitórias de antimicrobianos e sua transcrição causa resistência aos antimicrobianos ao ativar um *regulon* que inclui Rv1473 e o gene Tap (GEIMAN et al., 2006; MORRIS et al., 2005).

Além da resistência, bombas de efluxo desempenham um papel importante na sobrevivência de *M. tuberculosis* no hospedeiro (PIDDOCK, 2006a). No macrófago, a sobrevivência do bacilo depende na sua capacidade de obstruir a formação do fagolisossoma. Foi mostrado que genes homólogos a bombas de efluxo possuem relação com a interrupção da maturação do fagossomo (PETHE et al., 2004). A seguir

descreverei, resumidamente, as principais famílias de transportadores relacionados ao efluxo de antimicrobianos.

2.3.2 Bombas de efluxo em *Mycobacterium tuberculosis*

Nesta seção serão apresentadas o papel das famílias de bombas de efluxo em *M. tuberculosis*, e então as principais bombas de efluxo do bacilo serão descritas em subseções dedicadas.

A família ABC é uma das família de transportadores mais amplamente distribuída entre procariotas e eucariotas, sendo que o genoma do *M. tuberculosis* apresenta 38 transportadores desta família (XU; ZHOU; YAO, 2014). Os *clusters* de genes drrA-drrB-drrC e Rv2686c-Rv2687c-Rv2688c estão associados, respectivamente, com a resistência de amplo espectro a antimicrobianos clinicamente relevantes e com a resistência a ciprofloxacina quando sobre-expressados em *M. smegmatis* (CHOUDHURI et al., 2002; GUILFOILE; HUTCHINSON, 1991; PASCA et al., 2004).

A família RND tem transportadores de antimicrobianos muito frequentes nas bactérias gram-negativas. Em *M. tuberculosis*, o gene mmpL7 codifica um transportador que confere resistência de alto nível para INH quando sobre-expressado em *M. smegmatis* (PASCA et al., 2005). Da mesma família, a bomba de efluxo MmpS5-MmpL5 está associada a resistência de BDQ, um dos últimos antimicrobianos desenvolvidos para o tratamento da TB e recentemente introduzido nos esquemas terapêuticos para tratamento de TB-MDR (ALMEIDA et al., 2016; ANDRIES et al., 2014; RADHAKRISHNAN et al., 2014). Foi demonstrado que transportadores da família MmpL (Grandes Proteínas de Membrana de Micobactérias), geralmente estão acoplados a transportadores da família MmpS (Pequenas Proteínas de Membrana de Micobactérias), e tem como função fisiológica exportar lipídios micobacterianos para a síntese da parede celular (RADHAKRISHNAN et al., 2014).

Na família MATE, o gene MSMEG_2631 de *M. smegmatis* codifica para uma bomba de efluxo, existente em micobactérias inclusive *M. tuberculosis*. A deleção deste gene aumentou a sensibilidade para a amicacina, canamicina, capreomicina, cloreto de cetilpiridínio e outros antimicrobianos das famílias glicopeptídicos e sulfanomidas (MISHRA; DANIELS, 2013). Na família SMR, a bomba de efluxo Mmr confere resistência à acriflavina, brometo de etídio e eritromicina em *M. tuberculosis* quando expressado em um vetor multicópia (DE ROSSI et al., 1998).

Na família SMR, a bomba de efluxo Mmr também apresenta possível tolerância a INH, um dos dois fármacos de primeira linha do tratamento da TB (BOLLA et al., 2012; RODRIGUES et al., 2012).

A família MFS é outra ancestral família de transportadores e pelo menos 16 transportadores foram identificados em *M. tuberculosis*: Rv0037c, Rv0191, Rv0783c, Rv0849, Rv1250, Rv1258c, Rv1410c, Rv1634, Rv1877, Rv2333c, Rv2456c, Rv2459, Rv2846c (efpA), Rv28994, Rv3239c e Rv3728 (DE ROSSI et al., 2002). Destes, a proteína Rv1258c confere resistência à TET e aminoglicosídios, portanto é uma bomba de efluxo Tap (AÍNSA et al., 1998; DE ROSSI et al., 2002) e a proteína P55 (Rv1410c) confere resistência a STR (antimicrobiano usado na segunda linha do tratamento de TB), TET e RIF (DA SILVA et al., 2011; RAMÓN-GARCÍA et al., 2009).

A bomba de efluxo Tap, mostra um importante papel em *M. tuberculosis* apresentando tolerância a RIF, um dos dois principais fármacos no tratamento da TB, e associação com a TB-MDR (DA SILVA et al., 2011; GEIMAN et al., 2006; JIANG et al., 2008; MORRIS et al., 2005; SIDDIQI et al., 2004). A bomba de efluxo efpA, também da MFS, gera resistência a INH, o que mostra sua importância (MACHADO et al., 2012; RODRIGUES et al., 2012).

2.3.2.1 Bomba de Efluxo Mmr

A bomba de efluxo Mmr (Rv0365), da família SMR, gera resistência a compostos tóxicos, como a tetrafenilfosfônio, eritromicina, brometo de etídio, acriflavina, safranina O e pironina Y e trioridazina (BOLLA et al., 2012; DE ROSSI et al., 1998; LI; ZHANG; NIKAIDO, 2004). Um mutante com o gene Mmr nocauteado mostrou uma suscetibilidade maior a brometo de etídio, tetrafenilfosfônio e brometo cetrimetilamônio, enquanto a sobre-expressão causou uma menor suscetibilidade a brometo de etídio, acriflavina e safranina O, o que foi obliterado na presença dos IEs VERA e CCCP (RODRIGUES et al., 2013).

Foi mostrado que a bomba de efluxo Mmr estava significativamente sobre-expressa sob a exposição de INH em duas cepas sensíveis aos antibióticos de primeira linha e duas cepas clínicas monorresistentes à RIF (MACHADO et al., 2012). Cepas induzidas por INH apresentaram uma maior atividade de efluxo e sobreexpressão do gene Mmr (RODRIGUES et al., 2012).

2.3.2.2 Bomba de Efluxo efpA

A bomba de efluxo efpA pertence à família MFS (DE ROSSI et al., 2002) e quando foi sobre-expressada em cepas de *M. tuberculosis* expostas a altos níveis de INH apresentaram uma maior atividade de efluxo, que foi inibida por IEs (MACHADO et al., 2012; RODRIGUES et al., 2012).

A deleção do homólogo de efpA em *M. smegmatis* produziu maior sensibilidade a fluoroquinolonas, brometo de etidio e acriflavina, mas inesperadamente também resultou em diminuição da sensibilidade a rifamicinas, INH e cloranfenicol (LI; ZHANG; NIKAIDO, 2004). Além disso, efpA foi sobre-expresso em cepas de *M. tuberculosis* monorresistentes a RIF (LI et al., 2015).

2.3.2.3 Bomba de Efluxo MmpL5

Uma das causas da resistência a BDQ são mutações em Rv0678, que aumentam o efluxo a partir do complexo MmpS5-MmpL5 (ALMEIDA et al., 2016, p. 201; ANDRIES et al., 2014; RADHAKRISHNAN et al., 2014). A BDQ é o primeiro fármaco a ser aprovado para o tratamento de TB-MDR em décadas, assim ganhou aprovação acelerada como parte da terapia em casos no qual outra opção de tratamento não era possível (COHEN, 2013). Por isto, é um problema alarmante o surgimento da resistência a BDQ.

Resistência causada por efluxo foi identificada em isolados de pacientes tratados com BDQ, assim como em camundongos, onde foi confirmada a diminuição da eficácia bactericida. Apesar de não poder excluir a possibilidade de outras bombas de efluxo estarem envolvidas nessa resistência a BDQ, o fato de mutações no gene Rv0678 estarem presentes em todos os isolados do trabalho em questão e a sobrexpressão da bomba de efluxo MmpS5-MmpL5 vista por proteômica, reforçam que esta bomba de efluxo é responsável por resistência adquirida. Além disso, os dados de sobrexpressão desse artigo apontam para que BDQ seja substrato de MmpL5 (ANDRIES et al., 2014).

2.3.2.4 Bomba de Efluxo Tap

Foram caracterizadas a bomba de efluxo Tap de *M. tuberculosis*, que confere resistência a TET e resistência de baixo nível a ácido p-aminosalicílico (PAS, fármaco anti-TB de segunda linha), espectinomicina e acriflavina e sua análoga de *M. fortuitum* que confere resistência de baixo nível a aminoglicosídeos inclusive STR, TET, 2'-N-etilnetilmicina, e 6'-N-etilnetilmicina (AÍNSA et al., 1998; RAMÓN-GARCÍA et al., 2006, 2012). O gene tap apresentou maior expressão em amostras clínicas quando exposto a RIF (COELHO et al., 2015; JIANG et al., 2008; SIDDIQI et al., 2004), INH (COELHO et al., 2015; JIANG et al., 2008; MACHADO et al., 2012) e OFLO (SIDDIQI et al., 2004). Foi demonstrado que a deleção do gene tap do *M. bovis* BCG aumenta a

suscetibilidade do organismo à INH e RIF (DE ROSSI; AÍNSA; RICCARDI, 2006). Esta bomba de efluxo também foi associada ao desenvolvimento de resistência a fluoroquinolonas de segunda linha (MALINGA; STOLTZ; WALT, 2016).

Além da ação na resistência, as bombas de efluxo Tap estão associadas à importantes funções fisiológicas em *M. tuberculosis* como a divisão celular (DHAMDHERE; ZGURSKAYA, 2010; LAU; ZGURSKAYA, 2005) e a virulência (CAMACHO et al., 1999), possivelmente por serem responsáveis pela secreção de componentes do envelope celular (CAMACHO et al., 2001). Foi mostrado que a inativação da Tap reprimiu genes da biossíntese da parede celular, em particular da formação do peptidoglicano (RAMÓN-GARCÍA et al., 2012).

Tem sido demonstrado que diferentes compostos como carbonilcianeto m-clorofenil-hidrazona (CCCP), reserpina, verapamil (VERA) e clorpromazina (CPZ), inibiram o efluxo determinado pela Tap. Porém, não há nenhum IE em uso no tratamento para TB (SINGH et al., 2014). O uso de um IE com especificidade para a bomba de efluxo Tap poderia possibilitar: a introdução no tratamento da TB de antimicrobianos já disponíveis, porém não efetivos contra a TB, como espectinomicina ou TET; a maior eficácia de antimocrobianos da segunda linha do tratamento de TB como PAS e estreptomicina; a redução da duração do tratamento padrão, que por si só já é uma das causas de casos de resistência (RAMÓN-GARCÍA et al., 2012).

2.4 Estrutura tridimensional de bombas de efluxo

A chave para o entendimento da função das bombas de efluxo envolve a determinação de suas estruturas tridimensionais e a elucidação das mudanças conformacionais que acompanham a translocação dos antimicrobianos (LIU; WRIGHT; HOP, 2014; WALMSLEY; MCKEEGAN; WALMSLEY, 2003). A maior parte das informações estruturais disponíveis destes transportadores vem de previsões das

estruturas secundárias, a partir de suas estruturas primárias (WALMSLEY; MCKEEGAN; WALMSLEY, 2003; YE et al., 2014).

O planejamento de IEs clinicamente efetivos é lento e necessita de um desenvolvimento racional (WALMSLEY; MCKEEGAN; WALMSLEY, 2003). Isto inclui um entendimento da dinâmica funcional e dos mecanismos moleculares das mudanças conformacionais desse tipo de proteína (OPPERMAN; ST, 2015; OSWALD; TAM; POS, 2016; WANG et al., 2017). Desta forma, o estudo racional de fármacos é uma forma rápida e precisa de contribuir com a descoberta IEs clinicamente eficazes (LIU; WRIGHT; HOP, 2014; WALMSLEY; MCKEEGAN; WALMSLEY, 2003; YE et al., 2014).

A determinação de estruturas de bombas de efluxo por Cristalografia de Raio X e Espectroscopia de Ressonância Magnética Nuclear é dificultada pela natureza anfifílica e pela dificuldade de atingir pureza e quantidade (DIALLINAS, 2014). Apesar destas dificuldades, a cristalização tridimensional de algumas bombas de efluxo foi realizada com sucesso (DU et al., 2014; LEI et al., 2014). Estes dados de estruturas tridimensionais ficam depositados no Bancos de Dados de Proteínas (PDB), que podem ser utilizados em abordagens de modelagem por homologia (HILLISCH; PINEDA; HILGENFELD, 2004).

Ainda assim, além das dificuldades citadas para proteínas de membrana, estas técnicas são fastidiosas, demoradas e economicamente desvantajosas. Com a necessidade pelo conhecimento da estrutura de uma proteína para entender sua atividade, novas abordagens para esse estudo são importantes (WALMSLEY; MCKEEGAN; WALMSLEY, 2003). A modelagem molecular é uma ferramenta importante para determinar a estrutura de proteínas que ainda não foram cristalografadas (HILLISCH; PINEDA; HILGENFELD, 2004; MARTI-RENOM et al., 2000). Diversos estudos utilizam a modelagem molecular para determinar as estruturas de bombas de efluxo de *M. tuberculosis*, como a Mmr

(SURIYANARAYANAN; SAROJINI SANTHOSH, 2015), a MmpL5 e a MmpS5 (SANDHU; AKHTER, 2017) e a Tap (CLOETE et al., 2018). Dessa forma, nós realizamos um estudo que objetiva a modelagem molecular da bomba de Efluxo Tap de *M. tuberculosis* no Artigo I (SCAINI et al., 2019), Seção 6 desta Tese.

2.5 Modelagem molecular de proteínas

A modelagem molecular representa um conjunto de métodos, teóricos e computacionais, utilizados para modelar ou mimetizar o comportamento de moléculas. Recentemente, a biologia computacional tem apresentado importantes avanços em algoritmos de modelagem estrutural de proteínas (ESWAR et al., 2008; KELLEY; STERNBERG, 2009; ZHANG, 2008). O número de possíveis conformações possíveis para uma cadeia peptídica é de grande escala, e as predições de estrutura por modelagem molecular buscam resolver este problema (DURUP, 1998).

A modelagem por homologia se baseia na definição de que, durante o processo evolutivo, a estrutura terciária das proteínas permanece mais conservada que sua sequência de aminoácidos, assim proteínas com sequências diferentes podem manter a mesma função por possuírem a mesma estrutura. Portanto as homologias entre as sequências de aminoácidos implicam em semelhanças estrutural e funcional (CHOTHIA; LESK, 1986; KACZANOWSKI; ZIELENKIEWICZ, 2010). As proteínas homólogas apresentam conservadas suas regiões internas, majoritariamente constituídas por elementos de estrutura secundária (α-hélices e folhas-β) e as alterações estruturais entre proteínas homólogas ocorrem principalmente em regiões de alças (ECHAVE; SPIELMAN; WILKE, 2016).

A modelagem molecular por homologia é um método que, seguindo esses princípios, faz uso de estruturas homólogas à proteína de interesse como moldes para a construção do modelo tridimensional da proteína alvo (LUSHINGTON, 2015). Este método apresenta quatro etapas principais: 1) procura por sequências de proteínas

homólogas; 2) alinhamento das sequências; 3) construção e otimização dos modelos e 4) avaliação e validação das estruturas geradas (CAVASOTTO; PHATAK, 2009; D'ALFONSO; TRAMONTANO; LAHM, 2001; MARTI-RENOM et al., 2000).

A modelagem por *threading* é recomendada para proteínas sem estruturas homologas depositadas no PDB (ZHANG, 2008). Este método utiliza como molde proteínas com estrutura determinada com relação estrutural estatística, ou seja, levando em conta analogias evolutivas (ROY; KUCUKURAL; ZHANG, 2010).

A modelagem *ab initio* ou *de novo* determina a estrutura terciária de uma proteína a partir apenas da estrutura primária, sem necessidade de um molde. A predição do mecanismo de enovelamento das proteínas a partir da sequência de aminoácidos tem sido um desafio por mais de cinco décadas. A modelagem *ab initio* ainda tem pouca precisão, tendo sucesso em proteínas pequenas. Porém é um avanço importante para entender os mecanismos de enovelamento (LEE; FREDDOLINO; ZHANG, 2017).

2.6 *Docking* Molecular

Docking molecular é um método usado para estimar as orientações e conformações preferível em que uma molécula se liga a uma outra, formando um complexo estável. Este método também pode prever a força de ligação entre estas duas moléculas (MORRIS et al., 2009; TROTT; OLSON, 2010). Geralmente as duas moléculas em questão são uma macromolécula (receptor), como uma proteína, e uma molécula menor (ligante) (LORBER, 1999; LYBRAND, 1995). O *docking* molecular é eficaz no estudo das interações proteína-ligante, permitindo uma triagem de fármacos que pode ser utilizado tanto no planejamento de novos fármacos quanto no reuso de fármacos (HOU et al., 1999; ISLAM et al., 2020; VALDÉS-TRESANCO et al., 2020).

AutoDock Vina é um *software* de *docking* molecular de proteína-ligante (TROTT; OLSON, 2010) amplamente utilizada (A. MAIA et al., 2018; FORLI et al.,

2016; ISLAM et al., 2020; VALDÉS-TRESANCO et al., 2020). Este programa tem significativas melhoras na acurácia média nas predições de ligações em relação a versões anteriores. A força da ligação proteína-ligante é avaliada por uma função de *score* que estima a energia livre de ligação (FEB – *Free Energy of Binding*), quanto mais negativo o *score* de FEB, maior a afinidade (MORRIS et al., 2009; TROTT; OLSON, 2010).

O AutoDock Vina permite o usuário escolher qual sítio da proteína que será utilizado como receptor a partir de uma caixa, a *grid* box (TROTT; OLSON, 2010). O *framework* de triagem virtual proposto por SEUS et al., 2016 possibilita a variação da *grid box* do AutoDock Vina. Isso permite a avaliação da afinidade de IEs e antimicrobianos em diferentes sítios de uma bomba de efluxo, e assim avaliar a possibilidade de competição pelos mesmos. Isso é importante para testar a hipótese da competição inibitória, na qual o mecanismo de ação do IE seria a competição pelo mesmo sítio com o antimicrobiano, quando o IE é também um substrato da bomba de efluxo (DA SILVA JÚNIOR et al., 2017; LOMOVSKAYA et al., 2001; PUTMAN et al., 1999; SCAINI et al., 2019). Desta forma, nós estudamos a possibilidade da ação de IEs pela competição inibitória em um modelo molecular da bomba de efluxo Tap de *M. tuberculosis* utilizando o *docking* molecular no Artigo I (SCAINI et al., 2019), Seção 6.

2.7 Envelope celular das micobactérias

O envelope celular micobacteriano consiste de uma cápsula polissacarídica e protéica, a parede celular (PC) e a membrana plasmática. A PC robusta e impermeável é uma característica dominante da estrutura da célula das micobactérias em geral e do *M. tuberculosis* em particular, sendo responsável pela proteção da bactéria em ambientes hostis, resistência mecânica, transporte de solutos e proteínas e adesão a receptores de hospedeiros. Sob o ponto de vista terapêutico, enzimas envolvidas na síntese da PC são alvos de antimicrobianos como ETB, INH,

Etionamida e mutações nos genes que codificam estas enzimas são responsáveis pela resistência a estes antimicrobianos (DAFFÉ; DRAPER, 1998; GYGLI et al., 2017).

Uma forma de combater a resistência causada por antimicrobianos é o rompimento do envelope celular (BOAGS et al., 2017), como a MFL, um fármaco utilizado no tratamento de malária, que pode afetar a integridade de membranas procarióticas (BROWN; STANCATO; WOLFE, 1979) e que mostrou efeito antimicrobiano em *M. tuberculosi*s (BERMUDEZ; MEEK, 2014; GONALVES et al., 2012; JAYAPRAKASH et al., 2006; RODRIGUES-JUNIOR et al., 2016).

Vários lipídios únicos para micobactérias compõem este envelope, entre eles, os ácidos graxos de cadeia longa, ácidos micólicos, cuja abundância confere características particulares deste gênero (BRENNAN; GOREN, 1979; SARTAIN et al., 2011). A esses lipídios foram atribuídas várias das propriedades biológicas de micobactérias, como a alta resistência para um amplo espectro de antibióticos e sua reconhecida impermeabilidade à nutrientes (JARLIER; NIKAIDO, 1990). Por conta disso, a importância biológica destes lipídios são alvo de vários estudos que tentam elucidar suas estruturas e funções (CHIARADIA et al., 2017; SANCHO-VAELLO et al., 2017; SARTAIN et al., 2011).

A estrutura do envelope celular micobacteriano referida usada nesta tese é baseada na utilizada no artigo de BANSAL-MUTALIK; NIKAIDO, 2014, que realiza extração micelar dos lipídios de ambas parede celular e membrana plasmática, e valida o modelo de que lipídios da PC compõem uma ME. Desta forma, o envelope celular micobacteriano é composto pela ME, o complexo peptidoglicano-arabinogalactano e a MI (Figura 2) (BANSAL-MUTALIK; NIKAIDO, 2014).

No folheto externo da ME existe uma variedade de lipídios localizados de forma não covalente que são estruturalmente atípicos: ftiocerol dimicocerosato, dimecolato

de trealose, sulfolipídeos, PIMs, e lipoarabinomanano com extensos ramos metil que possuem uma estereoquímica sofisticada (ADHYAPAK et al., 2020; BANSAL-MUTALIK; NIKAIDO, 2014; BRENNAN; NIKAIDO, 1995). O folheto interno da ME é formado por ácidos micólicos, ácidos de cadeia longa com entre 60 e 90 átomos de carbono, que são covalentemente ligados aos arabinogalactanos do complexo peptidoglicano-arabinogalactano (BANSAL-MUTALIK; NIKAIDO, 2014).

Figura 2: Estrutura do envelope celular micobacteriano

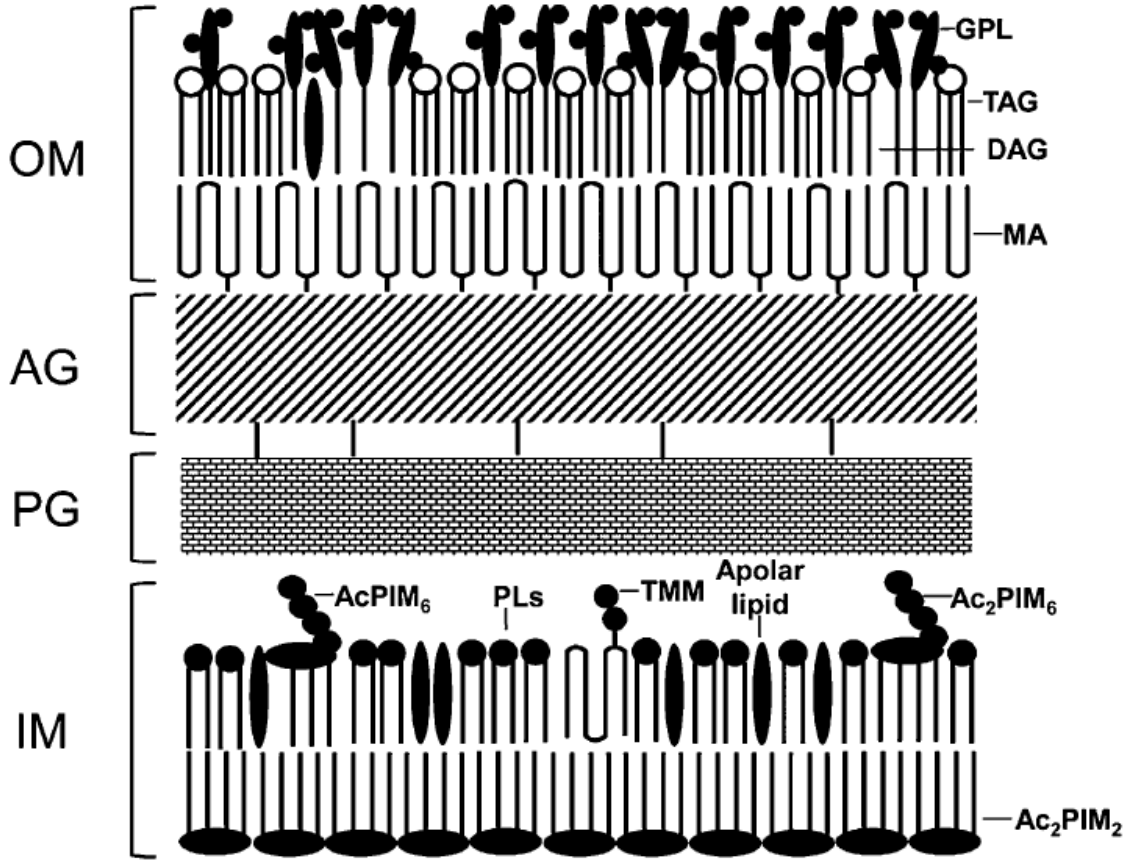

Estrutura do envelope celular micobacteriano. OM é a membrana externa, AG é o arabinogalactano, PG é o peptidoglicano e IM é a membrana interna (BANSAL-MUTALIK; NIKAIDO, 2014). Alguns lipídeos também estão representados na imagem:

GPL – glicopeptidiolipídeos, TAG – triacilglicerol, DAG – diacilglicerol, MA – ácido micólico, PL – fosfolipídios, além de lipídios apolares, AcPIM6, Ac2PIM6 e AC2PIM2.

O complexo PG-AG compreende o peptidoglicano covalentemente ligado ao arabinogalactano. O peptidoglicano é composto de unidades repetitivas de N-acetilglucosamina e N-acetil/glicolilmurâmico com peptídeos curtos. O arabinogalactano, por sua vez, é um heteropolissacarídeo que contém uma cadeia galactana composta de resíduos de D-galactofuranosil, sendo que três cadeiras de arabinano substituem a cadeira de D-galactano em *M. tuberculosis*. Em *M. tuberculosis*, dois terços dos *motifs* pentarabinosil terminais não-reduzidos são esterificados por ácidos micólicos, que como foi dito, ocupam o folheto interno da ME (ALDERWICK et al., 2015; DAFFÉ, 2015). O complexo PG-AG incluindo os ácidos micólicos (folheto interno da ME) formam o esqueleto da parede celular, que define a forma da célula micobacteriana (DAFFÉ, 2015). A parede celular é composta por este esqueleto e a ME (BANSAL-MUTALIK; NIKAIDO, 2014).

MI é composta de fosfolipídios típicos como cardiolipina (CL), PI e fosfatidiletanolamina (PE), constituindo ~ 10%, ~ 3% e ~ 4% da massa seca do extrato da MI, respectivamente. Também possui trealose monomicolato (TMM) constituindo ~ 10% da massa seca do extrato da MI. No entanto, o lipídio mais abundante é a forma tetra acilada dos PIM2 (Ac2PIM2), sendo até 42% da massa seca do extrato da MI. Outros glicolipídeos da família PIM, incluindo a forma triacilada de PIM2 (Ac1PIM2), as formas tri- e tetraaciladas de PI tetramanosídeos (Ac1PIM4 e Ac2PIM4, respectivamente) e as formas tri- e tetra aciladas de PI hexamanosídeos (Ac1PIM6 e Ac2PIM6, respectivamente; compõe até 26% da massa seca do extrato da MI. Ac2PIM2 é presente principalmente no folheto interno da MI, enquanto o folheto externo parece conter outros lipídios, incluindo Ac1PIM6 e Ac2PIM6, TMM, CL, PI e PE (BANSAL-MUTALIK; NIKAIDO, 2014). O ácido palmítico (C16: 0) e o ácido 10-

metiloctadecanóico (C19: 0) são os principais constituintes do ácido graxo da MI bioquimicamente isolada (DAFFÉ; DRAPER, 1998).

2.7.1 PIMs

Os PIMs são glicolipídeos únicos abundantes nas MI e ME de todas as micobactérias, sendo componentes estruturais do envelope celular. Estruturalmente, os PIMs são constituídos por um grupo PI contendo manosídeos esterificados no anel inositol (GUERIN et al., 2010). A família PIM compreende PI mono-, di-, tri-, tetra-, penta- e hexamanosídeos, com até quatro cadeias acil. As duas classes mais abundantes em *M. tuberculosis* são PIM2 e PI hexamanosídeos (PIM6) (SANCHO-VAELLO et al., 2017).

Como já foi dito, vários PIMs compõe uma grande parte da MI, incluindo Ac2PIM2, o lipídio mais abundante desta membrana, e também AcPIM2, AcPIM4, Ac2PIM4, Ac2PIM6 e Ac2PIM6 (BANSAL-MUTALIK; NIKAIDO, 2014). Além disso, são precursores dos dois principais lipoglicanos micobacterianos, o LM e o LAM, que são formas multiglicosiladas de PIM2 (CHATTERJEE et al., 1992; KHOO et al., 1995). PIMs e estes lipoglicanos são, além de componentes essenciais do envelope celular micobacteriano, fatores de virulência importantes em *M. tuberculosis*, e podem modular interações patógeno-hospedeiro (GUERIN et al., 2010; SANCHO-VAELLO et al., 2017). Como a PIM2 é a classe de PIMs mais abundante em *M. tuberculosis*, sendo a Ac2PIM2 o lipídio mais abundante da MI, e sendo os LM e LAM formas multiglicosiladas de PIM2, nós desenvolvemos um modelo estrutural de uma membrana de PIM2 utilizando a DM.

2.8 Dinâmica Molecular

A DM é uma técnica computacional desenvolvida para o estudo da dinâmica conformacional e posicional de átomos e moléculas (BORHANI; SHAW, 2012; RODRIGUEZ-BUSSEY; DOSHI; HAMELBERG, 2016). A DM utiliza lógica da

dinâmica newtoniana para simular a movimentação de todos os átomos de uma proteína em qualquer ambiente a partir do aumento de temperatura gerada pela velocidade de movimentação dos átomos, levando em consideração as forças de ligações e as forças que não são de ligação, que são calculadas a partir dos dados no campo de força (BORHANI; SHAW, 2012). O campo de força, por sua vez simula as forças reais que atuam nos átomos em um sistema macromolecular, utilizando valores obtidas de forma empírica (PIANA; LINDORFF-LARSEN; SHAW, 2011).

Simulações de DM tem sido usadas no planejamento racional no desenvolvimento de fármacos por possibilitar uma visão mais ampla e realista das afinidades dos fármacos com a proteína-alvo, assim como estruturas mais realistas por serem flexíveis (BORHANI; SHAW, 2012; RODRIGUEZ-BUSSEY; DOSHI; HAMELBERG, 2016). A observação do comportamento de uma proteína com átomos em movimento em um solvente é fundamental para a avaliação da qualidade da estrutura (FIGUEIREDO et al., 2014; PIANA; LINDORFF-LARSEN; SHAW, 2011).

GROMACS (BERENDSEN; VAN DER SPOEL; VAN DRUNEN, 1995) é um pacote de programas desenhado para a simulação computacional de moléculas bioquímicas como proteínas, lipídios e ácidos nucléicos. Possui algoritmos que calculam uma estimativa das forças intramoleculares, o que possibilita a simulação de moléculas complexas sob a atuação destas forças (ABRAHAM et al., 2015; PALL et al., 2014; PRONK et al., 2013).

2.8.1 Dinâmica Molecular em Membranas

A caracterização físico-química das membranas biológicas é fundamental para o entendimento do seu papel fisiológico (BOVIGNY et al., 2015). A elucidação dos mecanismos responsáveis pelas distintas conformações estruturais e morfologias, e a fusão e dissolução é essencial para compreender uma vasta gama de processos biológicos, como por exemplo a virulência (BAUMGART; HESS; WEBB, 2003; DE

VRIES; MARK; MARRINK, 2004). Para isso, uma das abordagens mais empregadas para entender o comportamento das membranas celulares são as simulações de DM. Este método *in silico* possibilita controle e uma análise detalhada das propriedades físicas e químicas da membrana e tem sido amplamente aplicado para fornecer informações sobre sua organização espacial e dinâmica temporal (DESERNO et al., 2014; FELLER, 2000; FRIGINI; LÓPEZ CASCALES; PORASSO, 2018).

Simulações de DM são capazes de produzir as configurações dinâmicas de moléculas de lipídios dispostas em membranas de bicamada e em um nível de detalhe atômico que não está disponível diretamente em estudos espectroscópicos (KLAUDA et al., 2008; SAPAY; TIELEMAN, 2008; SCHLENKRICH et al., 1996). Essas configurações são dependentes dos campos de força, que são otimizados para reproduzir uma gama de parâmetros experimentais que caracterizam a estrutura da bicamada (PASTOR; MACKERELL, 2011; VENABLE; BROWN; PASTOR, 2015).

Por conta de tudo isso, nós realizamos um estudo que objetiva o desenvolvimento de um modelo atomístico de DM de uma membrana de PIM2 de *M. tuberculosis* no Manuscrito II, Seção 7 desta Tese. Também utilizamos este modelo para estudar a hipótese de que a interação da MFL com o envelope celular é o motivo de seu sinergismo com outros antimicrobianos em *M. tuberculosis* no Manuscrito III, Seção 8 desta Tese.

2.9 Justificativa

Considerando que a Tap tem sido a bomba de efluxo mais frequentemente descrita como envolvida com resistência aos antimicrobianos em *M. tuberculosis*, além do seu possível papel na virulência, um IE com especificidade para esta bomba poderia possibilitar: a introdução, no tratamento da TB, de antimicrobianos já disponíveis, porém não efetivos contra a TB; a maior eficácia de antimicrobianos da segunda linha do tratamento de TB; a redução da duração do tratamento padrão. Para

tal, o estudo racional de IEs para Tap a partir de uma abordagem estrutural é uma forma efetiva para a descobrir IEs que possam ser utilizados clinicamente, tanto pelo desenvolvimento de novos IEs quanto pelo reposicionamento de IEs já utilizados para outros tratamentos. Assim, um estudo estrutural da bomba de efluxo Tap por ferramentas como a modelagem molecular, o *docking* molecular e a DM pode contribuir na adição de um IE no tratamento.

Para aumentar a acurácia dos estudos estruturais com bombas de efluxo, é importante a utilização de um modelo de membrana plasmática. No entanto, não há nenhum modelo molecular da membrana de *M. tuberculosis* que represente sua composição lipídica incomum. Portanto, seria importante desenvolver um modelo de membrana plasmática micobacteriana para permitir estudos estruturais que levassem em consideração sua real composição lipídica. Como citado antes, o PIM2 é um dos lipídios mais abundantes da MI, abundante na ME e precursor dos lipoglicanos LM e LAM, além de ser um fator de virulência importante em *M. tuberculosis*. Assim um modelo de membrana de PIM2 de *M. tuberculosis* possibilitaria uma gama de estudos que envolve este complexo envelope. Um destes estudos é a investigação da MFL, uma molécula que mostrou efeito antimicrobiano em *M. tuberculosis*, e que pode ser devido à sua possível interação com o envelope. Este estudo ganha um maior esclarecimento quanto ao mecanismo de ação físico e químico com o estudo da DM utilizando o modelo de membrana para *M. tuberculosis*.

3 Objetivos

3.1 Objetivo Geral

Desenvolver modelos atomísticos computacionais das estruturas de membrana de PIM2 e da bomba de efluxo Tap de *M. tuberculosis*, como alvos no estudo racional de antimicrobianos.

3.2 Objetivos Específicos

- Desenvolver e avaliar um modelo da bomba de efluxo Tap
- Avaliar a possibilidade de competição inibitória como mecanismo de ação de IEs no modelo de Tap
- Desenvolver e avaliar um modelo de membrana de PIM2 para *M. tuberculosis*
- Avaliar a interação do modelo da membrana de PIM2 com a bomba de efluxo Tap
- Avaliar o modelo de membrana de PIM2 na presença de mefloquina

4 Material e Métodos

A metodologia utilizada nesta tese está sintetizada na Figura 3. Dividido em o que foi utilizado em cada artigo. Os métodos são descritos nos artigos (seções 6, 7 e 8).

Figura 3: Fluxograma de Material e Métodos.

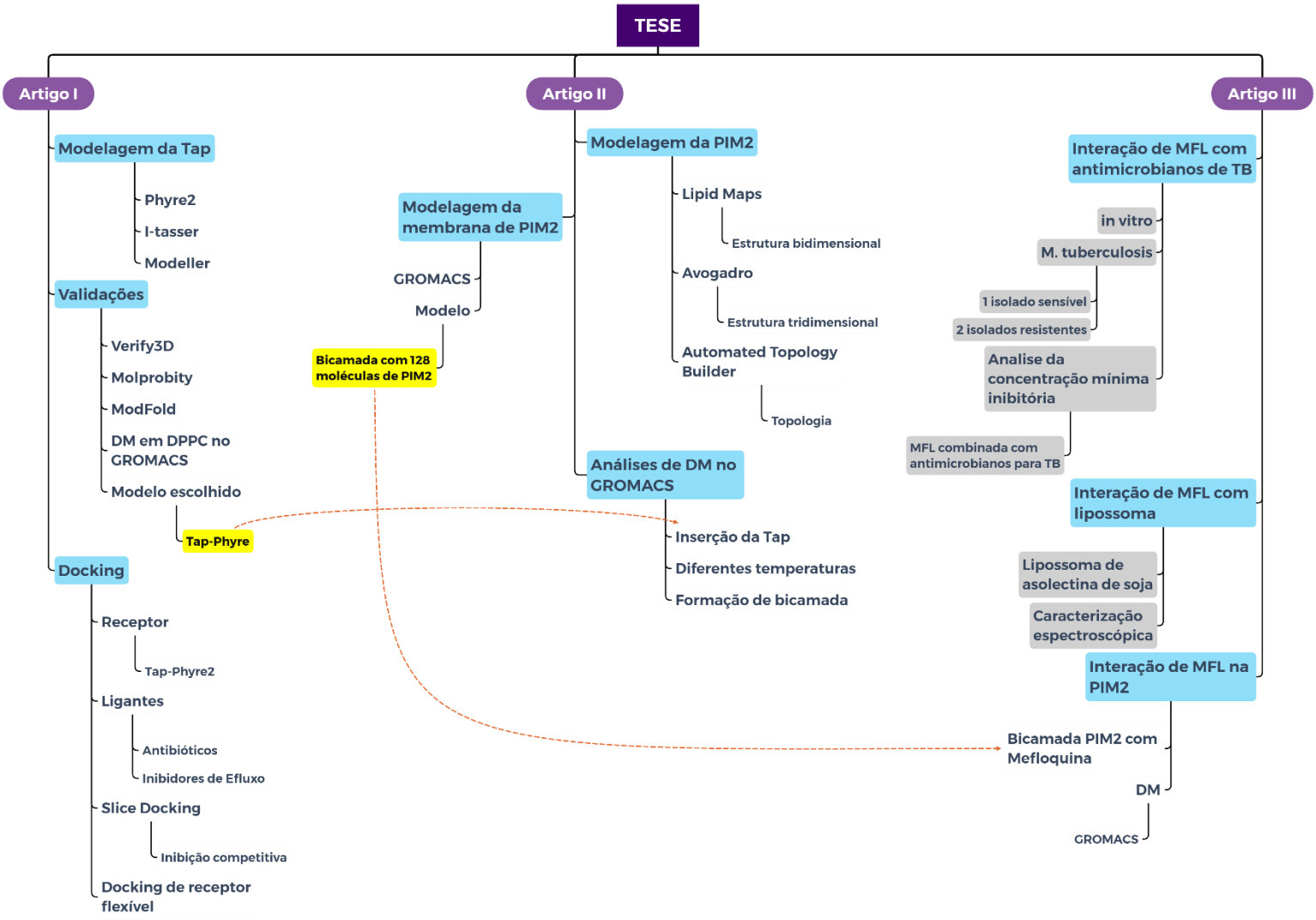

Fluxograma mostrando os métodos utilizados em cada etapa do trabalho.

5 Bibliografia

A. MAIA, R. et al. Crystal Engineering of Covalent Organic Frameworks Based on Hydrazine and Hydroxy-1,3,5-Triformylbenzenes. **Crystal Growth & Design**, v. 18, n. 9, p. 5682–5689, set. 2018.

ABRAHAM, M. J. et al. GROMACS: High performance molecular simulations through multi-level parallelism from laptops to supercomputers. **SoftwareX**, v. 1, p. 19–25, 2015.

ADHYAPAK, P. et al. Dynamical Organization of Compositionally Distinct Inner and Outer Membrane Lipids of Mycobacteria. **Biophysical Journal**, v. 118, n. 6, p. 1279–1291, 24 mar. 2020.

AÍNSA, J. A. et al. Molecular Cloning and Characterization of Tap, a Putative Multidrug Efflux Pump Present in Mycobacterium fortuitum and Mycobacterium tuberculosis. **Journal of Bacteriology**, v. 180, n. 22, p. 5836–5843, nov. 1998.

ALDERWICK, L. J. et al. The Mycobacterial Cell Wall--Peptidoglycan and Arabinogalactan. **Cold Spring Harbor Perspectives in Medicine**, v. 5, n. 8, p. a021113, 27 mar. 2015.

ALMEIDA, D. et al. Mutations in pepQ Confer Low-Level Resistance to Bedaquiline and Clofazimine in Mycobacterium tuberculosis. **Antimicrobial Agents and Chemotherapy**, v. 60, n. 8, p. 4590–4599, 22 jul. 2016.

ÁLVARO-MECA, A. et al. Incidence and mortality of tuberculosis disease in Spain between 1997 and 2010: Impact of human immunodeficiency virus (HIV) status. **Journal of Infection**, v. 68, n. 4, p. 355–362, 2014.

ANDRIES, K. et al. Acquired Resistance of Mycobacterium tuberculosis to Bedaquiline. **PLoS ONE**, v. 9, n. 7, 10 jul. 2014.

BANSAL-MUTALIK, R.; NIKAIDO, H. Mycobacterial outer membrane is a lipid bilayer and the inner membrane is unusually rich in diacyl phosphatidylinositol dimannosides. **Proceedings of the National Academy of Sciences of the United States of America**, v. 111, n. 13, p. 4958–4963, 1 abr. 2014.

BAUMGART, T.; HESS, S. T.; WEBB, W. W. Imaging coexisting fluid domains in biomembrane models coupling curvature and line tension. **Nature**, v. 425, n. 6960, p. 821–824, 23 out. 2003.

BERENDSEN, H. J.; VAN DER SPOEL, D.; VAN DRUNEN, R. GROMACS: a message-passing parallel molecular dynamics implementation. **Computer Physics Communications**, v. 91, n. 1–3, p. 43–56, 1995.

BERMUDEZ, L. E.; MEEK, L. Mefloquine and Its Enantiomers Are Active against Mycobacterium tuberculosis In Vitro and in Macrophages. **Tuberculosis Research and Treatment**, v. 2014, p. 1–5, 2014.

BLACK, P. A. et al. Energy Metabolism and Drug Efflux in Mycobacterium tuberculosis. **Antimicrobial Agents and Chemotherapy**, v. 58, n. 5, p. 2491–2503, maio 2014.

BOAGS, A. et al. Progress in Molecular Dynamics Simulations of Gram-Negative Bacterial Cell Envelopes. **The Journal of Physical Chemistry Letters**, v. 8, n. 11, p. 2513–2518, 1 jun. 2017.

BOLLA, J. R. et al. Structural and functional analysis of the transcriptional regulator Rv3066 of Mycobacterium tuberculosis. **Nucleic Acids Research**, v. 40, n. 18, p. 9340–9355, out. 2012.

BORHANI, D. W.; SHAW, D. E. The future of molecular dynamics simulations in drug discovery. **Journal of computer-aided molecular design**, v. 26, n. 1, p. 15–26, 2012.

BOVIGNY, C. et al. LipidBuilder: A Framework To Build Realistic Models for Biological Membranes. **Journal of Chemical Information and Modeling**, v. 55, n. 12, p. 2491–2499, 28 dez. 2015.

BRENNAN, P. J.; GOREN, M. B. Structural studies on the type-specific antigens and lipids of the mycobacterium avium. Mycobacterium intracellulare. Mycobacterium scrofulaceum serocomplex. Mycobacterium intracellulare serotype 9. **The Journal of Biological Chemistry**, v. 254, n. 10, p. 4205–4211, 25 maio 1979.

BRENNAN, P. J.; NIKAIDO, H. The envelope of mycobacteria. **Annual Review of Biochemistry**, v. 64, p. 29–63, 1995.

BROWN, R. E.; STANCATO, F. A.; WOLFE, A. D. THE EFFECTS OF MEFLOQUINE ON ESCHERICHIA COLI. **Vol .**, p. 8, 1979.

BURIAN, J. et al. WhiB7, a transcriptional activator that coordinates physiology with intrinsic drug resistance in Mycobacterium tuberculosis. **Expert review of anti-infective therapy**, v. 10, n. 9, p. 1037–1047, 2012.

CAMACHO, L. R. et al. Identification of a virulence gene cluster of Mycobacterium tuberculosis by signature-tagged transposon mutagenesis. **Molecular Microbiology**, v. 34, n. 2, p. 257–267, out. 1999.

CAMACHO, L. R. et al. Analysis of the phthiocerol dimycocerosate locus of Mycobacterium tuberculosis. Evidence that this lipid is involved in the cell wall permeability barrier. **The Journal of Biological Chemistry**, v. 276, n. 23, p. 19845–19854, 8 jun. 2001.

CAVASOTTO, C. N.; PHATAK, S. S. Homology modeling in drug discovery: current trends and applications. **Drug discovery today**, v. 14, n. 13, p. 676–683, 2009.

CHAN, Y. Y.; CHUA, K. L. Growth-related changes in intracellular spermidine and its effect on efflux pump expression and quorum sensing in Burkholderia pseudomallei. **Microbiology**, v. 156, n. 4, p. 1144–1154, 2010.

CHATTERJEE, D. et al. Lipoarabinomannan of Mycobacterium tuberculosis. Capping with mannosyl residues in some strains. **The Journal of Biological Chemistry**, v. 267, n. 9, p. 6234–6239, 25 mar. 1992.

CHIARADIA, L. et al. Dissecting the mycobacterial cell envelope and defining the composition of the native mycomembrane. **Scientific Reports**, v. 7, n. 1, p. 12807, 9 out. 2017.

CHOTHIA, C.; LESK, A. M. The relation between the divergence of sequence and structure in proteins. **The EMBO journal**, v. 5, n. 4, p. 823, 1986.

CHOUDHURI, B. S. et al. Overexpression and functional characterization of an ABC (ATP-binding cassette) transporter encoded by the genes drrA and drrB of Mycobacterium tuberculosis. **Biochemical Journal**, v. 367, n. Pt 1, p. 279–285, 1 out. 2002.

CLARK, T. G. et al. Elucidating emergence and transmission of multidrug-resistant tuberculosis in treatment experienced patients by whole genome sequencing. **PLoS One**, v. 8, n. 12, p. e83012, 2013.

CLOETE, R. et al. Molecular modelling and simulation studies of the Mycobacterium tuberculosis multidrug efflux pump protein Rv1258c. **PLOS ONE**, v. 13, n. 11, p. e0207605, 26 nov. 2018.

COELHO, T. et al. Enhancement of antibiotic activity by efflux inhibitors against multidrug resistant Mycobacterium tuberculosis clinical isolates from Brazil. **Frontiers in Microbiology**, v. 6, 28 abr. 2015.

COHEN, J. Approval of novel TB drug celebrated—with restraint. **Science**, v. 339, n. 6116, p. 130–130, 2013.

DA SILVA JÚNIOR, L. V. et al. In vitro and in silico analysis of the efficiency of tetrahydropyridines as drug efflux inhibitors in Escherichia coli. **International Journal of Antimicrobial Agents**, v. 49, n. 3, p. 308–314, 2017.

DA SILVA, P. E. A. et al. Efflux as a mechanism for drug resistance in Mycobacterium tuberculosis. **FEMS immunology and medical microbiology**, v. 63, n. 1, p. 1–9, out. 2011.

DAFFÉ, M. The cell envelope of tubercle bacilli. **Tuberculosis**, Supplement issue: Tuberculosis in Evolution. v. 95, p. S155–S158, 1 jun. 2015.

DAFFÉ, M.; DRAPER, P. The envelope layers of mycobacteria with reference to their pathogenicity. **Advances in Microbial Physiology**, v. 39, p. 131–203, 1998.

D'ALFONSO, G.; TRAMONTANO, A.; LAHM, A. Structural conservation in single-domain proteins: implications for homology modeling. **Journal of structural biology**, v. 134, n. 2, p. 246–256, 2001.

DE ROSSI, E. et al. Molecular Cloning and Functional Analysis of a Novel Tetracycline Resistance Determinant, tet(V), from Mycobacterium smegmatis. **Antimicrobial Agents and Chemotherapy**, v. 42, n. 8, p. 1931–1937, ago. 1998.

DE ROSSI, E. et al. The multidrug transporters belonging to major facilitator superfamily in Mycobacterium tuberculosis. **Molecular Medicine**, v. 8, n. 11, p. 714–724, nov. 2002.

DE ROSSI, E.; AÍNSA, J. A.; RICCARDI, G. Role of mycobacterial efflux transporters in drug resistance: an unresolved question. **FEMS microbiology reviews**, v. 30, n. 1, p. 36–52, jan. 2006.

DE VRIES, A. H.; MARK, A. E.; MARRINK, S. J. Molecular Dynamics Simulation of the Spontaneous Formation of a Small DPPC Vesicle in Water in Atomistic Detail. **Journal of the American Chemical Society**, v. 126, n. 14, p. 4488–4489, 1 abr. 2004.

DESERNO, M. et al. Computational Studies of Biomembrane Systems: Theoretical Considerations, Simulation Models, and Applications. In: BASCHÉ, T.; MÜLLEN, K.; SCHMIDT, M. (Eds.). . **From Single Molecules to Nanoscopically Structured Materials**. Advances in Polymer Science. Cham: Springer International Publishing, 2014. p. 237–283.

DHAMDHERE, G.; ZGURSKAYA, H. I. Metabolic shut-down in Escherichia coli cells lacking the outer membrane channel TolC. **Molecular microbiology**, v. 77, n. 3, p. 743–754, ago. 2010.

DIALLINAS, G. Understanding transporter specificity and the discrete appearance of channel-like gating domains in transporters. **Frontiers in pharmacology**, v. 5, 2014.

DU, D. et al. Structure of the AcrAB-TolC multidrug efflux pump. **Nature**, v. 509, n. 7501, p. 512–515, 2014.

DULBERGER, C. L.; RUBIN, E. J.; BOUTTE, C. C. The mycobacterial cell envelope — a moving target. **Nature Reviews Microbiology**, v. 18, n. 1, p. 47–59, jan. 2020.

DURUP, J. On “Levinthal paradox” and the theory of protein folding. **Journal of Molecular Structure: THEOCHEM**, A Faithful Couple: Qualitative and Quantitative Understanding of Chemistry. v. 424, n. 1, p. 157–169, 9 fev. 1998.

ECHAVE, J.; SPIELMAN, S. J.; WILKE, C. O. Causes of evolutionary rate variation among protein sites. **Nature Reviews Genetics**, v. 17, n. 2, p. 109–121, 2016.

ESCRIBANO, I. et al. Importance of the efflux pump systems in the resistance of Mycobacterium tuberculosis to fluoroquinolones and linezolid. **Chemotherapy**, v. 53, n. 6, p. 397–401, 2007.

ESWAR, N. et al. Protein structure modeling with MODELLER. **Structural proteomics: high-throughput methods**, p. 145–159, 2008.

FAVROT, L.; RONNING, D. R. Targeting the mycobacterial envelope for tuberculosis drug development. **Expert review of anti-infective therapy**, v. 10, n. 9, p. 1023–1036, 2012.

FELLER, S. E. Molecular dynamics simulations of lipid bilayers. **Current Opinion in Colloid & Interface Science**, v. 5, n. 3, p. 217–223, jul. 2000.

FIGUEIREDO, D. F. et al. Lessons from molecular modeling human α-l-iduronidase. **Journal of Molecular Graphics and Modelling**, v. 54, p. 107–113, 2014.

FORLI, S. et al. Computational protein-ligand docking and virtual drug screening with the AutoDock suite. **Nature protocols**, v. 11, n. 5, p. 905–919, maio 2016.

FRIGINI, E. N.; LÓPEZ CASCALES, J. J.; PORASSO, R. D. Molecular dynamics simulations of glyphosate in a DPPC lipid bilayer. **Chemistry and Physics of Lipids**, v. 213, p. 111–117, jul. 2018.

GEIMAN, D. E. et al. Differential gene expression in response to exposure to antimycobacterial agents and other stress conditions among seven Mycobacterium tuberculosis whiB-like genes. **Antimicrobial agents and chemotherapy**, v. 50, n. 8, p. 2836–2841, 2006.

GONALVES, R. S. B. et al. Mefloquine-oxazolidine derivatives, derived from mefloquine and arenecarbaldehydes: In vitro activity including against the multidrug-resistant tuberculosis strain T113. **Bioorganic and Medicinal Chemistry**, v. 20, n. 1, p. 243–248, 2012.

GUERIN, M. E. et al. Molecular Basis of Phosphatidyl-myo-inositol Mannoside Biosynthesis and Regulation in Mycobacteria. **The Journal of Biological Chemistry**, v. 285, n. 44, p. 33577–33583, 29 out. 2010.

GUILFOILE, P. G.; HUTCHINSON, C. R. A bacterial analog of the mdr gene of mammalian tumor cells is present in Streptomyces peucetius, the producer of daunorubicin and doxorubicin. **Proceedings of the National Academy of Sciences**, v. 88, n. 19, p. 8553–8557, 1991.

GUPTA, S. et al. Acceleration of Tuberculosis Treatment by Adjunctive Therapy with Verapamil as an Efflux Inhibitor. **American Journal of Respiratory and Critical Care Medicine**, v. 188, n. 5, p. 600–607, 1 set. 2013.

GYGLI, S. M. et al. Antimicrobial resistance in Mycobacterium tuberculosis: mechanistic and evolutionary perspectives. **FEMS microbiology reviews**, v. 41, n. 3, p. 354–373, 01 2017.

HILLISCH, A.; PINEDA, L. F.; HILGENFELD, R. Utility of homology models in the drug discovery process. **Drug Discov. Today**, v. 9, p. 659–669, 2004.

HOGAN, D.; KOLTER, R. Why are bacteria refractory to antimicrobials? **Current opinion in microbiology**, v. 5, n. 5, p. 472–477, 2002.

HØIBY, N.; CIOFU, O.; BJARNSHOLT, T. Pseudomonas aeruginosa biofilms in cystic fibrosis. **Future microbiology**, v. 5, n. 11, p. 1663–1674, 2010.

HOU, T. et al. Automated docking of peptides and proteins by using a genetic algorithm combined with a tabu search. **Protein Engineering**, v. 12, n. 8, p. 639–648, 1999.

HOUBEN, R. M. G. J.; DODD, P. J. The Global Burden of Latent Tuberculosis Infection: A Re-estimation Using Mathematical Modelling. **PLoS Medicine**, v. 13, n. 10, 25 out. 2016.

ISLAM, R. et al. A molecular modeling approach to identify effective antiviral phytochemicals against the main protease of SARS-CoV-2. **Journal of Biomolecular Structure & Dynamics**, p. 1–12, 12 maio 2020.

JARLIER, V.; NIKAIDO, H. Permeability barrier to hydrophilic solutes in Mycobacterium chelonei. **Journal of Bacteriology**, v. 172, n. 3, p. 1418–1423, mar. 1990.

JAYAPRAKASH, S. et al. Design, synthesis, and SAR studies of mefloquine-based ligands as potential antituberculosis agents. **ChemMedChem**, v. 1, n. 6, p. 593–597, 2006.

JIANG, X. et al. Assessment of efflux pump gene expression in a clinical isolate Mycobacterium tuberculosis by real-time reverse transcription PCR. **Microbial Drug Resistance (Larchmont, N.Y.)**, v. 14, n. 1, p. 7–11, mar. 2008.

KACZANOWSKI, S.; ZIELENKIEWICZ, P. Why similar protein sequences encode similar three-dimensional structures? **Theoretical Chemistry Accounts**, v. 125, n. 3–6, p. 643–650, 2010.

KAPP, E.; MALAN, S. F.; SAMPSON, S. L. Small Molecule Efflux Pump Inhibitors in Mycobacterium tuberculosis: a Rational Drug Design Perspective. **Mini Reviews in Medicinal Chemistry**, 9 maio 2017.

KELLEY, L. A.; STERNBERG, M. J. Protein structure prediction on the web: a case study using the Phyre server. **Nat. Protoc.**, v. 4, p. 363–371, 2009.

KHOO, K. H. et al. Structural definition of acylated phosphatidylinositol mannosides from Mycobacterium tuberculosis: definition of a common anchor for lipomannan and lipoarabinomannan. **Glycobiology**, v. 5, n. 1, p. 117–127, fev. 1995.

KLAUDA, J. B. et al. Chapter 1 Considerations for Lipid Force Field Development. In: FELLER, S. E. (Ed.). . **Current Topics in Membranes**. Computational Modeling of Membrane Bilayers. [s.l.] Academic Press, 2008. v. 60p. 1–48.

LAU, S. Y.; ZGURSKAYA, H. I. Cell Division Defects in Escherichia coli Deficient in the Multidrug Efflux Transporter AcrEF-TolC. **Journal of Bacteriology**, v. 187, n. 22, p. 7815–7825, nov. 2005.

LEE, J.; FREDDOLINO, P. L.; ZHANG, Y. Ab initio protein structure prediction. In: **From protein structure to function with bioinformatics**. [s.l.] Springer, 2017. p. 3–35.

LEI, H.-T. et al. Crystal structure of the open state of the Neisseria gonorrhoeae MtrE outer membrane channel. **PLoS One**, v. 9, n. 6, p. e97475, 2014.

LI, B. et al. Determination of MIC Distribution and Mechanisms of Decreased Susceptibility to Bedaquiline Among Clinical Isolates of Mycobacterium abscessus. **Antimicrobial Agents and Chemotherapy**, 30 abr. 2018.

LI, G. et al. Study of efflux pump gene expression in rifampicin-monoresistant Mycobacterium tuberculosis clinical isolates. **The Journal of Antibiotics**, v. 68, n. 7, p. 431–435, jul. 2015.

LI, X.-Z.; ZHANG, L.; NIKAIDO, H. Efflux Pump-Mediated Intrinsic Drug Resistance in Mycobacterium smegmatis. **Antimicrobial Agents and Chemotherapy**, v. 48, n. 7, p. 2415–2423, jul. 2004.

LIU, X.; WRIGHT, M.; HOP, C. E. Rational use of plasma protein and tissue binding data in drug design. **J. Med. Chem.**, v. 57, p. 8238–8248, 2014.

LOMOVSKAYA, O. et al. Identification and characterization of inhibitors of multidrug resistance efflux pumps in Pseudomonas aeruginosa: novel agents for combination therapy. **Antimicrobial Agents and Chemotherapy**, v. 45, n. 1, p. 105–116, jan. 2001.

LORBER, D. M. Computational drug design. **Chemistry & Biology**, v. 6, n. 8, p. R227–R228, 1999.

LOUW, G. E. et al. A balancing act: efflux/influx in mycobacterial drug resistance. **Antimicrob. Agents Chemother.**, v. 53, n. 8, p. 3181–3189, 2009.

LUSHINGTON, G. H. Comparative modeling of proteins. **Molecular Modeling of Proteins**, p. 309–330, 2015.

LYBRAND, T. P. Ligand—protein docking and rational drug design. **Current opinion in structural biology**, v. 5, n. 2, p. 224–228, 1995.

MACHADO, D. et al. Contribution of Efflux to the Emergence of Isoniazid and Multidrug Resistance in Mycobacterium tuberculosis. **PLoS ONE**, v. 7, n. 4, 6 abr. 2012.

MAHAMOUD, A. et al. Antibiotic efflux pumps in Gram-negative bacteria: the inhibitor response strategy. **J. Antimicrob. Chemother.**, v. 59, p. 1223–1229, 2007.

MALINGA, L.; STOLTZ, A.; WALT, M. V. D. Efflux Pump Mediated Second-Line Tuberculosis Drug Resistance. 2016.

MARQUEZ, B. Bacterial efflux systems and efflux pumps inhibitors. **Biochimie.**, v. 87, p. 1137–1147, 2005.

MARTÍNEZ, J. Effect of antibiotics on bacterial populations: a multi-hierarchical selection process [version 1; peer review: 2 approved]. **F1000Research**, v. 6, n. 51, 2017.

MARTINEZ, J. L. General principles of antibiotic resistance in bacteria. **Drug Discovery Today: Technologies**, v. 11, p. 33–39, 2014.

MARTI-RENOM, M. A. et al. Comparative protein structure modeling of genes and genomes. **Annu. Rev. Biophis. Biol.**, v. 29, p. 291–325, 2000.

MISHRA, M. N.; DANIELS, L. Characterization of the MSMEG_2631 Gene (mmp) Encoding a Multidrug and Toxic Compound Extrusion (MATE) Family Protein in Mycobacterium smegmatis and Exploration of Its Polyspecific Nature Using Biolog Phenotype MicroArray. **Journal of Bacteriology**, v. 195, n. 7, p. 1610–1621, abr. 2013.

MORRIS, G. M. et al. AutoDock4 and AutoDockTools4: Automated docking with selective receptor flexibility. **Journal of computational chemistry**, v. 30, n. 16, p. 2785–2791, 2009.

MORRIS, R. P. et al. Ancestral antibiotic resistance in Mycobacterium tuberculosis. **Proceedings of the National Academy of Sciences of the United States of America**, v. 102, n. 34, p. 12200–12205, 2005.

MULLER, M. P. et al. Characterization of Lipid-Protein Interactions and Lipid-mediated Modulation of Membrane Protein Function Through Molecular Simulation. **Chemical reviews**, v. 119, n. 9, p. 6086–6161, 8 maio 2019.

NIKAIDO, H. Multiple antibiotic resistance and efflux. **Current opinion in microbiology**, v. 1, n. 5, p. 516–523, 1998.

OPPERMAN, T. J.; ST, N. Recent advances toward a molecular mechanism of efflux pump inhibition. **Front. Microbiol.**, v. 6, n. 421, p. 1–16, 2015.

OSWALD, C.; TAM, H.-K.; POS, K. M. Transport of lipophilic carboxylates is mediated by transmembrane helix 2 in multidrug transporter AcrB. **Nature Communications**, v. 7, n. 1, p. 13819, 16 dez. 2016.

PALL, S. et al. **Tackling exascale software challenges in molecular dynamics simulations with GROMACS**. International Conference on Exascale Applications and Software. **Anais**...Springer, 2014

PASCA, M. R. et al. Rv2686c-Rv2687c-Rv2688c, an ABC Fluoroquinolone Efflux Pump in Mycobacterium tuberculosis. **Antimicrobial Agents and Chemotherapy**, v. 48, n. 8, p. 3175–3178, ago. 2004.

PASCA, M. R. et al. mmpL7 Gene of Mycobacterium tuberculosis Is Responsible for Isoniazid Efflux in Mycobacterium smegmatis. **Antimicrobial Agents and Chemotherapy**, v. 49, n. 11, p. 4775–4777, nov. 2005.

PASTOR, R. W.; MACKERELL, A. D. Development of the CHARMM Force Field for Lipids. **The Journal of Physical Chemistry Letters**, v. 2, n. 13, p. 1526–1532, 7 jul. 2011.

PAULSEN, I. T. et al. Comparative genomics of microbial drug efflux systems. **Journal of molecular microbiology and biotechnology**, v. 3, n. 2, p. 145–150, 2001.

PETHE, K. et al. Isolation of Mycobacterium tuberculosis mutants defective in the arrest of phagosome maturation. **Proceedings of the National Academy of Sciences of the United States of America**, v. 101, n. 37, p. 13642–13647, 2004.

PIANA, S.; LINDORFF-LARSEN, K.; SHAW, D. E. How robust are protein folding simulations with respect to force field parameterization? **Biophysical journal**, v. 100, n. 9, p. L47–L49, 2011.

PIDDOCK, L. J. Multidrug-resistance efflux pumps? not just for resistance. **Nature Reviews Microbiology**, v. 4, n. 8, p. 629–636, 2006a.

PIDDOCK, L. J. Clinically relevant chromosomally encoded multidrug resistance efflux pumps in bacteria. **Clinical microbiology reviews**, v. 19, n. 2, p. 382–402, 2006b.

PRONK, S. et al. GROMACS 4.5: a high-throughput and highly parallel open source molecular simulation toolkit. **Bioinformatics**, v. 29, n. 7, p. 845–854, 2013.

PUTMAN, M. et al. The secondary multidrug transporter LmrP contains multiple drug interaction sites. **Biochemistry**, v. 38, n. 42, p. 13900–13905, 19 out. 1999.

RADHAKRISHNAN, A. et al. Crystal Structure of the Transcriptional Regulator Rv0678 of Mycobacterium tuberculosis. **The Journal of Biological Chemistry**, v. 289, n. 23, p. 16526–16540, 6 jun. 2014.

RAMÓN-GARCÍA, S. et al. Characterization of tetracycline resistance mediated by the efflux pump Tap from Mycobacterium fortuitum. **The Journal of Antimicrobial Chemotherapy**, v. 57, n. 2, p. 252–259, fev. 2006.

RAMÓN-GARCÍA, S. et al. Role of the Mycobacterium tuberculosis P55 Efflux Pump in Intrinsic Drug Resistance, Oxidative Stress Responses, and Growth. **Antimicrobial Agents and Chemotherapy**, v. 53, n. 9, p. 3675–3682, set. 2009.

RAMÓN-GARCÍA, S. et al. Functional and Genetic Characterization of the Tap Efflux Pump in Mycobacterium bovis BCG. **Antimicrobial Agents and Chemotherapy**, v. 56, n. 4, p. 2074–2083, abr. 2012.

RICHARD, M. et al. Mechanistic and Structural Insights Into the Unique TetR-Dependent Regulation of a Drug Efflux Pump in Mycobacterium abscessus. **Frontiers in Microbiology**, v. 9, p. 649, 2018.

RODRIGUES, L. et al. Contribution of efflux activity to isoniazid resistance in the Mycobacterium tuberculosis complex. **Infection, Genetics and Evolution: Journal of Molecular Epidemiology and Evolutionary Genetics in Infectious Diseases**, v. 12, n. 4, p. 695–700, jun. 2012.

RODRIGUES, L. et al. Role of the Mmr Efflux Pump in Drug Resistance in Mycobacterium tuberculosis. **Antimicrobial Agents and Chemotherapy**, v. 57, n. 2, p. 751–757, fev. 2013.

RODRIGUES-JUNIOR, V. S. et al. Mefloquine and its oxazolidine derivative compound are active against drug-resistant Mycobacterium tuberculosis strains and in a murine model of tuberculosis infection. **International Journal of Antimicrobial Agents**, v. 48, n. 2, p. 203–207, 2016.

RODRIGUEZ-BUSSEY, I. G.; DOSHI, U.; HAMELBERG, D. Enhanced molecular dynamics sampling of drug target conformations. **Biopolymers**, v. 105, n. 1, p. 35–42, jan. 2016.

ROY, A.; KUCUKURAL, A.; ZHANG, Y. I-TASSER: a unified platform for automated protein structure and function prediction. **Nature protocols**, v. 5, n. 4, p. 725–738, 2010.

SANCHO-VAELLO, E. et al. Structural basis of phosphatidyl-myo-inositol mannosides biosynthesis in mycobacteria. **Biochimica et Biophysica Acta (BBA) - Molecular and Cell Biology of Lipids**, v. 1862, n. 11, p. 1355–1367, nov. 2017.

SANDHU, P.; AKHTER, Y. Siderophore transport by MmpL5-MmpS5 protein complex in Mycobacterium tuberculosis. **Journal of Inorganic Biochemistry**, v. 170, p. 75–84, maio 2017.

SAPAY, N.; TIELEMAN, D. P. Chapter 4 Molecular Dynamics Simulation of Lipid–Protein Interactions. In: FELLER, S. E. (Ed.). . **Current Topics in Membranes**. Computational Modeling of Membrane Bilayers. [s.l.] Academic Press, 2008. v. 60p. 111–130.

SARTAIN, M. J. et al. Lipidomic analyses of Mycobacterium tuberculosis based on accurate mass measurements and the novel “Mtb LipidDB”. **Journal of Lipid Research**, v. 52, n. 5, p. 861–872, maio 2011.

SCAINI, J. L. R. et al. Molecular modelling and competitive inhibition of a Mycobacterium tuberculosis multidrug-resistance efflux pump. **Journal of Molecular Graphics & Modelling**, v. 87, p. 98–108, mar. 2019.

SCHLENKRICH, M. et al. An Empirical Potential Energy Function for Phospholipids: Criteria for Parameter Optimization and Applications. In: MERZ, K. M.; ROUX, B. (Eds.). . **Biological Membranes: A Molecular Perspective from Computation and Experiment**. Boston, MA: Birkhäuser, 1996. p. 31–81.

SEUS, V. R. et al. **A framework for virtual screening**. Proceedings of the 31st Annual ACM Symposium on Applied Computing. **Anais**...ACM, 2016

SIDDIQI, N. et al. Mycobacterium tuberculosis isolate with a distinct genomic identity overexpresses a tap-like efflux pump. **Infection**, v. 32, n. 2, p. 109–111, abr. 2004.

SINGH, K. et al. Synthesis of new verapamil analogues and their evaluation in combination with rifampicin against Mycobacterium tuberculosis and molecular docking studies in the binding site of efflux protein Rv1258c. **Bioorganic & Medicinal Chemistry Letters**, v. 24, n. 14, p. 2985–2990, 15 jul. 2014.

SPIES, F. S. et al. Identification of Mutations Related to Streptomycin Resistance in Clinical Isolates of Mycobacterium tuberculosis and Possible Involvement of Efflux Mechanism. **Antimicrobial Agents and Chemotherapy**, v. 52, n. 8, p. 2947–2949, ago. 2008.

SUN, J.; DENG, Z.; YAN, A. Bacterial multidrug efflux pumps: Mechanisms, physiology and pharmacological exploitations. **Biochemical and Biophysical Research Communications**, v. 453, n. 2, p. 254–267, 2014.

SURIYANARAYANAN, B.; SAROJINI SANTHOSH, R. Docking analysis insights quercetin can be a non-antibiotic adjuvant by inhibiting Mmr drug efflux pump in Mycobacterium sp. and its homologue EmrE in Escherichia coli. **Journal of Biomolecular Structure & Dynamics**, v. 33, n. 8, p. 1819–1834, 2015.

TROTT, O.; OLSON, A. J. AutoDock Vina: improving the speed and accuracy of docking with a new scoring function, efficient optimization, and multithreading. **Journal of computational chemistry**, v. 31, n. 2, p. 455–461, 2010.

VADIJA, R. et al. Identification of small molecular inhibitors for efflux protein Rv2688c of Mycobacterium tuberculosis. **Biotechnology and Applied Biochemistry**, v. 65, n. 4, p. 608–621, jul. 2018.

VALDÉS-TRESANCO, M. S. et al. AMDock: a versatile graphical tool for assisting molecular docking with Autodock Vina and Autodock4. **Biology Direct**, v. 15, 16 set. 2020.

VENABLE, R. M.; BROWN, F. L. H.; PASTOR, R. W. Mechanical properties of lipid bilayers from molecular dynamics simulation. **Chemistry and Physics of Lipids**, v. 192, p. 60–74, nov. 2015.

VENABLE, R. M.; KRÄMER, A.; PASTOR, R. W. Molecular Dynamics Simulations of Membrane Permeability. **Chemical Reviews**, v. 119, n. 9, p. 5954–5997, 8 maio 2019.

VIVEIROS, M. et al. Inhibitors of mycobacterial efflux pumps as potential boosters for anti-tubercular drugs. **Expert Review of Anti-Infective Therapy**, v. 10, n. 9, p. 983–998, set. 2012.

WALMSLEY, M. I. B.; MCKEEGAN, K. S.; WALMSLEY, A. R. Structure and function of efflux pumps that confer resistance to drugs. **Biochem. J.**, v. 376, p. 313–338, 2003.

WANG, Z. et al. An allosteric transport mechanism for the AcrAB-TolC multidrug efflux pump. **eLife**, v. 6, p. e24905, 29 mar. 2017.

WORLD HEALTH ORGANIZATION. **Global tuberculosis report 2020**. Geneva: [s.n.].

WU, C.-P.; HSIEH, C.-H.; WU, Y.-S. The emergence of drug transporter-mediated multidrug resistance to cancer chemotherapy. **Molecular pharmaceutics**, v. 8, n. 6, p. 1996–2011, 2011.

XU, Z.; ZHOU, A.; YAO, Y. ATP-binding cassette transporters and transmembrane transport in Mycobacterium tuberculosis–a review. **Wei sheng wu xue bao= Acta microbiologica Sinica**, v. 54, n. 6, p. 608–615, 2014.

YE, C. et al. Correlation between AcrB trimer association affinity and efflux activity. **Biochemistry**, v. 53, n. 23, p. 3738–3746, 2014.

ZHANG, Y. I-tasser server for protein 3D structure prediction. **BMC Bioinform.**, v. 9, p. 1–8, 2008.

6 Artigo I

Molecular modelling and competitive inhibition of a *Mycobacterium tuberculosis* multidrug-resistance efflux pump

João L. R. Scaini, Alex D. Camargo, Vinicius R. Seus, Andrea von Groll, Adriano V. Werhli, Pedro E. A. da Silva, Karina S. Machado

Figura 4: Resumo gráfico do artigo I

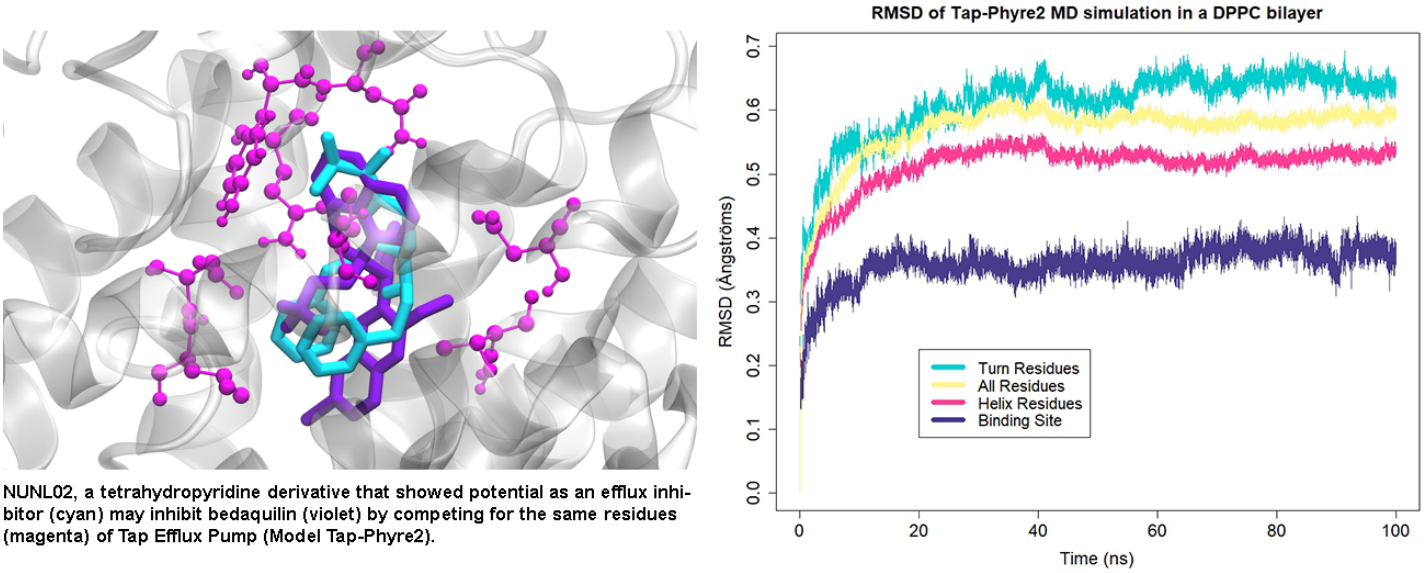

NUNL02, a tetrahydropyridine derivative that showed potential as an efflux inhibitor (cyan) may inhibit bedaquilin (violet) by competing for the same residues (magenta) of Tap Efflux Pump (Model Tap-Phyre2).

Imagem resume de forma gráfica os resultados do artigo. O artigo objetivou o desenvolvimento de um modelo tridimensional da Tap, que tem sua estabilidade representada no gráfico da direita por seu RMSD em uma DM dentro de uma membrana lipídica de dipalmitoilfosfatidilcolina (DPPC). O artigo também objetivou analisar a competição de sítios com os antimicrobianos como um possível mecanismo de ação de IEs. A imagem da esquerda mostra o resultado de um docking molecular mostrando em magenta os aminoácidos de ligação em comum entre o antimicrobiano e o IE.

Journal of Molecular Graphics and Modelling 87 (2019) 98e108

Contents lists available at ScienceDirect

Journal of Molecular Graphics and Modelling

journal homepage: www.elsevier.com/locate/JMGM

Molecular modelling and competitive inhibition of a Mycobacterium tuberculosis multidrug-resistance efflux pump

João Luís Rheingantz Scaini [a, b, *], Alex Dias Camargo [a], Vinicius Rosa Seus [a], Andrea von Groll [b], Adriano Velasque Werhli [a], Pedro Eduardo Almeida da Silva [b], Karina dos Santos Machado [a]

[a] Laboratory of Computational Biology, Computational Sciences Center of the Universidade Federal do Rio Grande, Avenida Itlia, Km8, Rio Grande, RS, Brazil

[b] Research Center in Medical Microbiology of the Universidade Federal do Rio Grande, Avenida Itlia, Km8, Rio Grande, RS, Brazil

article info

Article history:
Received 6 June 2018
Received in revised form
29 November 2018
Accepted 29 November 2018
Available online 3 December 2018

Keywords:
Tuberculosis
Tap effux pump
Efflux inhibitors
Molecular dynamics
Molecular docking

abstract

Tuberculosis is a major cause of mortality and morbidity in developing countries, and the emergency of multidrug and extensive drug resistance cases is an utmost issue on the control of the disease. Despite the efforts on the development of new antibiotics, eventually there will be strains resistant to them as well. Efflux plays an important role in the evolution of resistance in Mycobacterium tuberculosis. Tap is an important efflux pump associated with tuberculosis resistant to isoniazid, rifampicine and ofloxacin and with multidrug resistance. The development of efflux inhibitors for Tap could raise the effectiveness of second line drugs and reduce the duration of the current treatment. Therefore the objective of this study is to build a reliable molecular model of Tap efflux pump and test the possible competitive inhibition between efflux inhibitors and antibiotics in the optimized structure. We built twenty five Tap models with molecular modelling to elect the best according to the results of the validation analysis. The elected model went through to a 100 ns molecular dynamics simulation in a lipid bilayer, and the resulting optimized structure was used in docking studies to test if the used efflux inhibitors may act via competitive inhibition on antibiotics. The validation results pointed the model built by Phyre2 as the closest to a possible native Tap structure, and therefore it was the elected model. RSMD analysis revealed the model is stable, where the predicted binding site stabilized between 15 and 20 ns, maintaining the RMSD at around 0.35 Å throughout the molecular dynamics simulation in a lipid bilayer. Therefore this model is reliable and can also be used for further studies. The docking studies showed a possibility of competitive inhibition by NUNL02 on ofloxacin and bedaquiline, and by verapamil on ofloxacin and rifampicin. This presents the possibility that NUNL02 and verapamil are possible inhibitors of Tap efflux and highlights the importance of including efflux inhibitors as adjuvants to the tuberculosis therapy, as it indicates a possible extrusion of ofloxacin, rifampicin and bedaquilin by Tap.

© 2018 Elsevier Inc. All rights reserved.

1 Introduction

Tuberculosis (TB) is an important global health issue and a major cause of mortality and morbidity mainly in developing countries. The emergency of drug resistance in *Mycobacterium tuberculosis* is an utmost issue in TB control. In 2016, the World Health Organization estimated 6.3 million new TB cases and 490,000 new multidrug-resistance (MDR) cases, which are caused by strains resistant to at least isoniazid (INH) and rifampicin (RIF) [1]. Furthermore, the TB therapeutic options are limited as there is a growing incidence of MDR, and extensively drug-resistant (XDR) strains [2].

Efflux pumps in *M. tuberculosis* are associated to MDR-TB [3, 4], and even to bedaquilin (BDQ) resistance [5, 6], which is the first anti-TB drug in decades to be approved and used on the treatment of MDR-TB patients [1, 7]. Moreover, efflux plays an important role in the evolution to high levels of resistance in *M. tuberculosis* [3, 8, 9] as the exposure to subinhibitory antibiotic concentrations enhances the probability of drug resistant strains selection [10].

Tap (Rv1258c) [11, 12] is an efflux pump of *M. tuberculosis* associated to MDR-TB [13, 14]. The gene tap is part of the regulon WhiB7 that causes drug resistance phenotype and is induced by subinhibitory concentrations of erythromycin, tetracycline, and streptomycin [15, 16]. Previous studies show increase in the tap gene expression in exposure to RIF and ofloxacin (OFLO), used on the treatment of MDR-TB patients, and relates to the high level of resistance to this drugs [13]. It was also shown an increase in tap expression in a MDR clinic strain in the presence of INH and RIF [14].

A way to overcome and avoid the resistance related to efflux mechanism is to add efflux inhibitors (EI) as adjuvant to antimicrobial therapy [17, 18, 19]. The development of specific EI for Tap would allow the introduction of clinically available antibiotics that are up to now not effective against TB such as streptomycin or tetracycline in the TB treatment. It could also raise the effectiveness of second-line TB treatment drugs, such

as p-aminosalicylic acid and streptomycin. Furthermore, it would also reduce the duration of the current standard treatment, avoiding the development of antibiotic tolerance related with Tap efflux [20]. The mechanism of action of EIs may be elucidated by biochemical, computational and structural approaches [21]. Therefore, structure-based drug design can be a fast and accurate approach to discover clinically effective EI [22, 23, 24].

It is difficult to achieve enough quantity and purity for the structure determination of efflux pumps by X-Ray Crystallography and Nuclear Magnetic Resonance Spectroscopy due to the amphiphilic nature of those proteins [25]. Molecular Modeling allows the determination of a protein structure by computer algorithms that counts with experimental results and are faster and less expensive than the biophysical methods [26, 27, 28, 29, 30]. There is not any Tap three-dimensional structure published so far in the Protein Data Bank (https://www.rcsb.org/) [31], which would allow structure-based drug design studies.

A possible Tap Efflux Pump structure is expected to form a pore with 12 transmembrane helices, like Glycerol-3-Phosphate Transporter (PDB ID: 1PW4) or Lactose Permease (PDB ID: 1PV6), which are both sugar transporters of the family MFS, since Tap is also transporter from this family and has a sugar transporter signature [11]. The objective of this study is to build a reliable molecular model of Tap efflux pump and test the possibility of inhibitory competition between EIs and antibiotics in the optimized structure.

2 Methodology

The whole Methodology is represented in Figure 1. We built various Tap Efflux Pump models with molecular modelling to elect the best according to the validation results. The elected model was submitted to a molecular dynamics simulation in a lipid bilayer, and the resulting optimized structure was used in Docking studies to test if efflux inhibitors may act via competitive inhibition on antibiotics.

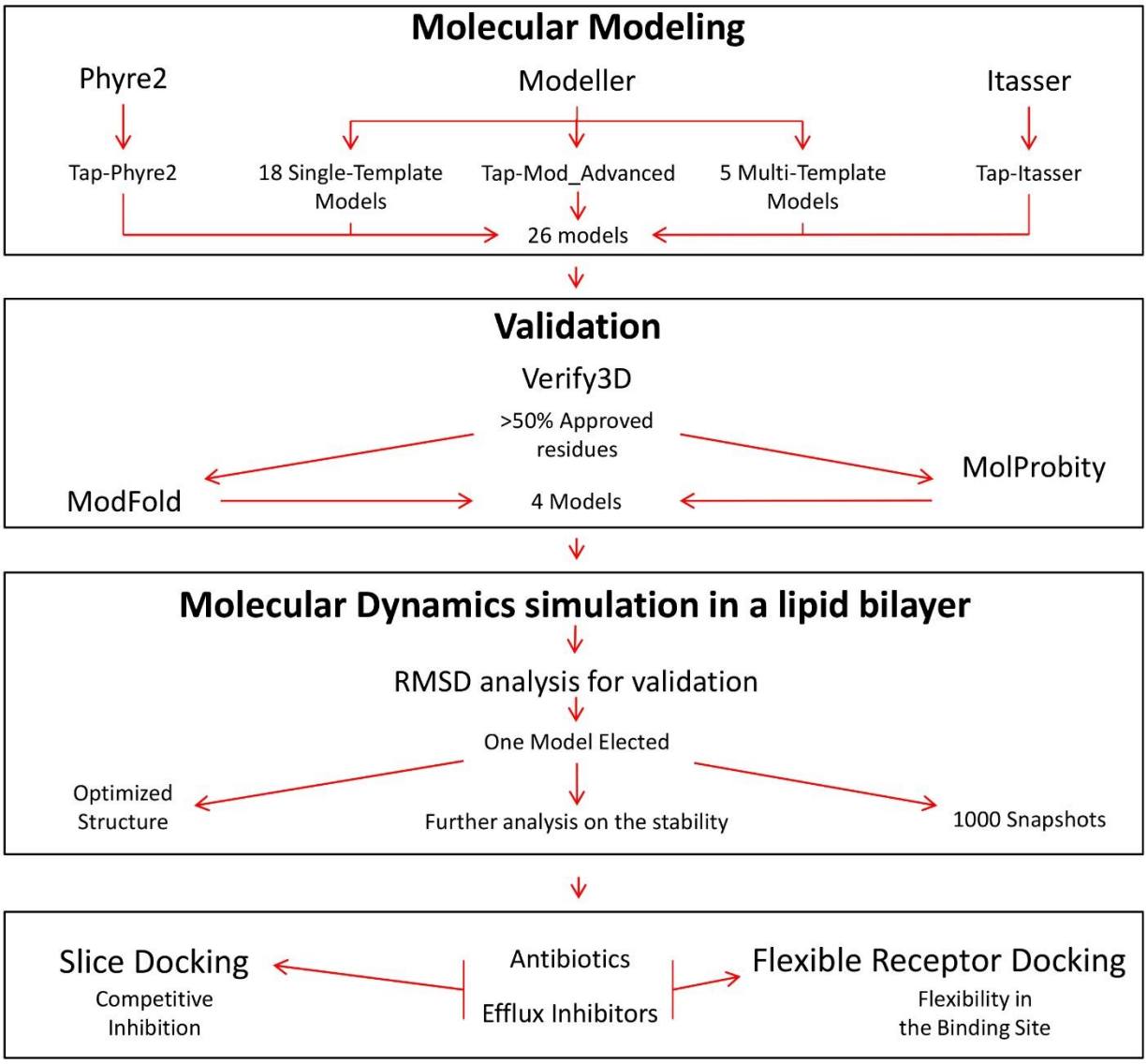

Figure 1: Fluxogram of the Methodology followed in this work.

2.1 Molecular Modelling

This study used three comparative modelling tools to build Tap efflux pump three-

dimensional models. Every model was built from the amino acid FASTA sequence of Tap (UNIPROT: P9WJX9-1) [32]. We created the figures of the protein strucutres with VMD [33].

2.1.1 Tap-Phyre2

This study used Phyre2 [30] to build Tap-Phyre2 model. Phyre2 uses its own structure database to find homologous proteins to use as templates. It builds models for each selected template and use those models to provide pairwise distance constraints to the tool Poing [34]. Poing builds a model based on this information and uses an *ab initio* procedure to complete the regions without coverage of homologous proteins. This model and all the selected templates are input to Modeller [35], that generates the final model [36].

2.1.2 Tap-Itasser

This study built Tap-Itasser using the software Itasser [37]. Itasser uses homologous proteins from its own database as templates to align with the target amino acid sequence. It then builds five models and determines the C-score and TM-score values for each of them. C-score values indicates the model quality varying from -5 to 2, where the higher C-score is, the closer to a possible native structure is the generated model. TM-score shows the model accuracy, where values between 0.5 and 1.0 indicate a correct topology related to the native protein. These scores are used to choose the best ranked model [38]. The structures used as templates by Itasser were GlpT Glycerol-3-Phosphtae transporter (PDB ID: 1PW4) and PePTSo Oligopeptide-proton symporter (PDB ID: 4D2B).

2.1.3 Modeller Models

This study used Modeller V9.14 [28] to build some models using different templates. The templates used were proteins with the highest amino acid identity (AAI) with Tap determined with BLAST [39]. We built single-template models from alignments between the Tap sequence and each template. An alignment between all the templates was aligned with Tap sequence to build the multi-template models. Finally, a Modeller script built five models and calculated a Discrete Optimized Protein Energy (DOPE) for each one. For each alignment, we chose the model with the lowest DOPE score, as it is the closest to a possible native protein structure [40].

One single-template model was built for each template determined by BLAST. Several multi-template models were created using different combinations of templates between the structures determined by BLAST. At last, a multi-template model was created following the Advanced tutorial in the official Modeller website [41].

2.2 Validation

We determined the quality of the models using validation tools to measure which model bears more physical and chemical resemblance to a native Tap structure.

This study used the online software Verify3D to determine the local errors on all models [42, 43]. This method validates the compatibility of the 3D structure with the primary structure using the 3D-1D matrix, which calculates the probability of each amino acid on its chemical environments. A 3D-1D score represents this probability, and approves a residue that scores 0.2 or higher [44]. Only the models that had more than 50% of its residues with a 3D-1D score higher than 0.2 on Verify3D were validated with ModFold [45, 46] and MolProbity [47, 48].

ModFold predicts both global and local 3D structure quality based on the distance of each residue in the model from its position on a possible native structure. ModFold server returns a global score and a p-value of the local scores showing the probability of

the model to be wrong. A global score higher than 0.4 means the structure is highly similar to a possible native structure. The software indicates the confidence of the structure according to the p-value [45, 46].

MolProbity is a software that generates a Ramachandran plot, an evaluation tool to assess the stereochemical quality of a given model through the analysis of *phi* and *psi* angles for all protein residues. The Ramachandran plot classifies residues varying from most favored to outliers [47, 48].

We elected the four models with the best results in these three tools to go through Molecular Dynamics (MD) simulations in order to analyze their stability.

2.3 Molecular Dynamics Simulation in a lipid bilayer

To determine the stability of the four best models, this study performed 100 ns MD simulations with each of the four best models inserted in a lipid bilayer. For such, we used GROMACS 2016.4 [49, 50, 51, 52] package on a Linux platform. The force field used was GROMOS96 53a6 force field [53] modified with Berger lipids for protein-lipid simulations [54]. These simulations followed a published protocol [55] with a few changes, as described.

This study obtained the coordinates and topology of a stable and flexible dipalmitoylphosphatidylcholine (DPPC) that was previously published [56]. The protein was inserted in the DPPC bilayer following the InflateGRO technique [57, 58] modified in accordance with the followed protocol [55]. It consists in inflating the lipid bilayer and deflating the area, with an EM after each deflation, slowly accommodating the membrane around the protein.

The incorporation of two 1 nm thick boxes of water model SPC on the top and bottom of the membrane with the protein solvated the system. Finally, the addition of five sodium ions in the water neutralized the charge of the system. GROMACS 2016.4

package [49, 50, 51, 52] executed the EM and equilibration with restraints for all heavy atoms of proteins, in order to shape the membrane around the protein. The equilibration also had restraints on the lipid phosphorus on the -axis, so that the lipids would not vertically leave their positions before the system is equilibrated. The equilibration consisted of a 100 ns temperature adjusting phase and a 1 ns pressure adjusting phase, maintaining the same temperature. At last, the production phase ran for 100 ns with no restraints and the temperature and pressure kept the same of the previous phase.

GROMACS 2016.4 package [49, 50, 51, 52] generated the files for the simulation plots, which were obtained using R 3.1.3 and R studio 0.99.491 [59, 60]. Two analysis were made by calculating the Root-mean-square deviation (RMSD) for each 2 ps along the entire MD simulations. The first one was the validation of four models according to their all atoms RMSD, to finally elect the best model considering this analysis and the other validation tools. The second was to further study the stability of the best model, analyzing the RMSD of the entire structure, of each secondary structure and of the binding site, predicted with COACH [61, 62].

2.4 Docking

Two different protein-ligand Docking methodologies were performed with Tap-Phyre2 and the antibiotics INH, RIF, OFLO, BDQ and the EIs chlorpromazine (CPZ), verapamil (VERA) and NUNL02. NUNL02 is a tetrahydropyridine derivative that showed potential as an efflux inhibitor [63]. This study used AutoDockTools 1.5.6 [64] and AutoDock Vina 1.1.2 [65, 66] to define the boxes and to perform the Docking simulations, respectively.

2.4.1 Slice Docking

In order to test the hypothesis of competitive inhibition we performed Slice

Docking, a previously published Docking strategy [63] consisting on the placement of many grid boxes along the receptor for the execution of a Docking simulation in each of them. This approach is because it has been suggested that efflux pumps can have more than one drug binding site [67, 68]. The receptor was the optimized structure of Tap-Phyre2 result of the 100 ns MD simulation in a DPPC bilayer. The ligands were considered flexible for higher accuracy. A framework for visual screening [69] prepared multiple boxes for the receptor.

Each box was constructed so that the size of the (44 Å) and (62 Å) covered the protein in these axis, that were the base of the box. The -axis corresponds to the height of the box; with a dimension of 18 Å for this parameter, after the ligands were measured with AutoDockTools, to make sure they fit well in the Docking box. The sizes considered for , and define the volume of the box and allow the ligands to assume all possible orientations inside them. The box size was constant throughout the Docking studies. Because the volume of the box was large (49104 cubic Å), the exhaustiveness was set to 128.

The first box was at the lowest position of the protein, with the coordinate centered at 10, therefore called box 10. AutoDock Vina determined the best binding position for this box. Next, the box changes only at the coordinate, adding 6 Å, defining box 16. AutoDock Vina calculates the Free Energy of Biding (FEB) and determines the best binding position of the ligand for the new box. This procedure is repeated until box 52 (Supplementary Material). Since adjacent boxes have a superposition of 12 Å, the procedure allows the possibility of near boxes having the same best binding positions. Eight boxes were used to determine the best affinity sites between Tap and each ligand.

For each box, this study considered the best binding position for a ligand the one with the strongest FEB. We calcutated the average coordinates for each ligand in each box. Plotting the average coordinates against the FEB for each box, joining adjacent

points, allowed the construction of the Energy Distribution Curves (EDCs). LigPlot+ [70] identified the residues that shared interactions with the ligands. Supplementary material shows the aligned residues of all the ligands in the two boxes that got the strongest FEBs between antibiotics and EIs. We created the figures of the protein strucutre and the ligands with VMD [33].

2.4.2 Flexible Receptor Docking

Most of docking algorithms consider the ligand flexibility. However, the inclusion of receptor flexibility remains a challenge. Proteins are flexible on their cellular environment and frequently this flexibility is important to their functions and ligands interactions [71, 72, 73]. In order to evaluate the impact of Tap flexibility on docking simulations, as well as to verify the most important residues of the proposed model binding site, we performed docking simulations incorporating the flexibility of Tap receptor.

Diverse approaches have been developed to take into account the receptor flexibility on docking simulations as reviewed by previous works [71, 72, 74, 75]. Soft docking was one of the first proposed approaches and was developed to incorporate conformational changes allowing small overlaps between receptor and ligand atoms [76]. Diverse approaches incorporate the receptor flexibility considering some side chains on the binding site as flexible [64, 77].

Soft docking and flexibility of side chains consider only local movements in some residues on the binding site, but cannot capture the global effects of the receptor flexibility. To overcome these limitations, it was proposed the *Ensemble docking* where different structures of the receptor can be combined on one structure or a set of molecular docking simulations is performed considering in each simulation one different conformation of a receptor [78, 71, 79].

In this paper, we are performing the *Ensemble docking* considering a set of protein

conformations obtained from the performed molecular dynamics simulation with the Tap-Phyre2 model. From the Tap-Phyre2 MD simulation of 100 ns we selected a snapshot every 100ps totalizing 1,000 snapshots. Thus, we performed 1,000 docking simulations with each ligand. On these dockings we consider the ligand as rigid and the exhaustiveness was set to 64 to reduce computational cost. The docking box was defined to involve the amino acids of the predicted binding site and was configured with size 24, 34 and 28 Å in , and -axis, respectively, and centered at 43, 34 and 25 Å in , and -axis respectively. To configure all the docking simulations we used the framework for virtual screening [69] and for analyses the receptor conformations-ligands interactions we applied LigPlot+ [70].

3 Results and Discussion

3.1 Molecular Modelling

This study built one model with Phyre 2 (Tap-Phyre2) [30], one model with I-Tasser (Tap-Itasser) [37], and the other models with Modeller [28]. There were eighteen possible templates based on their BLAST AAI with Tap (Table 1). Thus, we built eighteen single-template models, one for each found template, and five multi-template models based on combinations between those templates.

PDB	AAI with Tap	Super-family / family	Species
4APS	56.00%	MFS / POT	*Streptococcus thermophilus* LMG 18311
4D2B	56.00%	MFS / POT	*S. thermophilus* LMG 18311
4M64	56.00%	MFS	*Salmonella enterica* LT2
2XUT	38.00%	MFS / POT	*Shewanella oneidensis* MR-1
4IU8	37.00%	MFS / NNP	*Eschirichia coli* K-12
2GFP	36.00%	MFS	*E. coli*

4LEP	35.00%	MFS / POT	*Shewanella oneidensis* MR-1
2Y5Y	33.00%	MFS	*E. coli* K-12
4OH3	33.00%	MFS	*Arabidopsis thaliana*
3WDO	33.00%	MFS	*E. coli*
4Q65	32.00%	MFS / POT	*E. coli K-12*
3MKT	31.00%	MATE	*Vibrio cholerae* str. N16961
3O7P	29.00%	MFS	*E. coli* K-12
3O7Q	29.00%	MFS	*E. coli* K-12
4J05	29.00%	MFS	*Piriformospora indica*
1PV6	28.00%	MFS	*E. coli*
2CFQ	28.00%	MFS	*E. coli*
1PW4	24.00%	MFS	*E. coli*

Table 1: Templates used to build Tap models using Modeller. The PDB column shows the templates PDB ID. The AAI with Tap column shows the BLAST amino acid identity (AAI) for the alignment between the amino acid sequences of both the template and Tap. The Super-Family / Family column shows in which protein family is that protein. The Species column shows which bacteria, fungus, or plant species which this protein was isolated from for the crystallization.

	ModFold			MolProbity		Verify3D
Model	Global	P-Value	Confidence	Favored (%)	Outlier (%)	Approved (%)
Tap-Phyre2	**0.4867**	**5.727E-3**	**HIGH**	**91.37**	**3.36**	**67.54**
Tap-Itasser	**0.4831**	**5.943E-3**	**HIGH**	**91.61**	**3.60**	**75.42**
Tap-Mod_1PW4	**0.4065**	**1.318E-2**	**MEDIUM**	**91.85**	**2.16**	**52.03**

Tap-Mod_Advanced	**0.3881**	**1.596E-2**	**MEDIUM**	**94.00**	**1.68**	**60.86**
Tap-Mod_2CFQ	0.3674	1.98E-2	MEDIUM	89.45	2.88	55.13
Tap-Mod_2Y5Y	0.3347	2.78E-2	MEDIUM	89.69	2.16	51.79
Tap-Mod_4J05	0.2890	4.469E-2	MEDIUM	89.69	2.88	59.43
Tap-Mod_4OH3	0.2734	5.257E-2	MEDIUM	88.25	3.12	60.62
Tap-Mod_7	0.2699	5.455E-2	LOW	90.41	3.86	69.21
Tap-Mod_3WDO	0.2636	5.824E-2	LOW	92.81	1.92	61.58
Tap-Mod_3	0.1821	1.359E-1	POOR	92.57	1.92	59.43
Tap-Mod_5	0.1209	2.566E-1	POOR	91.13	2.88	54.42
Tap-Mod_4Q65	0.0408	5.899E-1	LOW	92.09	3.36	61.34
Tap-Mod_4D2B	0	9.017E-1	POOR	92.09	3.60	55.37

Table 2: Validation results for the Tap models. These are only the models which more than 50% of its residues scored higher than 0.2 on Verify3D. The first column shows the identification of the models. The second column shows ModFold global scores, third the p-value the fourth local score confidence according to the p-value. The fifth column shows the percentage of Ramachandran favored residues and the sixth is the percentage of Ramachandran outliers of each model according to MolProbity. The seventh column shows the percentage of residues that scored higher than 0.2 on each model according to Verify 3D. The four lines in bold represent the models elected as the best and were submitted to the MD in a lipid bilayer.

The AAI with Tap (Table 1) determined the templates used to build the multi-template models. Tap-Mod_18 included all proteins on the list as templates. The twelve proteins with AAI higher than 30% were templates to Tap-Mod_12. Tap-Mod_7 had all the seven proteins with AAI higher than 35% as templates. Tap-Mod_5 included the five best

proteins ranked by AAI. The three templates with AAI higher than 50% based Tap-Mod_3. In addition, one model was built following the Advanced tutorial in the Modeller website [41]. For this one, we tried to cluster each template determined by BLAST in a family using DBAli v2.0 [80]. Only lactose permease (PDB ID: 1PV6) and sugar free lactose permease (2CFQ) formed any cluster. Both structures formed the same cluster, with four structures of lactose permease (PDB ID: 1PV6, 1PV7, 2CFQ and 2CFP). The residues from 401 to 410 formed a loop that was poorly modelled, according to DOPE score, so we refined this region using a Modeller script. This range of possibilities from various templates was generated to look for the best possible model.

A published work also built a structural model of Tap Efflux Pump [81]. They used Protein Preparation Wizard [82], which has the advantage of having different tools to edit the protein and is specific for virtual screening.

3.2 Validation

We used Verify3D (Table 2) to validate all Tap models built and analyzed them by the quantity of approved residues (residues that scored 0.2 or higher). Tap-Itasser obtained the highest number of approved residues (75.42%), followed by Tap-Mod_7 (69.21%) and Tap-Phyre2 (67.54%). All models with more than 50% approved residues were also validated with MolProbity and ModFold (Table 2).

ModFold considers a model with a global score higher than 0.4 close to a possible native structure. High ModFold confidence indicate there is 1% chance that the model is wrong. Tap-Phyre2 got the best ModFold score (high confidence, global score of 0.4867), followed by Tap-Itasser (high confidence, global score of 4.831) and Tap-Mod_1PW4 (medium confidence, global score of 4.065) (Table 2). According to MolProbity, the model with the most Ramachandran favored residues and less Ramachandran outliers was Tap-Mod_Advanced (Table 2).

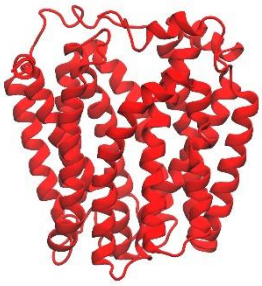

(a) Tap-Phyre2

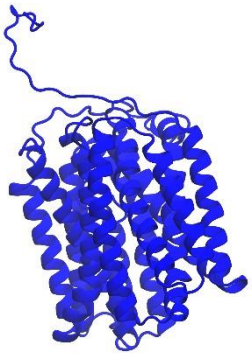

(b) Tap-Itasser

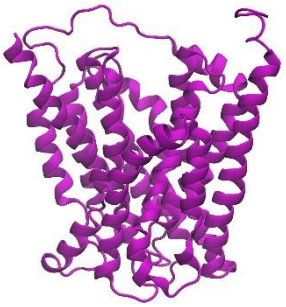

(c) Tap-Mod_1PW4

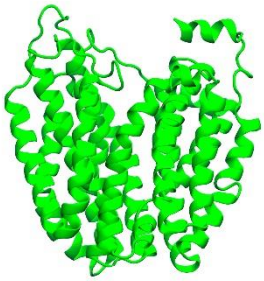

(d) Tap-Mod_Mod-Advanced

Figure 2: The four generated Tap efflux pump models elected as best according to the Verify3D, ModFold and MolProbity results.

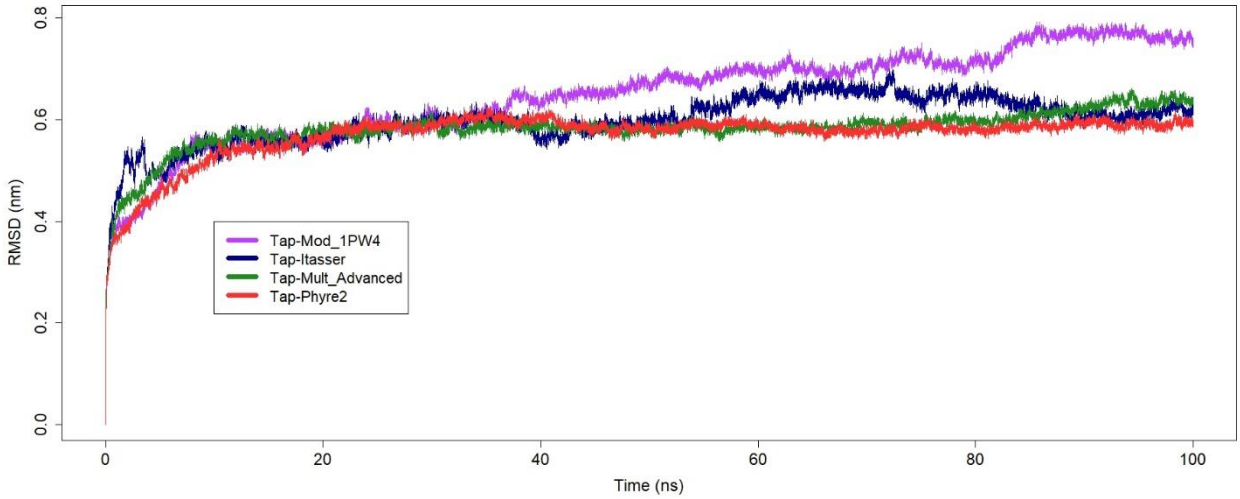

Figure 3: RMSD of the four best models in a 100 ns MD simulation in a DPPC bilayer. -axis represents the RMSD in nm and the -axis represents the time in ns.

Thus, we elected four models (Figure 3.2) to test their stability with MD simulations using GROMACS. Tap-Phyre2 (Figure 3.2) and Tap-Itasser (Figure 3.2) were the two best models according to the previous validation results. Tap-Mod_1PW4 (Figure 3.2) got the best ModFold score within all the Modeller models and one of the only three with a global score higher than 0.4, despite its low Verify3D score (52.03%) (Table 2). And finally, Tap-Mod_Advanced (Figure 3.2) had the highest MolProbity scores, fourth highest Verify3D score, with 60.86% of residues approved, and the fourth highest ModFold score (medium confidence, global score of 0.3881). All four models obtained more than 90% residues on most-favored regions in MolProbity Ramachandran plot (Supplementary Material).

The four elected models have the uniform topology of 12 transmembrane alpha helices, which is a characteristic of the MFS proteins [83]. The most important difference between the four elected models are how the helices are disposed, in Tap-

Phyre2 and Tap-Mod_Advanced they have a similar disposition, Tap-Itasser has more parallel helices, and Tap-Mod_1PW4 more open ones. That is relevant because the flexibility of the loops is what will affect this disposition, and therefore determine the stability of the model.

3.3 Molecular Dynamics Simulation in a lipid bilayer

In order to choose the best model, and then further analyze its structure, we performed a 100 ns MD simulation with the four elected models (Figure 3.2). The MD simulation in a lipid bilayer allowed an insight on the stability and quality of the models [84], which fits the purpose to elect the best model, as Tap is a transport protein that is found embedded in a lipid membrane. Therefore, the RMSD of all atoms during the 100 ns MD was analyzed on the four best models, and one model was elected as the best considering the results from this analysis and from the validation tools.

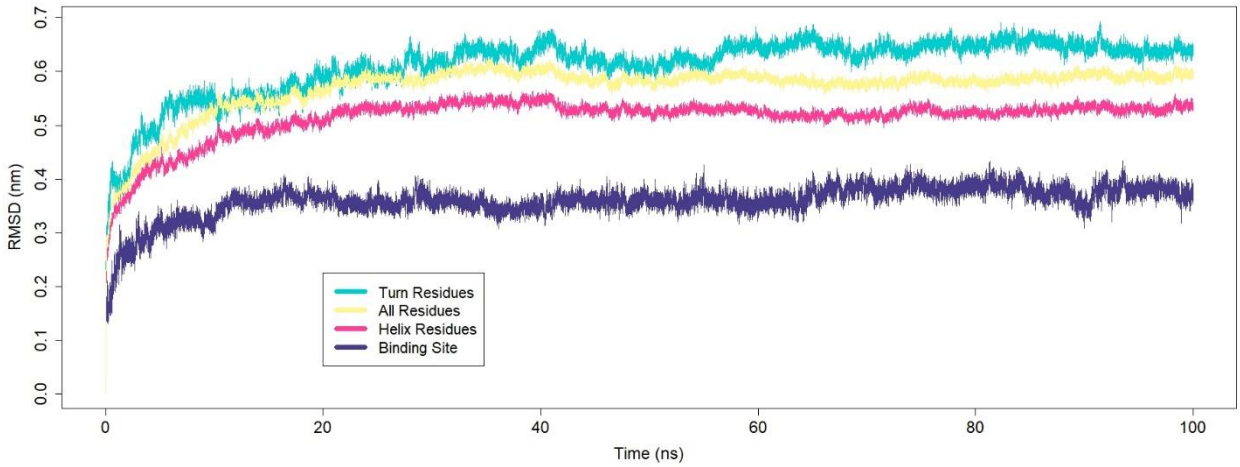

Figure 4: RMSD of Tap-Phyre2 100 ns MD simulation in a DPPC bilayer. -axis represents the RMSD in nm and the -axis represents the time in ns.

Tap-Mod_1PW4 (purple) had its RMSD raising since the beginning of the simulation, reaching almost 0.8 nm from 80 ns to the end of the simulation (Figure 3.2). It had the worst stability from all models. Tap-Itasser (blue) had its RMSD fluctuating

around 0.5 and 0.6 nm between 10 and 50 ns. From 50 to 85 ns the RMSD raised to almost 0.7 nm, lowering to 0.6 nm from 90 ns to the end of the simulation (Figure 3.2). It had too much variation in its conformation, therefore showing low stability.

Tap-Mod_Advanced (green) stabilized with less than 0.6 nm between 10 and 20 ns, but it got higher after 90 ns (Figure 3.2). This model showed high stability and also got the best Molprobity scores, thus it is the best Modeller model. Tap-Phyre2 (red) had its RMSD stabilized at around 20 and 40 ns, maintaining an RMSD of less than 0.6 nm (Figure 3.2) until the end of the simulation. It had the fewest fluctuations along the 100 ns of the MD simulation, therefore showing the highest stability.

We chose Tap-Phyre2 (Figure 3.2) as the best model because it had the best score with ModFold, good scores with MolProbity and Verify3D and showed to have most stable structure, with the smallest RMSD and with the least fluctuations and from the starting position.

The MD simulations also provides information on protein stability in a solvent, allowing a better insight in the folding and unfolding processes [85, 86]. Therefore, this tool can be used for structural model evaluation [87, 88, 89]. For this purpose, we analyzed the RMSD of Tap-Phyre2 in four different ways: considering all of its residues, the helix, the turn and the predicted binding site residues.

The overall structure, represented by the RMSD considering all residues, stabilized between 20 and 40 ns, maintaining an RMSD from the starting position of less than 0.6 nm. The delay on the stabilization seems to be mainly because of the Turns, which had a variation of around 1 nm at this same time. The Turns might also have raised the RMSD of all residues, since the Turn residues RMSD floated between 0.6 nm and 0.7 nm from the starting position throughout the end of the simulation (Figure 3.3).

The helix residues stabilized early, between 20 and 25 ns, and kept an RMSD of around 0.5 nm from the starting position. Therefore, the helixes were a more rigid secondary structure. The binding site was predicted to test its stability during the

Dynamics, since it is a more rigid structure that may better reflect the quality of the model. The RMSD stabilized between 15 and 20 ns, and it maintained an RMSD of around 0.35 nm from the starting position (Figure 3.3). The results show an stable behaviour that reflect a model of good quality. Also, the overall protein stabilized in a way that optimized the structure, which is therefore ready for the Docking simulations.

3.4 Docking

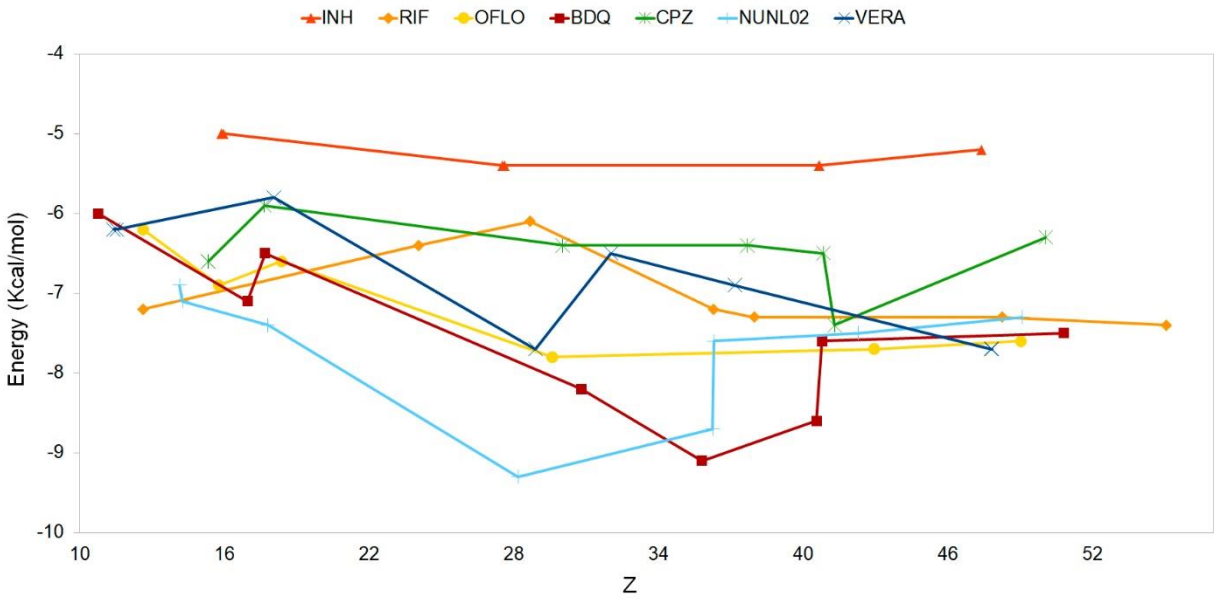

Figure 5: Energy Distribution Curves of the Slice Docking of Tap-Phyre2 with the antibiotics RIF, INH, OFLO and BDQ, and the EIs CPZ, NUNL2 and VERA. -axis represents the FEB in kcal/mol and -axis represent the center of each grid box in the -axis. The points represent the FEB for each box against the average coordinates.

3.4.1 Slice Docking

Docking simulations can give insights in the affinity of an efflux pump interaction to its substrate [90]. We used the optimized Tap-Phyre2 structure result of the 100 ns MD simulation in a DPPC bilayer for a Slice Docking simulation to investigate the possibility of competitive inhibition between the antibiotics INH, RIF, OFLO and BDQ

and the EIs CPZ, VERA and NUNL02.

A visual inspection of the EDCs (Figure 3.4) allows a comparison of the FEBs and binding positions along the -axis between the compounds tested. Even though the real FEB may not be fully represented by the calculated FEB: since all Docking simulations followed the same methodology, the EDCs indicate the relative FEB difference between the substrate and compounds [63].

The EDCs (Figure 3.4) show overall strong FEBs of OFLO, used in the MDR-TB treatment, and RIF, on the first line TB treatment [1]. Resistance of both OFLO and RIF has been related to Tap Efflux Pump [13, 14]. Therefore, this result corroborates the hypothesis that OFLO and RIF are substrates of Tap Efflux Pump. It also reinforces that Tap-Phyre2 is an accurate model for drug discovery studies.

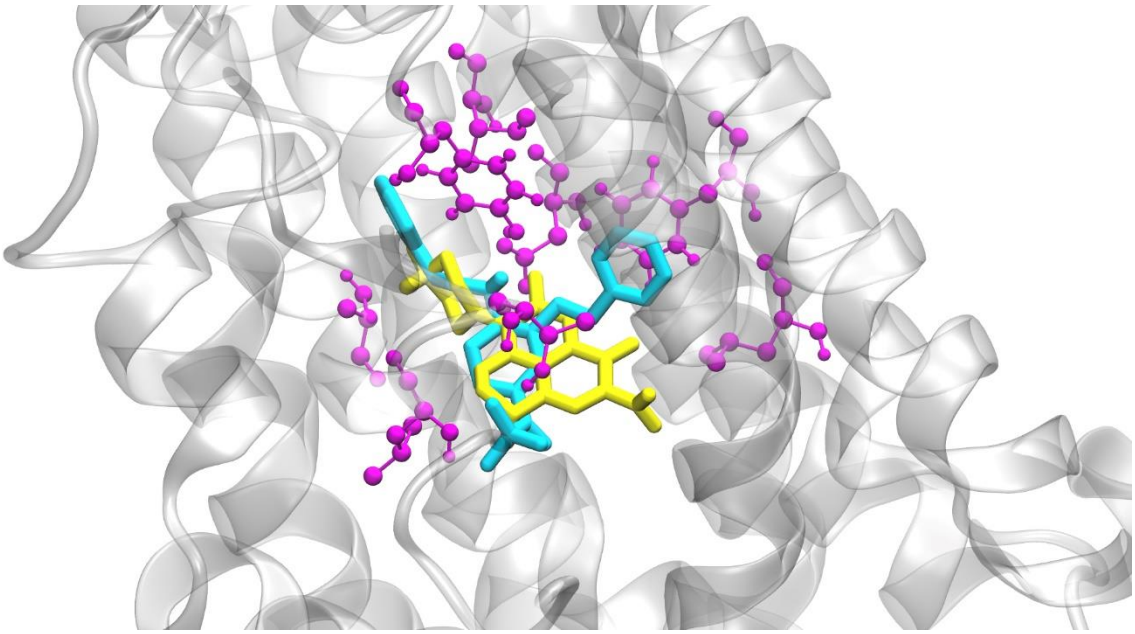

(a) OFLO and NUNL02 at box z28

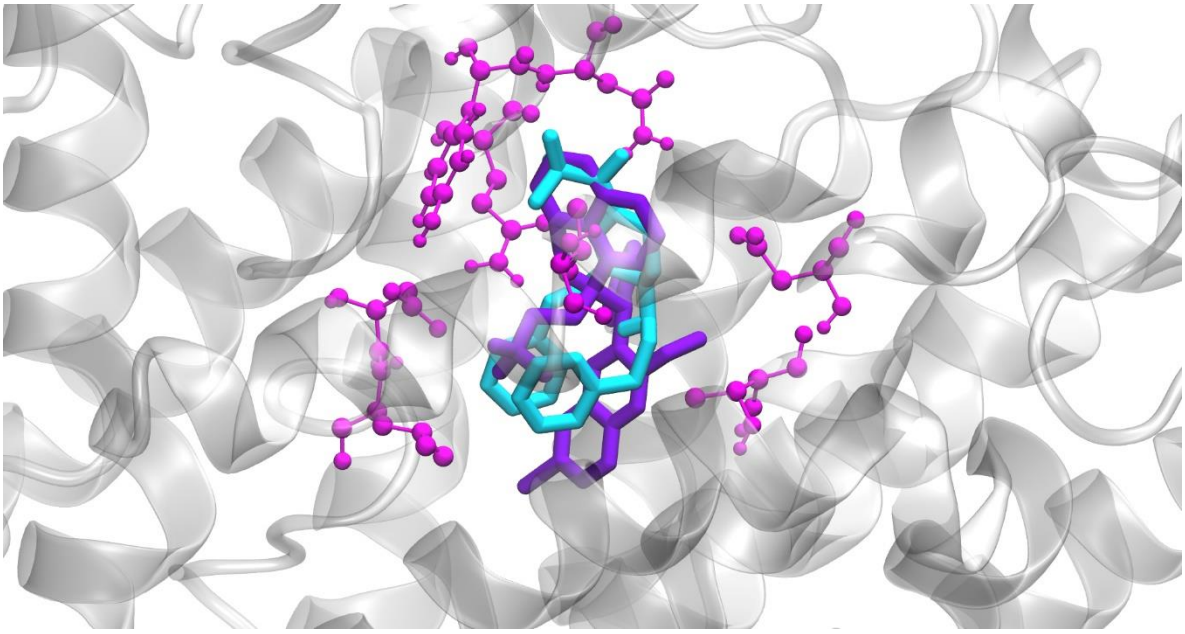

(b) BDQ and NUNL02 at box z34

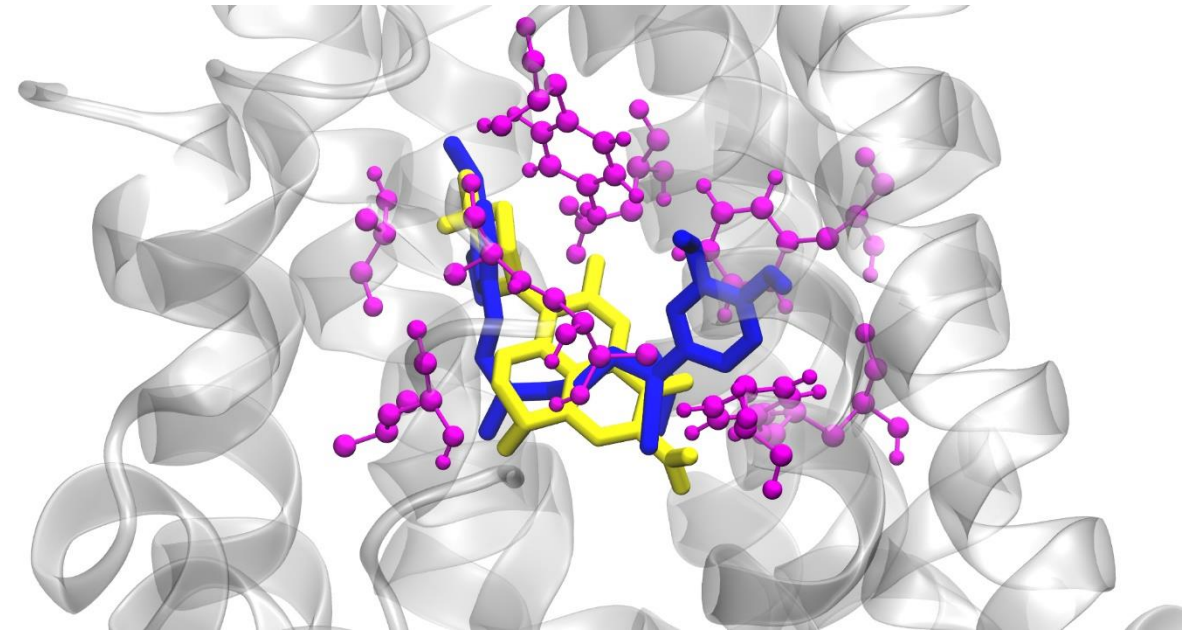

(c) OFLO and VERA at box z28

Figure 6: Tap-Phyre2 residues in interaction with both antibiotic and inhibitor (magenta). NUNL02 in cyan. VERA in blue. OFLO in yellow. BDQ in purple.

BDQ is the first antibiotic approved for TB treatment in decades, used to treat MDR-TB [7], and there are cases of BDQ resistance due to efflux [5, 6]. The overall strong FEB of BDQ highlights the importance of studying the efflux and its inhibition on Tap efflux pump, as it may indicate that this antibiotic is a possible substrate.

The EDCs allows the search of the best binding positions for the compounds along the -axis of Tap-Phyre2. The valleys in the EDCs indicate the strongest FEBs. Thus, we used the valleys to verify whether these positions between antibiotics and EIs are nearby, indicating that the compounds may share preferences for the same binding positions and protein residues. Therefore it may indicate the possibility of competitive inhibition, which is further tested by verifying the coincident biding residues (Supplementary Material).

Competition for the same binding position could be the mechanism for efflux inhibition when the inhibitor is also a substrate [68, 63]. The three inhibitors, but mainly VERA and NUNL02 showed strong FEBs (Figure 3.4), which corroborates the evidences in literature that they may act as efflux pump substrates [68, 63]. Also, it has been indicated that VERA inhibits Tap [91], therefore its EDC also reinforces that Tap-Phyre2 is an accurate model for drug discovery studies.

In the EDCs (Figure 3.4), NUNL02 has a valley (-9.3 kcal/mol) close to the OFLO valley (FEB -7.8 kcal/mol) at box 28, and they interact to 8 coincident residues (Figure 2). NUNL02 has the next strongest FEB (-8.7 kcal/mol) close the BDQ valley (-9.1 kcal/mol) at box 34, and they also interact to 8 coincident residues (Figure 3).

VERA has a valley in its EDC (FEB -7.7 kcal/mol), also close to the OFLO valley (-7.8 kcal/mol) at box 28, and they interact to 9 coincident residues (Figure 4). VERA has another valley (FEB -7.7 kcal/mol) close to a RIF strong FEB (-7.3 kcal/mol) at box 46, and they interact to 3 coincident residues. None of the antibiotics showed valleys near CPZ valley at box 46.

The EDCs plus the coincident residues showed a possibility of competitive

inhibition [68, 63] by NUNL02 on OFLO and BDQ, which highlights NUNL02 as an effective EI. The results also shows a possible competitive inhibition by VERA on OFLO and RIF, which corroborates with the use of VERA as an effective EI. This is important because VERA is a wildly studied EI that has shown success on efflux inhibition in animal models [92].

3.4.2 Flexible Receptor Docking

We performed docking considering 1,000 snapshots of the Tap-Phyre2 MD simulation to evaluate the impact of the Tap flexibility on docking simulations as well as to verify the most important residues of the Tap-Phyre2 model binding site (we believe that the residues that interacts most frequently with the ligands during the flexible receptor docking simulations are important to characterize and confirm the Tap binding site). To compare the flexible and rigid receptor docking results we considered as rigid the docking result with the last MD snapshot (the same snapshot used on slice docking). Besides performing docking simulations we used LigPlot+ to analyze all the receptor snapshots-ligands interactions. Table 3 presents the results of these docking simulations and receptor-ligands interaction analyses.

	FEB (*kcal/mol*)				Total amount of receptor residues interacting				
	Rigid	Flexible Receptor: 1000 snapshots			Rigid	Flexible receptor - 1000 snapshots			
Ligand		Min	Max	Average		−10%	10−50%	50−70%	+70%
BDQ	−8.2	−11.0	−6.0	-8.47 ± 0.77	17	87	16	9	1
CPZ	−6.6	−7.9	−5.9	-6.77 ± 0.35	7	91	22	4	0
NUNL02	−9.4	−10.6	−6.5	-8.40 ± 0.81	11	89	21	4	3
OFLO	−7.8	−9.4	−6.1	-7.78 ± 0.42	11	86	20	3	2
VERA	−7.2	−8.8	−5.1	-7.10 ± 0.60	15	92	18	10	2
INH	−5.4	−6.9	−4.6	-5.50 ± 0.36	7	86	27	0	0
RIF	−6.4	−10.8	−5.7	-7.08 ± 1.04	11	94	13	3	1

Table 3: Results of the docking simulations with flexible receptor. The first column lists the ligands. The second column corresponds to the FEB value in *kcal/mol* for the Rigid docking with snapshot 1,000 and the next columns 3, 4 and 5 describes the minimum, maximum and average with standard deviation values of FEB for flexible receptor. The next five columns are related with the total amount of receptor residues that interacts

(hydrogen bonds or non-bonded contacts) with the respective snapshot(s)).

Regarding the FEB results presented on Table 3 (Columns 2-5) it is possible to note that the best FEB values are for the ligands NUNL02, BDQ, OFLO and VERA in rigid and flexible docking results, the same observed on slice docking (Figure 3.4). The fifth column on Table 3 shows the average values of FEB with the standard deviation. The values of standard deviation shows that we have variation of FEB values between the 1,000 snapshots. Besides regarding the minimum values of FEB (Table 3, third column) we can see that we can obtain more negative values of FEB when considering the flexible receptor model where we highlight the RIF minimum FEB value (almost 4 *kcal/mol* of difference with the average FEB).

Table 3 columns 6-10 shows the total amount of receptor residues interacting with the ligands in the rigid and flexible docking results. The sixth column corresponds to the number of receptor residues interaction with the ligands on the Rigid simulation (snapshot 1,000). Columns 7, 8, 9 and 10 corresponds to the total amount of residues interaction with -10%, 10-50%, 50-70% and more than 70% of the 1,000 considered snapshots respectively. We can observe that up to 94 different residues can interact with RIF in some snapshot during the flexible receptor docking. The same happens for the other ligands: VERA interacts with 92 different residues, CPZ with 91 residues, and so on. Regarding the rigid results this number of residues is smaller even if you compare with the 10-50% frequent residues. Thus we can suppose that Tap-Phyre2 model has a flexible binding site that is important to taking into account to the search for new inhibitors.

For BDQ and VERA we observe that 10 residues that interacts with the rigid receptor are the same as observed for more the 50% of the snapthots and corresponds to the residues ASP23, LEU55, PRO118, MET121, LEU150, PHE154, THR236, TYR239, TYR325, GLN329. For CPZ, 4 of these 10 residues are also interacting with more the 50% of the snapthots: ASP23, PHE154, THR236 and TYR239 . However for

CPZ the 7 residues are different from the most frequent on the ensemble docking. It means that this ligand on the rigid simulation is positioned in a not frequent region of the binding site when compared with the ensemble docking.

Considering NUNL02, most of the residues in rigid and ensemble docking are the same (7/11) and 5 of these 7 are in common with BDQ: ASP23, LEU55, PHE154, THR236, TYR239. The other two most frequent residues are ILE27 and ALA114. For OFLO, the five most frequent residues are the same as BDQ or NUNL02: ASP23, LEU55, PHE154, THR236 and TYR239 and the rigid result present 5 residues in common with the ensemble docking. INH does not have residues with more the 50% of frequency and for the rigid result all the residues are different comparing with the other ligands. Finally for RIF the 4 most frequent residues are different from the other ligands. This can be explained because this ligand has more atoms than the other and probably its positions on the binding site is different.

4 Conclusions

We concluded that Tap-Phyre2 is the best model tested and that it can be used in the studies of EIs for Tap. Tap-Phyre2 got the best results during the validation techniques, including the 50 ns MD in water. On the 100 ns MD simulation of Tap-Phyre2 in a DPPC bilayer, it can be seen that the model is consistent, as it structure was able to stabilize, and that its binding site is highly stable.

Our results also highlight Phyre2, I-Tasser and Modeller as reliable programs for molecular modelling purposes. The model with the best structure was built using Phyre2. The reason might be the fact that Phyre2 uses a large variety of templates and Tap is a protein without any template with close homology. Our results show that it is important to use more than one model built with different software to determine the efficiency of each structure, as different models had considerable differences. It can also be noticed that Verify3D, ModFold and Molprobity had coherent results with the validation MD simulations. ModFold seems to be the software with most agreement

with the final results of this work. However, the validation techniques show to be better used in combination, for they analyse different characteristics of the protein structure.

The Docking results can be considered relevant, as Tap-Phyre2 is a reliable model and is even closer to a native Tap structure after the 100 ns MD simulation in a lipid bilayer. About the slice docking, these results corroborates the hypothesis that OFLO and RIF are possible substrates of Tap, and shows that BDQ can also be extruded by Tap, which reinforces the importance of Tap Efflux Pump in the drug resistance of *M. tuberculosis*. We also found that VERA and NUNL02 possibly act as substrates on Tap Efflux Pump via inhibitory competition over important TB antibiotics. This means those two molecules are possible inhibitors of Tap efflux, and highlights the importance of including EIs as adjuvants to the anti-TB therapy. In respect of the flexible receptor docking results we obtained information about important residues on the binding site of Tap-Phyre2.

5 Acknowledgments

The authors acknowledge the support from CNPq (Process number 477462/2013-8), CAPES (*Edital Biologia Computacional* â€“ Process number 051/2013) and FAPERGS (*Edital* PqG - Process Number 1896-2551/13-1). The first author received a CAPES Master Degree fellowship.

References

[1] World Health Organization, Global tuberculosis report 2017, World Health Organization, Geneva, 2017.

[2] D. R. Silva, M. Dalcolmo, S. Tiberi, M. A. Arbex, M. Munoz-Torrico, R. Duarte, L. D'Ambrosio, D. Visca, A. Rendon, M. Gaga, A. Zumla, G. B. Migliori, New and repurposed drugs to treat multidrug- and extensively drug-resistant tuberculosis, Jornal Brasileiro De Pneumologia: Publicacao Oficial Da Sociedade Brasileira De Pneumologia E Tisilogia 44 (2) (2018) 153–160. doi:10.1590/s1806-37562017000000436 .

[3] T. Coelho, D. Machado, I. Couto, R. Maschmann, D. Ramos, A. von Groll, M. L. Rossetti, P. A. Silva, M. Viveiros, Enhancement of antibiotic activity by efflux inhibitors against multidrug resistant mycobacterium tuberculosis clinical isolates from brazil, Front. Microbiol. 6 (2015) 330. doi:10.3389/fmicb.2015.00330 .

[4] G. Li, J. Zhang, Q. Guo, Y. Jiang, J. Wei, L. L. Zhao, X. Zhao, J. Lu, K. Wan, Efflux pump gene expression in multidrug-resistant mycobacterium tuberculosis clinical isolates, PLoS One 10 (2) (2015) e0119013. doi:10.1371/journal.pone.0119013 .

[5] D. Almeida, T. Ioerger, S. Tyagi, S.-Y. Li, K. Mdluli, K. Andries, J. Grosset, J. Sacchettini, E. Nuermberger, Mutations in pepQ Confer Low-Level Resistance to Bedaquiline and Clofazimine in Mycobacterium tuberculosis , Antimicrobial Agents and Chemotherapy 60 (8) (2016) 4590–4599. doi:10.1128/AAC.00753-16 .
URL https://www.ncbi.nlm.nih.gov/pmc/articles/PMC4958187/

[6] B. Li, M. Ye, Q. Guo, Z. Zhang, S. Yang, W. Ma, F. Yu, H. Chu, Determination of MIC Distribution and Mechanisms of Decreased Susceptibility to Bedaquiline Among Clinical Isolates of Mycobacterium abscessus, Antimicrobial Agents and Chemotherapy doi:10.1128/AAC.00175-18 .

[7] J. Cohen, Approval of novel TB drug celebratedâ€”with restraint, Science 339 (6116) (2013) 130–130.

[8] D. Machado, I. Couto, J. PerdigÃ£o, L. Rodrigues, I. Portugal, P. Baptista, B. Veigas, L. Amaral, M. Viveiros, Contribution of efflux to the emergence of isoniazid and multidrug resistance in mycobacterium tuberculosis, PLoS One 7 (2012) e34538. doi:10.1371/journal.pone.0034538 .

[9] M. Viveiros, M. Martins, L. Rodrigues, D. Machado, I. Couto, J. Ainsa, L. Amaral, Inhibitors of mycobacterial efflux pumps as potential boosters for anti-tubercular drugs, Expert Rev. Anti-Infe. 9 (2012) 983–998. doi:10.1586/eri.12.89 .

[10] J. L. MartÃ-nez, Effect of antibiotics on bacterial populations: a multi-hierachical selection process , F1000Research 6. doi:10.12688/f1000research.9685.1 .

URL https://www.ncbi.nlm.nih.gov/pmc/articles/PMC5247793/

[11] J. A. Aínsa, M. C. Blokpoel, I. Otal, D. B. Young, K. A. De Smet, M. C., Molecular cloning and characterization of tap, a putative multidrug efflux pump present in mycobacterium fortuitum and mycobacterium tuberculosis, J. Bacteriol. 180 (1998) 5836–5843.

[12] E. De Rossi, P. Arrigo, M. Bellinzoni, P. A. Silva, C. Martn, J. A. Ansa, P. Guglierame, G. Riccardi, The multidrug transporters belonging to major facilitator superfamily in mycobacterium tuberculosis., Mol. Medicine 8 (11) (2002) 714–724.

[13] N. Siddiqi, R. Das, N. Pathak, S. Banerjee, N. Ahmed, V. M. Katoch, S. E. Hasnain, Mycobacterium tuberculosis isolate with a distinct genomic identity overexpresses a tap-like efflux pump , Infect. 32 (2004) 109–111.
URL 10.1007/s15010-004-3097-x

[14] X. Jiang, W. Zhang, Y. Zhang, F. Gao, C. Lu, X. Zhang, H. Wang, Assessment of efflux pump gene expression in a clinical isolate mycobacterium tuberculosis by real-time reverse transcription pcr, Microb. Drug Resist. 14 (2008) 7–11. doi:10.1089/mdr.2008.0772 .

[15] R. P. Morris, L. Nguyen, J. Gatfield, K. Visconti, K. Nguyen, D. Schnappinger, S. Ehrt, Y. Liu, L. Heifets, J. Pieters, G. Schoolnik, C. J. Thompson, Ancestral antibiotic resistance in mycobacterium tuberculosis, Proc. Natl. Acad. Sci. USA 102 (2005) 12200–12205. doi:10.1073/pnas.0505446102 .

[16] D. E. Geiman, T. R. Raghunand, N. Agarwal, W. R. Bishai, Differential gene expression in response to exposure to antimycobacterial agents and other stress conditions among seven mycobacterium tuberculosis whib-like genes, Antimicrob. Agents. Chemother. 50 (2006) 2836–2841. doi:10.1128/aac.00295-06 .

[17] B. Marquez, Bacterial efflux systems and efflux pumps inhibitors, Biochimie. 87 (2005) 1137–1147. doi:10.1016/j.biochi.2005.04.012 .

[18] A. Mahamoud, J. Chevalier, S. Alibert-Franco, W. V. Kern, J. M. Pag‘es, Antibiotic efflux pumps in gram-negative bacteria: the inhibitor response strategy, J. Antimicrob. Chemother. 59 (2007) 1223–1229. doi:10.1093/jac/dkl493 .

[19] S. Gupta, S. Tyagi, D. V. Almeida, M. C. Maiga, N. C. Ammerman, W. R. Bishai, Acceleration of tuberculosis treatment by adjunctive therapy with verapamil as an efflux inhibitor, Am. J. Respir. Crit. Care Medicine 188 (5) (2013) 600–607.

[20] S. Ramón-García, V. Mick, E. Dainese, C. Martín, C. J. Thompson, E. De Rossi, R. Manganelli, J. A. Aínsa, Functional and genetic characterization of the tap efflux pump in mycobacterium bovis bcg, Antimicrob. Agents. Chemoth. 56 (2012) 2074–2083. doi:10.1128/aac.05946-11 .

[21] T. J. Opperman, N. St., Recent advances toward a molecular mechanism of efflux pump inhibition, Front. Microbiol. 6 (421) (2015) 1–16. doi:10.3389/fmicb.2015.00421 .

[22] M. I. B. Walmsley, K. S. McKeegan, A. R. Walmsley, Structure and function of efflux pumps that confer resistance to drugs, Biochem. J. 376 (2003) 313–338. doi:10.1042/bj20020957 .

[23] C. Ye, Z. Wang, W. Lu, M. Zhong, Q. Chai, Y. Wei, Correlation between acrb trimer association affinity and efflux activity, Biochem. 53 (2014) 3738–3746. doi:10.1021/bi5000838 .

[24] X. Liu, M. Wright, C. E. Hop, Rational use of plasma protein and tissue binding data in drug design, J. Med. Chem. 57 (2014) 8238–8248. doi:10.1021/jm5007935 .

[25] G. Diallinas, Understanding transporter specificity and the discrete appearance of channel-like gating domains intransporters, Front. Pharmacol. 5 (2014) 1–17. doi:10.3389/fphar.2014.00207 .

[26] M. A. Marti-Renom, A. C. Stuart, A. Fiser, R. Sanchez, F. Melo, A. Sali, Comparative protein structure modeling of genes and genomes, Annu. Rev. Biophis.

Biol. 29 (2000) 291–325. doi:10.1146/annurev.biophys.29.1.291 .

[27] A. Hillisch, L. F. Pineda, R. Hilgenfeld, Utility of homology models in the drug discovery process, Drug Discov. Today 9 (2004) 659–669. doi:10.1016/s1359-6446(04)03196-4 .

[28] N. Eswar, B. Webb, M. A. Marti-Renom, M. Madhusudhan, D. Eramian, M. Shen, U. Pieper, A. Sali, Comparative protein structure modeling using modeller, Curr. Protoc. Protein Sci. 5 (6) (2006) 2.9.1–2.9.31. doi:10.1002/0471140864.ps0209s50 .

[29] Y. Zhang, I-tasser server for protein 3d structure prediction, BMC Bioinform. 9 (2008) 1–8. doi:10.1186/1471-2105-9-40 .

[30] L. A. Kelley, M. J. Sternberg, Protein structure prediction on the web: a case study using the phyre server, Nat. Protoc. 4 (2009) 363–371. doi:10.1038/nprot.2009.2 .

[31] H. M. Berman, J. Westbrook, Z. Feng, G. Gilliland, T. N. Bhat, H. Weissig, I. N. Shindyalov, P. E. Bourne, The Protein Data Bank , Nucleic Acids Research 28 (1) (2000) 235–242.
URL https://www.ncbi.nlm.nih.gov/pmc/articles/PMC102472/

[32] S. T. Cole, R. Brosch, J. Parkhill, T. Garnier, C. Churcher, D. Harris, S. V. Gordon, K. Eiglmeier, S. Gas, B. C. E. 3rd, F. Tekaia, K. Badcock, D. Basham, D. Brown, T. Chillingworth, R. Connor, R. Davies, K. Devlin, T. Feltwell, S. Gentles, N. Hamlin, S. Holroyd, T. Hornsby, K. Jagels, A. Krogh, J. McLean, S. Moule, L. Murphy, K. Oliver, J. Osborne, M. A. Quail, M. A. Rajandream, J. Rogers, S. Rutter, K. Seeger, J. Skelton, R. Squares, S. Squares, J. E. Sulston, K. Taylor, S. Whitehead, B. G. Barrell, Deciphering the biology of mycobacterium tuberculosis from the complete genome sequence, Nature 393 (1998) 537–544. doi:10.1038/31159 .

[33] W. Humphrey, A. Dalke, K. Schulten, Vmd: visual molecular dynamics, J. Mol. Graph. 14 (1) (1996) 33–38.

[34] B. R. Jefferys, L. A. Kelley, S. Mje., Protein folding requires crowd control in a simulated cell, J. Mol. Biol. 397 (5) (2010) 1329–1338. doi:10.1016/j.jmb.2010.01.074 .

[35] T. Liu, G. W. Tang, E. Capriotti, Comparative modeling: the state of the art and protein drug target structure prediction, Comb. Chem. High. T. Scr. 14 (2011) 532–547. doi:10.2174/138620711795767811 .

[36] L. A. Kelley, S. Mezulis, C. M. Yates, M. N. Wass, M. J. E. Sternberg, The phyre2 web portal for protein modeling, prediction and analysis, Nat. Protoc. 10 (2015) 845–858. doi:10.1038/nprot.2015.053 .

[37] A. Roy, A. Kucukural, Y. Zhang, I-tasser: a unified platform for automated protein structure and function prediction, Nat. Protoc. 5 (2007) 725–738.

[38] Y. Zhang, J. Skolnick, Scoring function for automated assessment of protein structure template quality, Proteins: Struct. Funct. Bioinform. 57 (2004) 702–710. doi:10.1002/prot.21643 .

[39] S. F. Altschul, A protein alignment scoring system sensitive at all evolutionary distances, J. Mol. Evol. 36 (1993) 290–300. doi:10.1007/bf00160485 .

[40] M. Shen, A. Sali, Statistical potential for assessment and prediction of protein structures, Protein Sci. 15 (2006) 2507–2524. doi:10.1110/ps.062416606 .

[41] B. W. Andrej Sali, Tutorial - Advanced Example. Modeling of a protein-ligand complex based on multiple templates, loop refinement and user specified restraints. , 23 (2015).
URL https://salilab.org/modeller/tutorial/advanced.html

[42] D. Eisenberg, D. LÃ¼thy, B. J. U., Methods in enzymology: Verify3d: assessment of protein models with three-dimensional profiles, Methods Enzymol. 277 (1997) 396–404. doi:10.1016/s0076-6879(97)77022-8 .

[43] R. E. D. Luthy, B. J. U., Assessment of protein models with three-dimensional profiles, Nat. 356 (1992) 83–85. doi:10.1038/356083a0 .

[44] J. U. Bowie, R. Luthy, D. Eisenberg, A method to identify protein sequences that fold into a known three-dimensional structure, Science 253 (1991) 164–170. doi:10.1126/science.1853201 .

[45] L. J. McGuffin, The modfold server for the quality assessment of protein structural models, Bioinform. 24 (2008) 586–587. doi:10.1093/bioinformatics/btn014 .

[46] L. J. McGuffin, M. T. Buenavista, D. B. Roche, The modfold4 server for the quality assessment of 3d protein models, Nucleic Acids Res. 41 (2013) W368–W372. doi:10.1093/nar/gkt294 .

[47] R. A. Laskowski, D. S. Moss, J. M. Thornton, Main-chain bond lengths and bond angles in protein structures, J. Mol. Biol. 231 (1993) 1049–1067. doi:10.1006/jmbi.1993.1351 .

[48] I. W. Davis, A. Leaver-Fay, V. B. Chen, J. N. Block, G. J. Kapral, X. Wang, L. W. Murray, L. W. Arendall, J. Snoeyink, J. S. Richardson, D. C. Richardson, Molprobity: all-atom contacts and structure validation for proteins and nucleic acids, Nucleic Acid Res. 35 (2007) W375–W383. doi:10.1093/nar/gkm216 .

[49] S. Páll, M. J. Abraham, C. Kutzner, B. Hess, E. Lindahl, Tackling exascale software challenges in molecular dynamics simulations with gromacs, in: Solving Software Challenges for Exascale, Springer International Publishing, 2015, pp. 3–27. doi:10.1007/978-3-319-15976-8_1 .

[50] M. J. Abraham, T. Murtola, R. Schulz, S. PÃ¡ll, J. C. Smith, B. Hess, E. Lindahl, GROMACS: High performance molecular simulations through multi-level parallelism from laptops to supercomputers, SoftwareX 1 (2015) 19–25.

[51] M. J. Abraham, D. van der Spoel, E. Lindahl, B. Hess, the GROMACS

development team, GROMACS User Manual version 2016.4 (2017).
URL www.gromacs.org

[52] S. Pronk, S. PÃ¡ll, R. Schulz, P. Larsson, P. Bjelkmar, R. Apostolov, M. R. Shirts, J. C. Smith, P. M. Kasson, D. van der Spoel, others, GROMACS 4.5: a high-throughput and highly parallel open source molecular simulation toolkit, Bioinformatics 29 (7) (2013) 845–854.

[53] C. Oostenbrink, A. Villa, A. E. Mark, W. F. Van Gunsteren, A biomolecular force field based on the free enthalpy of hydration and solvation: the GROMOS force-field parameter sets 53a5 and 53a6, Journal of computational chemistry 25 (13) (2004) 1656–1676.

[54] O. Berger, O. Edholm, F. JÃ¤hnig, Molecular dynamics simulations of a fluid bilayer of dipalmitoylphosphatidylcholine at full hydration, constant pressure, and constant temperature, Biophysical Journal 72 (5) (1997) 2002–2013. doi:10.1016/S0006-3495(97)78845-3 .

[55] Justin Lemkul, KALP-15 in DPPC. (2015).
URL http://www.bevanlab.biochem.vt.edu/Pages/Personal/justin/gmx-tutorials/membrane_protein/01_pdb2gmx.html

[56] Peter Tieleman, State-of-the-art computational models of lipids and membrane proteins. (2015).
URL http://wcm.ucalgary.ca/tieleman/downloads

[57] J. Nagle, Area/lipid of bilayers from NMR, Biophysical journal 64 (5) (1993) 1476–1481.

[58] C. Kandt, W. L. Ash, D. P. Tieleman, Setting up and running molecular dynamics simulations of membrane proteins, Methods 41 (4) (2007) 475–488.

[59] R. C. Team, et al., R: A language and environment for statistical computing , Vienna, Austria (2013).

URL http://www.rstudio.com/

[60] RStudio Team, RStudio: Integrated Development Environment for R , RStudio, Inc., Boston, MA (2015).
URL http://www.rstudio.com/

[61] J. Yang, A. Roy, Y. Zhang, Protein-ligand binding site recognition using complementary binding-specific substructure comparison and sequence profile alignment, Bioinform. 29 (2013a) 2588–2595. doi:10.1093/bioinformatics/btt447 .

[62] J. Yang, A. Roy, Y. Zhang, Biolip: a semi-manually curated database for biologically relevant ligand-protein interactions, Nucleic Acids Res. 41 (2013b) D1096–D1103. doi:10.1093/nar/gks966 .

[63] L. S. Jr, L. L. Carrion, A. v. Groll, S. S. Costa, E. Junqueira, D. F. Ramos, J. Cantos, V. R. Seus, I. Couto, L. d. S. Fernandes, H. G. Bonacorso, M. A. P. Martins, N. Zanatta, M. Viveiros, K. S. Machado, P. E. A. d. Silva, In vitro and in silico analysis of the efficiency of tetrahydropyridines as drug efflux inhibitors in Escherichia coli , International Journal of Antimicrobial Agents 49 (3) (2017) 308 – 314. doi:https://doi.org/10.1016/j.ijantimicag.2016.11.024 .
URL https://www.sciencedirect.com/science/article/pii/S0924857917300262

[64] G. M. Morris, R. Huey, W. Lindstrom, M. F. Sanner, R. K. Belew, D. S. Goodsell, A. J. Olson, Autodock4 and autodocktools4: automated docking with selective receptor flexiblity, J. Comput. Chem. 16 (2009) 2785–2791. doi:10.1002/jcc.21256 .

[65] O. Trott, A. J. Olson, AutoDock Vina: improving the speed and accuracy of docking with a new scoring function, efficient optimization, and multithreading, J. Comput. Chem. 31 (2) (2010) 455–461.

[66] V. Y. Tanchuk, V. O. Tanin, A. I. Vovk, G. Poda, A New, Improved Hybrid Scoring Function for Molecular Docking and Scoring Based on AutoDock and AutoDock Vina, Chem. Biol. Drug Des. 87 (4) (2016) 618–625.

[67] M. Kolaczkowski, M. van der Rest, A. Cybularz-Kolaczkowska, J. P. Soumillion, W. N. Konings, A. Goffeau, Anticancer drugs, ionophoric peptides, and steroids as substrates of the yeast multidrug transporter Pdr5p, The Journal of Biological Chemistry 271 (49) (1996) 31543–31548.

[68] M. Putman, L. A. Koole, H. W. van Veen, W. N. Konings, The secondary multidrug transporter LmrP contains multiple drug interaction sites, Biochemistry 38 (42) (1999) 13900–13905.

[69] V. R. Seus, L. Silva, J. Gomes, da Silva Pea, A. V. Werhli, K. S. Machado, A framework for virtual screening, in: Symposium on Applied Computing, Association for Computer Machinery, New York, NY, USA, 2016, pp. 1205–1218.

[70] R. A. Laskowski, M. B. Swindells, LigPlot+: multiple ligand-protein interaction diagrams for drug discovery, Journal of Chemical Information and Modeling 51 (10) (2011) 2778–2786. doi:10.1021/ci200227u .

[71] H. Alonso, A. A. Bliznyuk, J. E. Gready, Combining docking, molecular dynamic simulations in drug design, Med. Res. Rev. 26 (2006) 531–568.

[72] P. Cozzini, G. E. Kellogg, F. Spyrakis, D. J. Abraham, G. Costantino, A. Emerson, F. Fanelli, H. Gohlke, L. A. Kuhn, G. M. Morris, M. Orozco, T. A. Pertinhez, M. Rizzi, C. A. Sotriffer, Target flexibility: An emerging consideration in drug discovery and design., J. Med. Chem. 51 (20) (2008) 6237–6255.

[73] A. Ganesan, M. L. Coote, K. Barakat, Molecular dynamics-driven drug discovery: leaping forward with confidence, Drug Discovery Today 22 (2) (2017) 249 – 269. doi:http://dx.doi.org/10.1016/j.drudis.2016.11.001 .

[74] B.-R. Chandrika, J. Subramanian, S. D. Sharma, Managing protein flexibility in docking and its applications, Drug discovery today 14 (7-8) (2009) 394–400.

[75] I. A. Guedes, C. S. de Magalhães, L. E. Dardenne, Receptor–ligand molecular docking, Biophysical reviews 6 (1) (2014) 75–87.

[76] F. Jiang, S.-H. Kim, â€œsoft dockingâ€• : matching of molecular surface cubes, Journal of molecular biology 219 (1) (1991) 79–102.

[77] A. R. Leach, Ligand docking to proteins with discrete side-chain flexibility, Journal of molecular biology 235 (1) (1994) 345–356.

[78] J.-H. Lin, A. L. Perryman, J. R. Schames, J. A. McCammon, The relaxed complex method: Accommodating receptor flexibility for drug design with an improved scoring scheme., Biopolymers 68 (1) (2003) 47–62.

[79] K. S. Machado, E. K. Schroeder, D. D. Ruiz, E. M. L. Cohen, O. Norberto de Souza, Fredows: a method to automate molecular docking simulations with explicit receptor flexibility and snapshots selection., BMC Genomics 12 (2011) S6.

[80] M. A. Marti-Renom, U. Pieper, M. S. Madhusudhan, A. Rossi, N. Eswar, F. P. Davis, F. Al-Shahrour, J. Dopazo, A. Sali, Dbali tools: mining the protein structure space, Nucleic acids research 35 (suppl_2) (2007) W393–W397.

[81] K. Singh, M. Kumar, E. Pavadai, K. Naran, D. F. Warner, P. G. Ruminski, K. Chibale, Synthesis of new verapamil analogues and their evaluation in combination with rifampicin against Mycobacterium tuberculosis and molecular docking studies in the binding site of efflux protein Rv1258c, Bioorganic & Medicinal Chemistry Letters 24 (14) (2014) 2985–2990. doi:10.1016/j.bmcl.2014.05.022 .

[82] G. Madhavi Sastry, M. Adzhigirey, T. Day, R. Annabhimoju, W. Sherman, Protein and ligand preparation: parameters, protocols, and influence on virtual screening enrichments , Journal of Computer-Aided Molecular Design 27 (3) (2013) 221–234. doi:10.1007/s10822-013-9644-8 .
URL https://doi.org/10.1007/s10822-013-9644-8

[83] C. J. Law, P. C. Maloney, D.-N. Wang, Ins and outs of major facilitator superfamily antiporters, Annu. Rev. Microbiol. 62 (2008) 289–305.

[84] R. J. Law, C. Capener, M. Baaden, P. J. Bond, J. Campbell, G. Patargias, Y. Arinaminpathy, M. S. P. Sansom, Membrane protein structure quality in molecular dynamics simulation, Journal of Molecular Graphics & Modelling 24 (2) (2005) 157–165. doi:10.1016/j.jmgm.2005.05.006 .

[85] V. Daggett, Molecular dynamics simulations of the protein unfolding/folding reaction, Acc. Chem. Res. 35 (6) (2002) 422–429. doi:10.1021/ar0100834 .

[86] K. Lindorff-Larsen, N. Trbovic, P. Maragakis, S. Piana, S. D. E., Structure and dynamics of an unfolded protein examined by molecular dynamics simulation, J. Am. Chem. Soc. 134 (8) (2012) 3787â€“3791. doi:10.1021/ja209931w .

[87] K. Takemura, H. Guo, S. Sakuraba, N. Matubayasi, A. Kitao, Evaluation of protein-protein docking model structures using all-atom molecular dynamics simulations combined with the solution theory in the energy representation, J Chem Phys. 137 (21) (2012) 215105. doi:10.1063/1.4768901 .

[88] S. Della-Longa, A. A., Structural and functional insights on folate receptor alpha (fralpha) by homology modeling ligand docking and molecular dynamics, J. Mol. Graph. Model. 44 (2013) 197–207. doi:10.1016/j.jmgm.2013.05.012 .

[89] K. Kulleperuma, S. M. Smith, D. Morgan, B. Musset, J. Holyoake, N. Chakrabarti, V. V. Cherny, T. E. DeCoursey, R. PomÃ¨s, Construction and validation of a homology model of the human voltage-gated proton channel hhv1, J. Gen. Physiol. 141 (2013) 445–465. doi:10.1085/jgp.201210856 .

[90] R. J. Ferreira, M. U. Ferreira, D. J. V. A. Santos, Molecular docking characterizes substrate-binding sites and efflux modulation mechanisms within p-glycoprotein, J. Chem. Inf. Model. 53 (7) (2013) 1747–1760. doi:10.1021/ci400195v .

[91] K. N. Adams, K. Takaki, L. E. Connolly, H. Wiedenhoft, K. Winglee, O. Humbert, P. H. Edelstein, C. L. Cosma, L. Ramakrishnan, Drug Tolerance in Replicating Mycobacteria Mediated by a Macrophage-Induced Efflux Mechanism , Cell 145 (1) (2011) 39–53. doi:10.1016/j.cell.2011.02.022 .

URL https://www.ncbi.nlm.nih.gov/pmc/articles/PMC3117281/

[92] S. Gupta, S. Tyagi, W. R. Bishai, Verapamil Increases the Bactericidal Activity of Bedaquiline against Mycobacterium tuberculosis in a Mouse Model , Antimicrobial Agents and Chemotherapy 59 (1) (2015) 673–676. doi:10.1128/AAC.04019-14 .
URL https://www.ncbi.nlm.nih.gov/pmc/articles/PMC4291418/

7 Manuscrito II

All-atom Molecular Dynamics model for mycobacterial plasma membrane

João L. R. Scaini, Adriano V. Werhli, Vânia R. de Lima, Pedro E. A. da Silva, José R. Bordin, Karina S. Machado

O manuscrito objetivou o desenvolvimento de um modelo de membrana de PIM2 com DM. A análise deste modelo é realizada com experimentos de DM utilizando variação de temperatura, agregação espontânea e inserção da bomba de efluxo Tap, cujo modelo foi desenvolvido no Artigo I na Seção 6.

A Molecular Dynamics study of PIM $_2$ lipid bilayermembranes

João L. R. Scaini [*,†], Adriano V. Werhli [†], Vânia R. de Lima [‡], Pedro E. A. da Silva [¶], José R. Bordin [*,§] and Karina S. Machado [†]

† Laboratório de Biologia Computacional do Centro de Ciências Computacionais, Universidade Federal do Rio Grande.

‡ Escola de Química e Alimentos, Universidade Federal do Rio Grande.

¶ Núcleo de Pesquisa em Microbiologia Médica, Universidade Federal do Rio Grande.

§ Departamento de Física, Instituto de Física e Matemática, Universidade Federal de Pelotas, Caixa Postal 354, 96010-900, Pelotas, Rio Grande do Sul, Brazil

E-mail: jlrscaini@yahoo.com.br; jrbordin@ufpel.edu.br

Abstract

Phosphatidyl-myo-inositol mannosides (PIMs) are an essential component of the cell envelope and the most predominant lipid in the inner membrane (IM) of *M. tuberculosis*. In this work, we propose a Molecular Dynamics (MD) model for PIM $_2$ lipids and analyze the properties of membranes composed of this lipid. The study is divided in three parts: influence of the temperature in the PIM $_2$ membrane stability, self-assembly abilities of the PIM $_2$ lipid and the behavior when a trans membrane protein is inserted in PIM $_2$ membrane. Our results show that the model is able to reproduce the gel phase observed at 310.0 K and a fluid phase at 363.15 K. Also, the spontaneous self-assembly of randomly

distributed lipids in a vesicular aggregate was observed. Finally, we observe that the PIM_2 membrane is more stable than DPPC membranes when a Tap protein is inserted. Once Tap efflux pump is related to multidrug resistance of *M. tuberculosis*, this result indicates that the use of the proper lipid model is essential to the appropriate depiction and modeling of these systems.

Introduction

Tuberculosis (TB) is an important infecto-contagious disease caused mainly by *Mycobacterium tuberculosis* being a major cause of mortality and morbidity, especially in developing countries. It was estimated that TB have caused over 1.4 million deaths in 2019. The incidence per year for TB has been growing since 2013. In 2019, 10 million new cases were estimated. One of the factors attributed to this increase is the emergence of multidrug-resistant (MDR) TB, which correspond to 362,000 new cases in 2019 [1]. In addition to the acquired resistance, *M. tuberculosis* presents high degree of intrinsic resistance related to its cellular ultrastructure. One of the major reasons for the intrinsic resistance to therapeutic agents, and also host defense mechanisms, is the unusual lipid-rich robust and impermeable cell envelope [2].

M. tuberculosis is covered by a complex envelope, composed by the inner plasma membrane (IM), the peptidoglycan-arabinogalactan complex, and the outer membrane (OM) that is covalently linked to the arabinogalactan [3]. Lipids that are unique to the species or to mycobacteria compose this envelope. The abundance and biological importance of these lipids reflect in extensive studies to elucidate their structures and functions [4].

Phosphatidyl-myo-inositol mannosides (PIMs) are unique glycolipids abundant in both IM and OM of all mycobacteria, being structural components of the cell envelope. Structurally, PIMs are consisted of a phosphatidyl-myo-inositol (PI) group containing mannosides esterified to the inositol ring [5]. The PIM family comprises phosphatidyl-myo-inositol mono-, di-, tri-, tetra-, penta-, and hexamannosides, with up to four acyl chains. The two most abundant classes in *M. tuberculosis* are Phosphatidyl-myo-inositol dimannosides (PIM_2) and Phosphatidyl-myo-inositol hexamannosides (PIM_6) [6].

Diacyl phosphatidyldimannoside (Ac_2PIM_2) is the most abundant lipid in the

mycobacterial IM, accounting for up to 42% of all lipids extracted. Other PIMs such as AcPIM $_2$, AcPIM $_4$, Ac $_2$PIM $_4$, AcPIM $_6$ and Ac $_2$PIM $_6$ account to up to 26% [3]. Furthermore, they are precursors of the lipoglycans (lipomannan and lipoarabinomannan), which are multiglycosylated forms of PIM $_2$ [7,8]. PIMs and lipoglycans are important virulence factors in *M. tuberculosis* and may modulate to host-pathogen interactions [5].

The physicochemical characterization of biological membranes in fundamental to understand their physiological role [9]. Elucidation of the mechanisms responsible for the distinct structural conformations and morphologies, and the fusion and dissolution is essential to understand a wide range of biological processes, as for example virulence [10,11]. To this end one of the most employed approach to understand the behavior of cell membranes is Molecular Dynamics (MD) simulations. This *in silico* method allows a complete control on the system properties and has been extensively applied to provide information on both their spatial organization and temporal dynamics [12-14].

Recent MD studies about mycobacterial membrane include membranes based in dipalmitoylphosphatidylcholine (DPPC), dioleoylphosphatidylcholine (DOPC), palmitoyloleoylphosphatidylglycerol (POPG), 1-palmitoyl-2-oleoyl phosphatidylethanolamine (POPE) [15-17]. Nevertheless, there are no specific membrane molecular model with such uncommon and unique lipids as the ones observed in the *M. tuberculosis*. Therefore, it is important to develop a mycobacterial membrane model to allow structural studies that takes in consideration its actual lipid composition. As cited before, PIM $_2$ is one of the most abundant PIMs, and is precursor of lipoglycans and the other PIMs with higher amount of mannosides. In this way, the main objective of this study is to propose a PIM $_2$ lipid model for MD simulations, analyze its behavior and viability for a more accurate *M. tuberculosis* IM modeling.

In this sense, this study was performed in three parts. First, we investigate the

temperature effect on a PIM_2 bilayer to validate it in comparison to its natural behavior. We considered 310 K (36.85 ^oC) as the normal lungs temperature – where a gel phase is expected – and 363.15 K (90 ^oC) – temperature above the phase transition for mycobacterial membrane [18]. The second part of this study aimed to analyze the occurrence of spontaneous aggregation of the lipid molecules forming a bilayer structure [19] of PIM_2, as another form of validation of the model. Finally, we studied the behavior of the PIM_2 bilayer with insertion of a protein that is naturally inserted on *M. tuberculosis* IM and is associated to MDR-TB, the tetracycline/aminoglycoside resistance (Tap) efflux pump [20,21].

Data reported in this work will contribute to establish a membrane model which may provide more accurate protein-membrane studies related to mycobacteria as well as drugs' structure-activities relationships to improve the MDR-TB therapy.

Methodology

PIM_2 Bilayer at different temperatures

To obtain the two-dimensional structure of the PIM_2 molecule we use the Lipid Maps [22] (LM ID: LMGP15010062) [4]. The hydrogen from the hydroxyl group is removed to get the net charge -1. The three-dimensional structure is obtained using Avogadro 1.2.0 [23] minimization with the force field Universal Force Field (UFF). The topology was obtained with the Automated Topology Builder (ATB) [24] (ATB ID: KJII) from the submission of the minimized three-dimensional structure. The topology was manually edited in order to ensure that the names of atoms correspond to the parameters of "Berger lipids" [25] modification for GROMOS96 53a6 force field [26] – this topology is available in the Supplementary Information. The electrostatic interaction was handled using the Particle

Mesh Ewald method.

Molecular Dynamics simulations were performed using the GROMACS 2016.4 package [27,28]. GROMACS editconf was used to create a 128 lipid bilayer perpendicular to the z-axis. A short 50 step minimization and a short 250 step production phase were performed to make the structure flexible. Then, two boxes of water model SPC with a thickness of 0.6 nm were added to both sided of the bilayer solvated the system. In order to neutralize the system, 128 sodium ions were added to the solvent.

The solvated system went through energy minimization (EM), equilibration and production. The equilibration was performed with restraints on lipid phosphorus in the z-axis, preventing them from leave the position vertically. The equilibration consisted of two phases. The first was a 10.0 ns NVT simulation for temperature adjustment (EQ 1), where the temperature was fixed in 310.0 K or 363.15 K using the velocity rescale. The second was a 10.0 ns NPT simulation (EQ 2) keeping the temperature fixed in 310.0 K or 363.15 K by the Nosè-Hoover thermostat and the pressure fixed in 1.0 bar by the Parrinello-Rahman semi-isotropic barostat – the pressure in the z-direction was not fixed. Finally, the system went to a 100.0 ns NPT simulation for the production phase. Here no restraints were applied, and the same temperature and pressure control from the equilibration phase were used.

PIM $_2$ Bilayer formation

MD simulations were performed to test if PIM $_2$ molecules would spontaneously aggregate in a bilayer structure. The initial system was a box with 12.0 nm $\times$ 12.0 nm $\times$ 6 nm box in the x, y and z directions with 128 randomly distributed PIM $_2$ molecules. The box was then fully solvated. The system was neutralized with 128 sodium ions. The simulations were conducted with the same conditions as the bilayer MDs, and the same

steps: energy minimization, two equilibration steps - 10.0 ns equilibration for temperature coupling and 10.0 ns equilibration for pressure coupling, which were respectively designated EQ1 and EQ2 - and 100.0 ns production. The temperature was fixed in 310.0 K. The box had equal sizes at x and y axes, and a smaller size at z axis because of the membrane formation. Also, the volume was not conserved in EQ2 and the production steps in order to respect anisotropy.

PIM $_2$ bilayer with Tap protein inserted

To test the bilayer as an IM model, we performed a MD simulation with a Tap protein [29,30] inside the PIM $_2$ bilayer. The Tap model used was proposed in a previous study of our group [17]. The same software and force field of the previous sections were employed. The PIM $_2$ bilayer final structure from the 100.0 ns 310.0 K MD simulation was used for the insertion. To compare the stability of Tap protein inside of the PIM $_2$ bilayer, a simulation with Tap inserted in a dipalmitoylphosphatidylcholine (DPPC) bilayer was performed, following the same protocol. We used coordinates and topology of a previously published stable and flexible DPPC membrane [31]. The DPPC topology was also edited to the parameters of the "Berger lipids" [25] modification for GROMOS96 53a6 force field [26], this topology is available in the Supplementary Information.

The insertion of the protein in the lipid bilayer followed the InflateGRO technique [32,33] modified according to the protocol of Lemkul [34]. Briefly stated, it consists in inflating the bilayer area in the xy-plane by 4 times, and then deflate the area for 0.95 times, with an EM after each deflation. This allows a more natural accommodation of the lipid bilayer around the protein. Six lipids were removed from the system during this process, the system has now 122 lipid molecules. The water from the lipid bilayer is also removed in the InflateGRO procedure. Therefre, the system was then solvated in the same way as described above, but the water boxes had 1.5 nm at the z axis. Here we added 122 sodium

and 5 chlorine ions in the water to neutralize the charge of the system. Next, the system went through EM and two equilibration phases with the same configurations as previous section, adding now restraints for the heavy atoms of the protein. This allows shaping the lipid bilayer around the protein. Finally, the same 100.0 ns production phase at 310.0 K and 1 bar was performed to analyze the protein inside the distinct bilayer membranes.

Analysis

GROMACS provided the calculation for some analysis that were plotted using R 3.1.3 and R studio 0.99.491 software [35,36]. The Root-mean-square deviation (RMSD) was calculated at each 2 ps along the entire MD simulations to determine the mobility of the bilayer in different temperatures and with Tap protein. In addition, the RMSD of Tap protein inserted in the bilayer was calculated. The density profile of different atom groups (water, lipid head groups, acyl chains, and protein, when present) was calculated along the z-axis to have an overview of the distribution. The deuterium order parameters of the acyl chains of the bilayer were calculated in order to determine how rigid the bilayer is. The lateral diffusion of the lipid bilayer was calculated to determine its fluidity. The thickness of the membrane was calculated using GridMAT-MD [37] and plotted using Matplotlib.

Results and Discussion

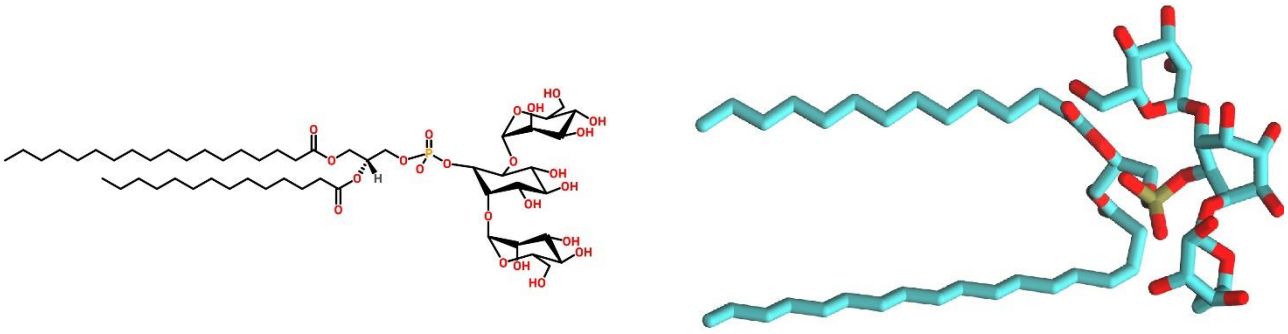

2D 3D

Figure 1: Structure of PIM_2.

The PIM_2 bi-dimensional and three-dimensional structures are shown in the Figures 3 and 3, respectively. As cited before, the MD results were described and discussed as follows: first, the influence of the temperature in the PIM_2 bilayer. Then, the description of PIM_2 bilayer formation. Finally, the effect of Tap in the PIM_2 bilayer properties. Considering the fact that computational MD simulation data related to gel-phase lipid membranes are closest to their correspondent experimental results, when compared to membranes in fluid phase [38], the PIM_2 bilayer formation process and the effects of Tap on its properties were studied at 310 K.

PIM_2 bilayer at different temperatures

MD simulations data related to PIM_2 bilayer structure at the lungs temperature (310 K) and at a temperature above the phase transition for mycobacterial membrane (363.15 K) [18] are shown in Figures 3.4 and 3.1, respectively. From these data, five different properties were analyzed and compared: partial density, RMSD, deuterium order

parameters, thickness and lateral diffusion.

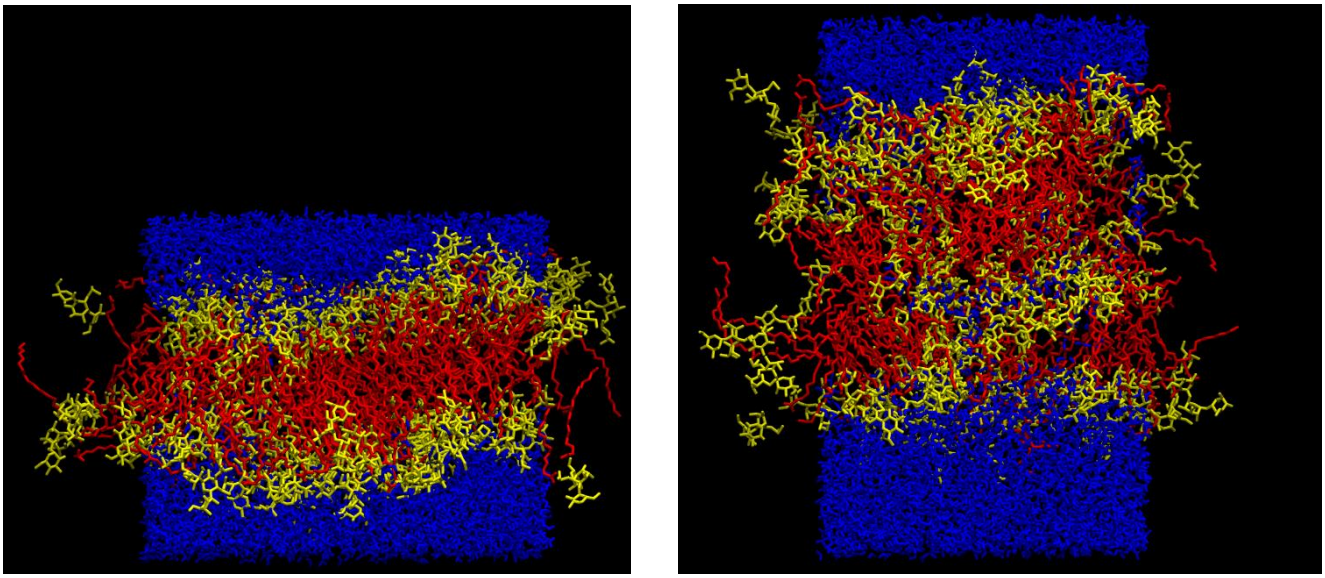

PIM $_2$ 310 K PIM $_2$ 363.15 K

Figure 2: Final structure of PIM $_2$ bilayer in two different MD simulations, (a) bilayer at 310 K, (b) bilayer at 363.15 K. Water in blue, lipid headgroups in yellow, lipid acyl chains in red.

Partial density

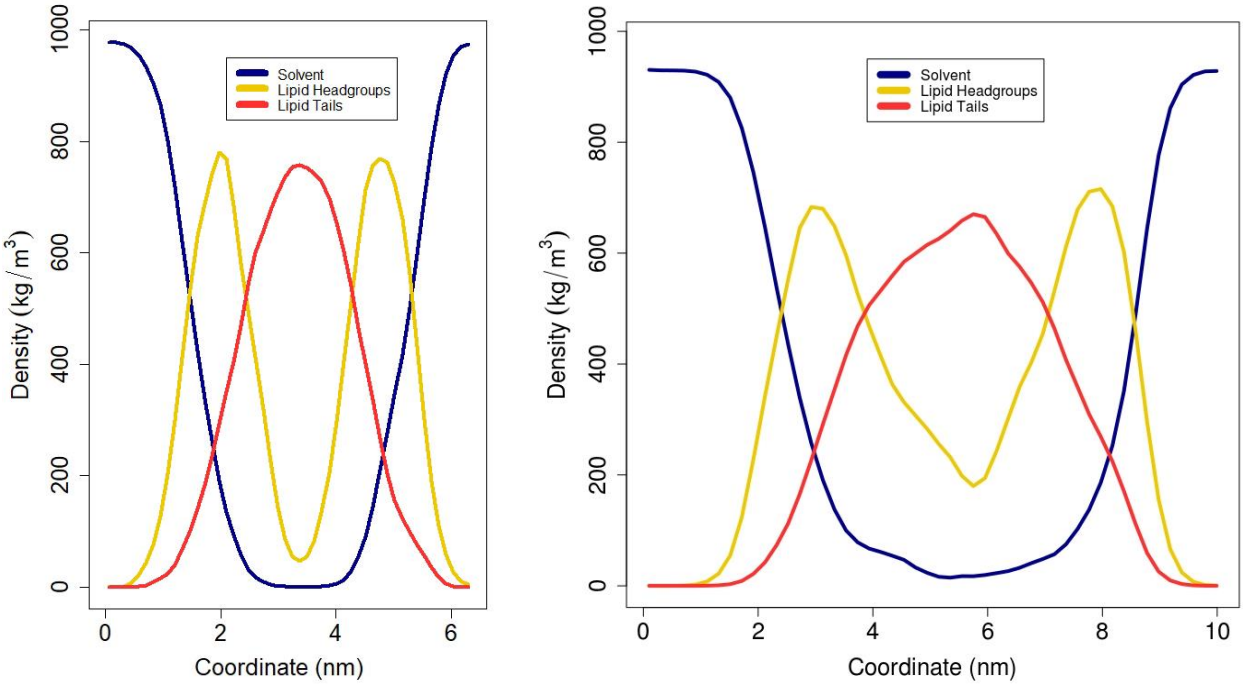

310 K

363.15 K

Figure 3: Partial density of PIM $_2$ bilayer at different temperatures, y-axis represents the density and the x-axis represents the coordinates. Lipid headgroups correspond to the inositol phosphate and mannosides polar groups, while the Lipid tails correspond to acyl chains hydrophobic region, and the solvent correspond to the water.

The partial density was calculated to analyze the density distribution of three regions (lipid head groups, lipid acyl chains and water) of the PIM $_2$ bilayer system and the temperature effect on it. The partial density of PIM $_2$ at 310 K is showed in Figures 3.1.1 and 3.4 and the PIM $_2$ correspondent property at 363.15 K is showed in Figures 3.1.1 and 3.1. The whole membrane is less dense at 363.15 K, but occupy a larger region

at z axis, compared to the model at 310 K. The temperature increase promoted a decrease in the density of membrane headgroups and hydrophobic region, indicating a disorganization effect in the bilayer structure. Here, it is interesting to note that, at 310 K, water remained in the extremes of the z-axis and did not penetrate toward the PIM_2 hydrophobic acyl chains – this reflects the stronger interaction between water molecules and the hydrophilic lipid head groups. However, at 363.15 K, the water seems to have penetrated deeper in the membrane, reaching the lipid acyl chains (Figure 3.1). The water displacement toward the PIM_2 hydrophobic region indicates a decrease in membrane packing or a reduction of area per lipid molecule in the bilayer plane [39]. The results corroborate to an expected fluid phase related to PIM_2 at 363.15 K.

Thickness

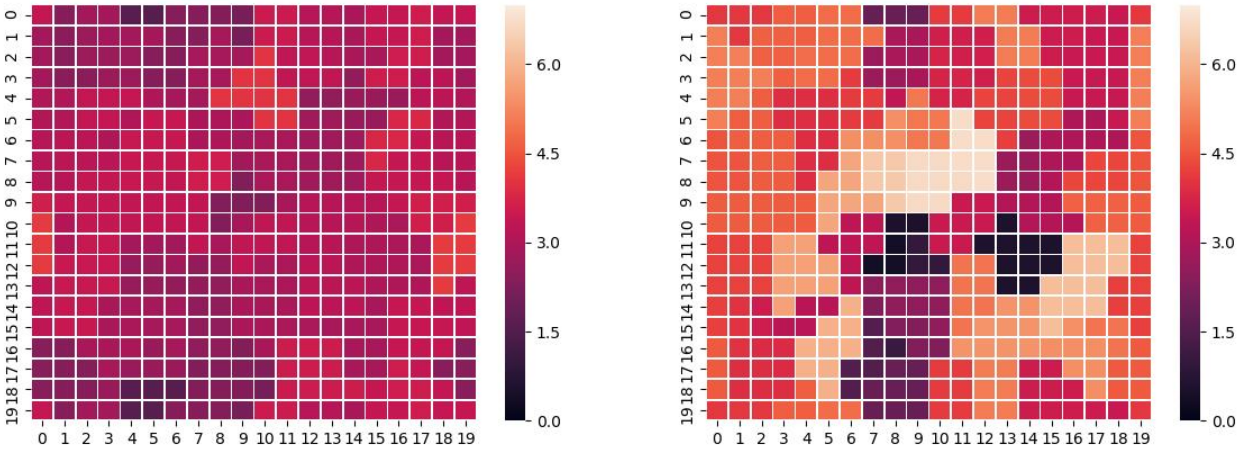

310 K 363.15 K

Figure 4: Bilayer Thickness of PIM_2 bilayer at different temperatures. y-axis and x-axis are a 20 x 20 points grid box representing the PIM_2 bilayer area. The z-axis is represented by a color gradient indicating the thickness (nm), where lighter colors are thicker regions.

The effect of different temperatures in the thickness of PIM_2 bilayer system was evaluated and is shown in Figure 3.1.2. The PIM_2 bilayer at 310 K showed 4.5% of its structure with thickness over 4 nm, where the thickest region corresponds to 4.13 nm. At 363.15 K, 60.75% of the PIM_2 bilayer was thicker than 4 nm, with the thickest region equivalent to 6.73 nm. Considering PIM_2 saturated hydrophobic chains, it is expected a considerable molecular package which, at higher temperature, is disrupted by water entry (see Partial Density section), promoting changes in the molecular conformation as well as in the headgroup sugars dipolar interactions. This may had reflected in an increase of the bilayer thickness. A direct relationship between the bilayer thicknes and the membrane swelling, was considered before by Kuklin and co-workers (2020) [40] and Zhang and co-workers (1995) [41].

Deuterium order parameters

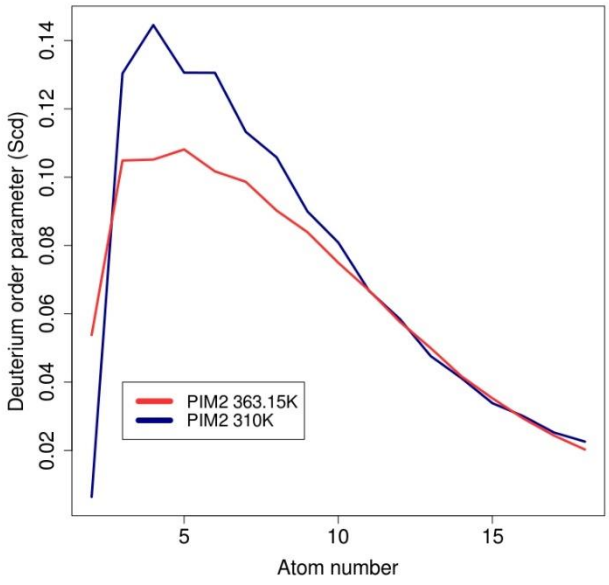

Acyl chain 1

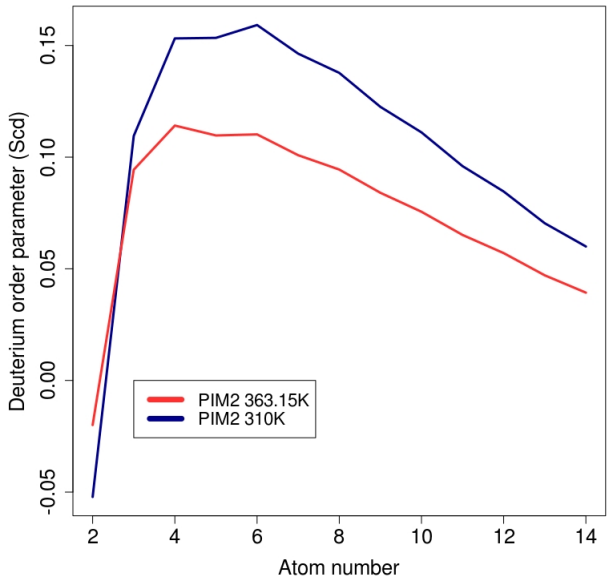

Acyl chain 2

Figure 5: Deuterium order parameters of PIM_2 bilayer acyl chains at different temperatures. y-axis represents the deuterium order parameter and the x-axis represents the atom number.

Deuterium order parameters were calculated to analyze how ordered were the acyl chains of the PIM_2 bilayer system and the temperature influence on it, shown in Figure 3.1.3. Both acyl chain 1, shown in the Figure 3.1.3, and acyl chain 2, Figure 3.1.3, are less ordered at 363.15 K. Once more ordered acyl chains are indicative that the membrane is directed toward the gel phase, it is a coherent result that indicates a PIM_2 bilayer at fluid state at 363.15K. It is interesting to note that, for lipid acyl chains, the correlation of time and order parameters related to the molecular overall motion are the same for all methylene and methyl groups. Both acyl chains 1 and 2, in both temperatures, are more ordered at the beginning of the chain, closest to the head groups. It is expected, once that chain conformation and *trans- gauche* isomerism rate show a flexibility gradient, raising from the first chain methylene to the terminal methyl group. As *trans-gauche* isomerism increases toward and above the melting temperature, it is expected a reduction in the S_{cd} values related to the model at 363.15 K, compared to the values observed at 310 K [42].

Lateral Diffusion

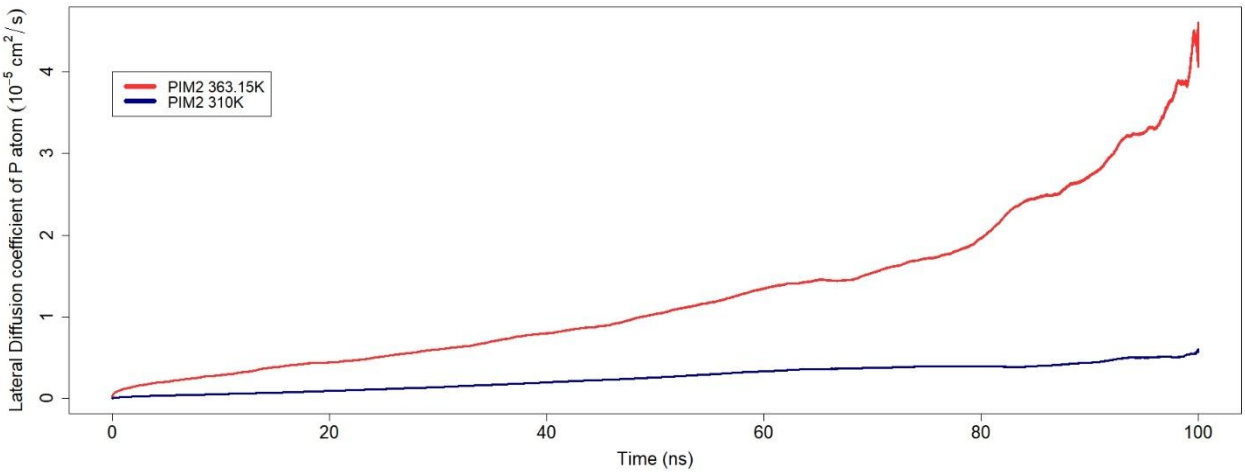

Figure 6: Lateral diffusion coefficient of the PIM_2 bilayer in 100 ns MD simulations at different temperatures. y-axis represents the MSD in nm and the x-axis represents the time in ns.

The Mean squared displacement (MSD) of the lateral diffusion coefficient of the P atom was calculated to analyze the lateral diffusion in PIM_2 and the temperature influence on it (Figure 3.1.4). The lateral diffusion coefficient of PIM_2 at 363.15 K reaches above 4×10^{-5} cm^2/s, while at 310 K it reaches 0.7×10^{-5} cm^2/s. For entire dimyristoyl phosphatidylcholine molecules the lateral diffusion value is 17×10^{-8} cm^2 in the fluid phase. When the lipid is in the gel phase, this value is equivalent to 7×10^{-8} cm^2/s (considering DMPC melting temperature equivalent to 297.15 K). The typical increase of lateral diffusion as the membrane transits from gel to fluid phase was also observed to PIM_2 bilayer. It is coherent to what is expected, once the phase transition temperature makes the membrane more flexible, therefore increasing the lateral diffusion coefficient.

RMSD

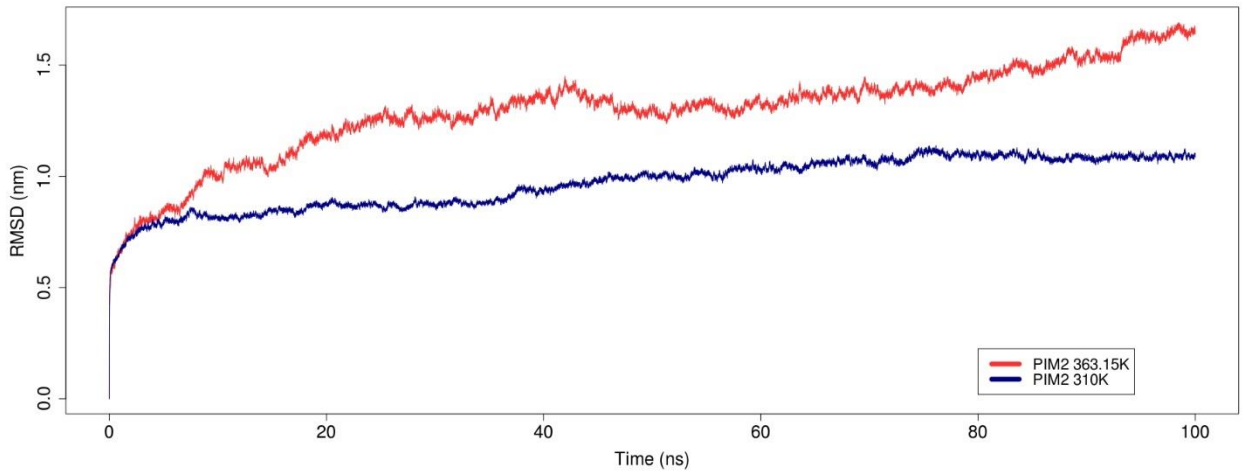

Figure 7: RMSD of PIM $_2$ bilayer in the 100.0 ns MD simulations at different temperatures. y-axis represents the RMSD in nm and the x-axis represents the time in ns.

The RMSD of the PIM $_2$ bilayer was calculated to analyze its stability and the influence of different temperatures on it, shown in Figure 3.1.5. PIM $_2$ bilayers at 310 K has a lower RMSD that stabilized from around 80 ns at around 1 nm, which shows the stability of the structure. The lipid bilayer stability is expected as the *M. tuberculosis* membrane exists at this temperature in the lungs and thus it should be ordered. PIM $_2$ at 363.15 K showed a higher RMSD, reaching over 1.5 nm at the end of the simulation, while still raising, and did not stabilize. Therefore, this higher and more unstable RMSD from PIM $_2$ at 363.15K agrees what is expected for the fluid state, which reinforces a disordering process above the lipid phase transition temperature.

Analysis of PIM $_2$ bilayer at different temperatures

All MD simulation data related to PIM $_2$ bilayer at 363.15 K are consistent to a highly disordered structure, typical of systems at temperatures above to their correspondent phase transition temperature. Data also corroborates to a higher membrane permeability,

as observed by the water penetration into the bilayer. It is known that the lipid arrangement, order and fluidity in the mycobacterial membrane modulate its properties, such as the nutrients uptake, protein transport and drug interaction profiles [43]. Indeed, mycobacteria membranes lipid arrangement is consisted by a gradient of, or an intermittent ordered-disordered lipid regions and domains [43], which is also attributed to the duration of treatment and resistance. Here, it is interesting to note that, despite saturated lipids in gel phase are unusual in cellular membranes, it is precisely the mycobacterial membrane acyl chains saturations that lead to a high conformational freedom and acyl chains fluctuations on it [43]. The primary results concerning the study of PIM_2 bilayer model in two different temperatures agrees with the expected state-of-phase behaviour, and allows further studies which will contribute to the design of simple and accurate tests evolving the mycobacterial membrane role in TB processes, resistance and therapy. Considering the fact that, in the lungs temperature, 310 K, PIM_2 bilayer model behaves as a gel-ordered membrane, such as in mycobacteria, and this state-of-phase is also related to a close relationship with experimental results [38], this was the chosen temperature to assays related to PIM_2 bilayer and vesicular formation, as well as the protein-membrane interaction approaches, which are reported as follows.

PIM_2 Bilayer Formation

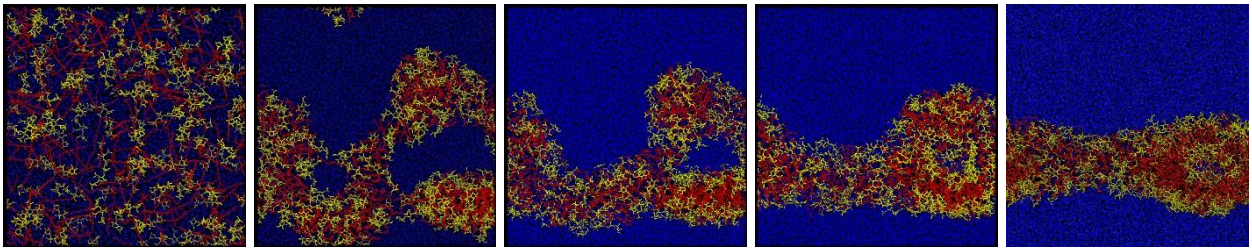

(a) 0 ns (b) 5 ns EQ 1 (c) 10 ns EQ 1 (d) 10 ns EQ 2 (e) 100 ns MD

Figure 8: Snapshots of Molecular Dynamics simulation of PIM_2 aggregation in water. Lipid head groups (yellow); acyl chains (red); water (blue). (a) is the first frame. (b) is a snapshot from EQ 1. (c) is the final structure from EQ 1. (d) is the final structure from EQ2. (e) is the final structure from production MD.

In order to test the PIM_2 property of aggregation in water, we performed a simulation with the lipids starting at random positions. Snapshots of the aggregation process can be seen at Figure 3.3. It started with 128 lipids randomly distributed in the box (Figure 3.3). During the first 10 ns equilibration phase (EQ 1), one aggregate containing two vesicular portions was observed at 5 ns (Figure 3.3), and at the end of this phase, all lipids form one aggregate including a vesicular portion, as shown in Figure 3.3. At the end of the second 10 ns equilibration the structure takes a more clear horizontal form containing one more defined vesicular portion, as shown in Figure 3.3. Finally, at the end of the 100 ns production phase, there is the final aggregate including a well defined vesicular portion containing one pore-like defect (Figure 3.3). Sprott and co-workers (2004) [18] reported the experimental mycobacteria lipid-based liposomes formation only at conditions above each lipid phase transition temperatures. Below the phase transition temperature, they observed clumps of lipids. In our MD simulation model, however, it was possible to observe unstable vesicular aggregates that, at the second equilibration,

showed a "finger" shape. Studies of charged species permeation in membrane show the formation of a water process finger defects in the membrane [44]. Other explanation for the observed defect is the transient pore formation mechanism, which stability depends to the proton transport through membrane [45]. Also, systems with self-assembly properties may require even longer simulation to relax to the final configuration [46], which may also explain why the other portions of the aggregate have not a well defined form. Despite the reported above, considering that liposomes which contains PIM lipids are useful to the proinflammatory cytokines production [18], the obtained results may contribute to MD simulations of vesicles containing associations between PIM_2 and other lipids.

PIM_2 bilayer with insertion of Tap

In order to validate the PIM_2 model, we analyzed its behavior with a transmembrane protein found in *M. tuberculosis* IM, Tap efflux pump. For this end, we compare the structural differences of PIM_2 bilayer during the MD simulation with Tap protein inserted (Figure 3.4) with the MD simulation of the PIM_2 bilayer at 310 K previously discussed (Figure 3.4), once both simulation were performed at the same temperature.

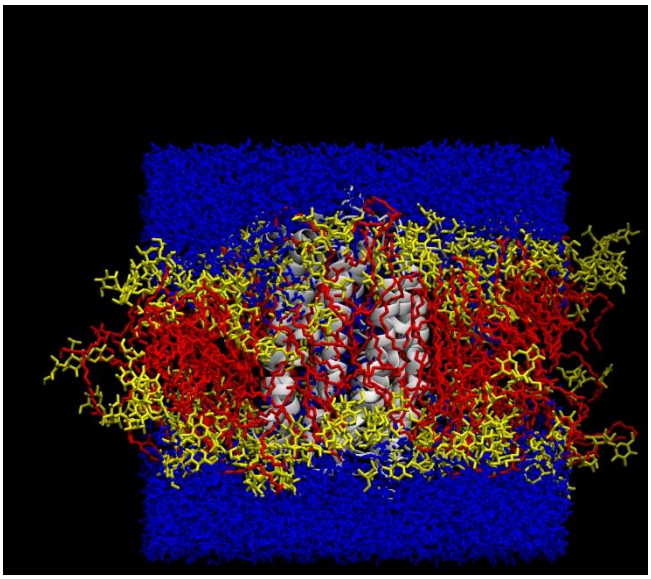

Figure 9: Final structure of PIM_2 bilayer in two different MD simulations, (a) bilayer at 310 K, (b) bilayer with Tap protein insertion at 310 K. Lipid head groups (yellow), Lipid acyl chains (red), water (blue) and protein (white).

Partial Density

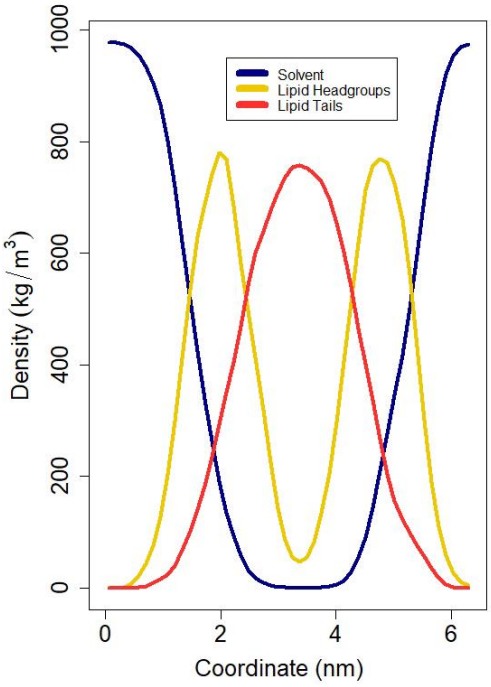

PIM $_2$

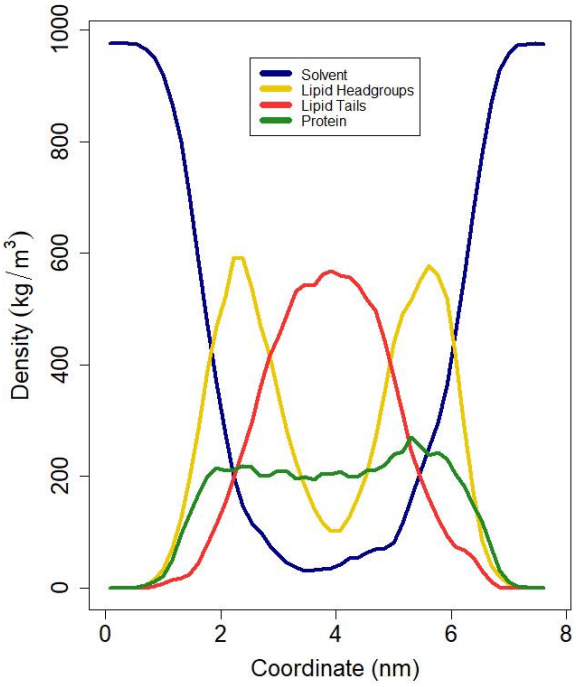

PIM $_2$ with Tap

Figure 10: Partial density of PIM $_2$ bilayer without (a) and with Tap protein insertion (b). y-axis represents the density and the x-axis represents the coordinates. Lipid headgroups correspond to the inositol phosphate and mannosides polar groups, while the Lipid tails correspond to acyl chains hydrophobic region, the protein correspond to Tap and the solvent correspond to the water.

The partial density shown in Figure 3.4.1 was calculated to analyze the distribution of four regions (lipid head groups, lipid acyl chain, water and protein) in the PIM $_2$ bilayer system and the effect of Tap protein insertion on it. In both systems, water stayed in the extremes of the z-axis, did not penetrate toward the acyl chains, and interacted with the head groups. Although there is water inside the protein in the system with Tap (Figures 3.4.1 and 3.4), as expected. The protein was across the whole bilayer. Lipid headgroups

and acyl chains were less dense in the system with Tap, but this system also had a thicker bilayer, mainly at the interface between lipid headgroups and acyl chains. An experimental study concerning changes in membrane thickness induced by transmembrane peptides reported the peptide orientation and the bilayer adaptation to the hydrophobic mismatch as contributing factors to these variations [47]. The membrane thickness may be observed if the lenght of the peptide is higher than the bilayer hydrophobic thickness and, consequently, an adjustment of the acyl chains is performed in order to relax the hydrophobic mismatch between the peptide lenght and the effective membrane thickness [47]. The contributing factors proposed by Grage and co-workers [47] may be considered to explain the Tap protein effect on PIM_2 bilayer partial density, reinforcing the reliability of the membrane model for MD simulation studies.

Bilayer Thickness

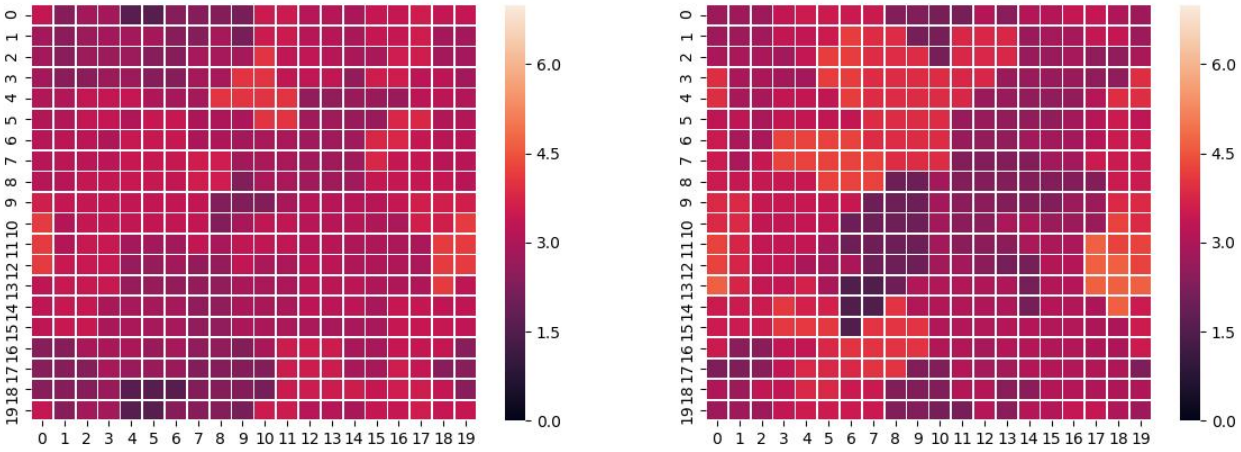

PIM_2 PIM_2 with Tap

Figure 11: Bilayer Thickness of PIM_2 bilayer with Tap protein insertion (b) and without it (a). y-axis and x-axis are a grid box representing the PIM_2 bilayer area. The z-axis is

represented by a color gradient indicating the thickness (nm), where lighter colors are thicker regions.

The thickness of PIM_2 bilayer system with Tap protein insertion, shown in Figure 3.4.2, was calculated to analyze the difference of its thickness and the influence of Tap insertion on it. The PIM_2 bilayer with Tap had 11.5% of its structure thicker than 4 nm, where the thickest region is 4.66 nm. The bilayer with Tap is thicker in comparison to PIM_2 bilayer without Tap, that had 4.5% of its structure thicker than 4 nm, where thickest region is 4.13 nm. These thicker regions can be explained because the system is more crowded, and therefore had to agglutinate more. But it can be observed that the thickest regions of PIM_2 with Tap are in extreme regions, which are far from the protein. The bilayer structure around the protein is compact and stable near the protein, which is the most important when studying proteins inserted in membranes, and also shows an adequate behavior that reinforces our bilayer as a efficient *M. tuberculosis* IM model. Thickness results corroborates to the partial density data, as well as to the discussion concerning the possible contributing factors to increase the membrane thickness cited by Grage and co-workers (2016) [47].

Deuterium Order Parameters

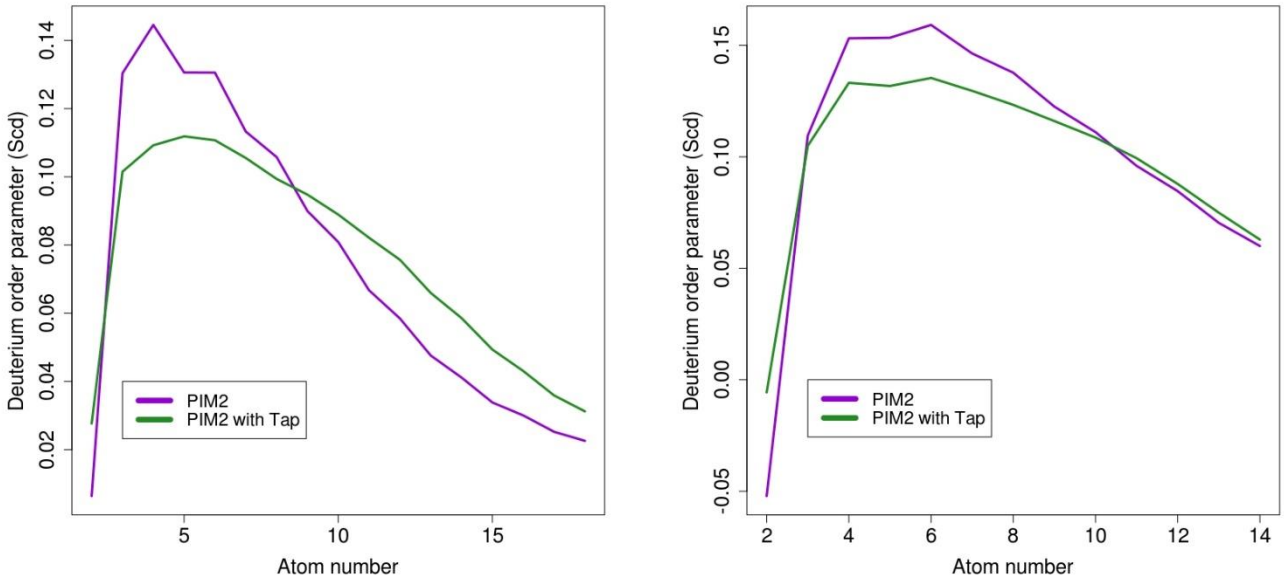

Acyl chain 1

Acyl chain 2

Figure 12: Deuterium order parameters of PIM_2 bilayer acyl chains with and without Tap protein insertion. y-axis represents the deuterium order parameter and the x-axis represents the atom number.

Deuterium order parameters were calculated to analyze how ordered were the acyl chains of the PIM_2 bilayer with Tap protein insertion and the influence of Tap insertion on it (Figure 3.4.3). A higher deuterium order means a more ordered structure. Both acyl chains have higher deuterium parameters in PIM_2 without Tap in comparison to PIM_2 with Tap on the first atoms, and reverse it and the end, more close to the hydrophobic nucleus, more evident on acyl chain 1. This may indicate the acyl chains atoms closer to the hydrophobic nucleus are more affected and therefore organized in the structure with the Tap inserted inside. While, probably the crowdedness can affect the atoms closer to the headgroup, which are charged. Here, it is also possible to correlate the Tap effect on PIM_2 bilayer order parameters to the adjustment of acyl chains to relax to the lipid-protein hydrophobic mismatch, cited in Partial Density section [47].

Lateral Diffusion

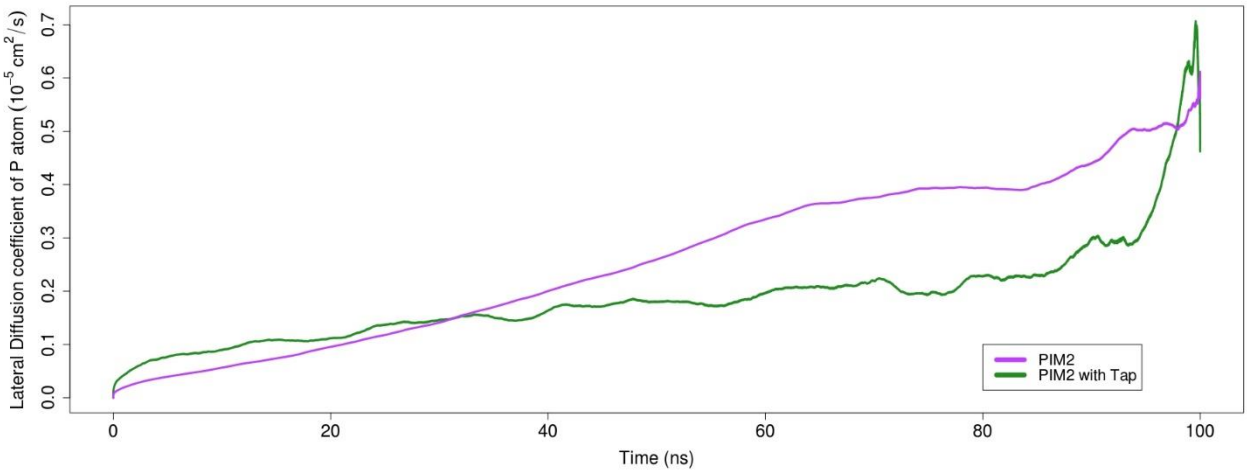

Figure 13: Lateral diffusion coefficient of the PIM_2 bilayer in 100 ns MD simulations with and without Tap protein insertion. y-axis represents the MSD in nm and the x-axis represents the time in ns.

The MSD of the lateral diffusion coefficient of the P atoms were calculated to analyze the lateral diffusion in PIM_2 bilayer system with Tap protein insertion and the

influence of Tap insertion on it, as shown in the Figure 3.4.4. The lateral diffusion of PIM_2 with Tap insertion, reaches around 0.4×10^{-5} cm^2/s, and is lower than PIM_2 without the protein, that reaches around 0.7×10^{-5} cm^2/s. This indicates that the protein insertion makes the bilayer more ordered. Considering the partial density data, deuterium order parameters analyses, as well as the behavior concerning the membrane thickness, the Tap-induced reduction in the lipid lateral diffusion was expected. It seems that the main order effect induced by Tap occurs at membrane interface-polar regions, followed by the adjustment at hydrophobic regions to mismatch relaxation.

Bilayer RMSD

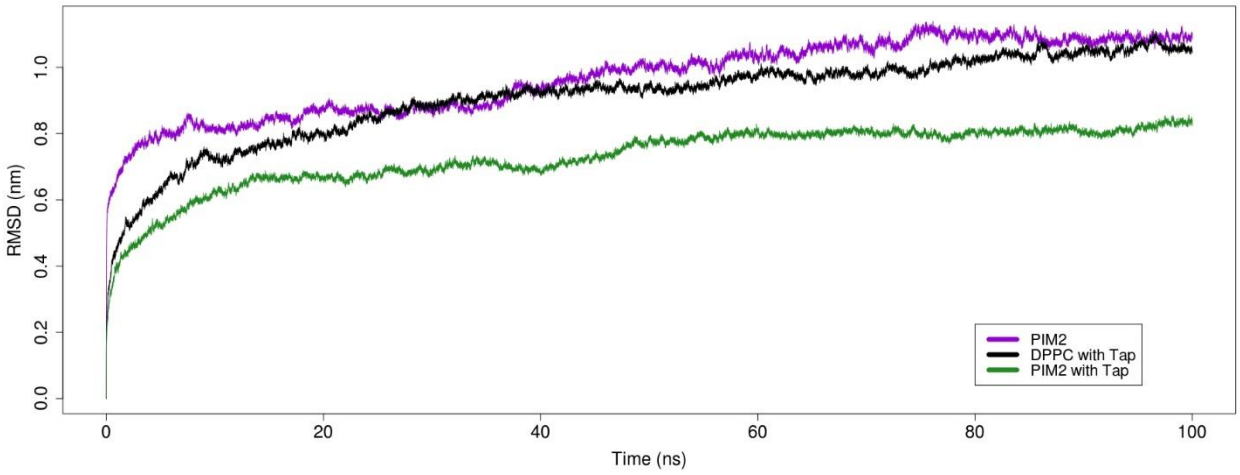

Figure 14: RMSD of PIM_2 bilayer in 100 ns MD simulations with and without Tap protein insertion, and also of a DPPC bilayer with Tap protein insertion. y-axis represents the RMSD in nm and the x-axis represents the time in ns.

The RMSD of PIM_2 bilayer with Tap (Figure 3.4.5) allowed the analysis of the effect of the protein in the membrane model stability. The RMSD of PIM_2 bilayer without Tap stabilized from around 80 ns at around 1 nm, as previously analyzed. PIM_2 bilayer with Tap showed a lower RMSD that stabilized from around 50 ns at around 0.7 nm. This shows a higher stabilization of the PIM_2 model in the presence of Tap.

For further comparison, we added the analysis of the DPPC bilayer with the insertion of the same Tap model, where the DPPC membrane stabilized at around 0.95 nm from 90 ns. This indicates a higher stabilization of PIM_2 with Tap in comparison to DPPC with Tap. This results show the lowest RMSD in PIM_2 bilayer model with the Tap insertion, and therefore reinforces the PIM_2 bilayer as a *M. tuberculosis* IM model, that has transmembrane proteins like Tap naturally inserted in it.

Protein RMSD

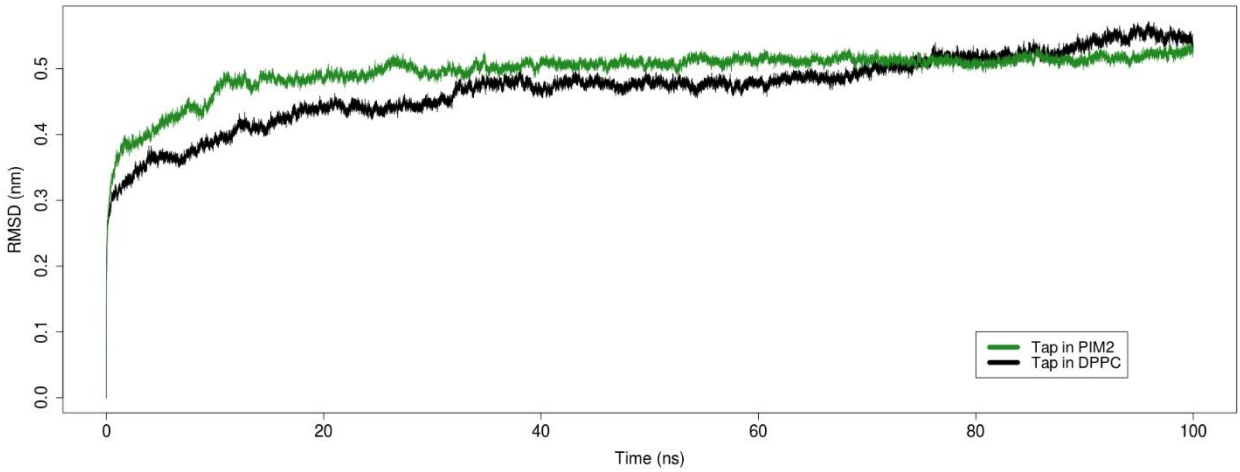

Figure 15: RMSD of Tap Helix during 100 ns MD simulations in PIM_2 and DPPC bilayers. y-axis represents the RMSD in nm and the x-axis represents the time in ns.

Finally, we analyze the stability of Tap inserted in the PIM_2 bilayer. For this end, we use RMSD calculations for the MD simulations of both Tap in PIM_2 and Tap in DPPC, both at 310 K, shown in the Figure 3.4.6. The atoms from the helices were accounted, once they are a more rigid structure than the turns and are the most predominant [17]. Tap in DPPC did not stabilize until the end, with a RMSD over 5 nm and higher than Tap in PIM_2. Tap in PIM_2 has a higher RMSD at first, but it was stabilized early, at around 0.5 nm from 15 ns. This stabilization reinforces the PIM_2 role of anchor lipid, allowing the protein typical from *M. tuberculosis* IM to stabilize, and

therefore maintain a functional structure. This result show that the choice of the appropriate lipid to compose the membrane can affect the transmembrane protein behavior. Therefore the lipid type and model should be carefully chosen. This final data reinforces the necessity of models for PIMs lipids.

Analysis of PIM_2 bilayer with insertion of Tap

Density, thickness and deuterium order parameters analyses point out that the bilayer is thicker with the insertion of Tap mainly at the regions further away from the protein, possibly because of how the protein made the system more crowded, as well as ordering effects at polar-interfacial regions and mismatch adjustments at the hydrophobic one. Lateral diffusion and RMSD are lower with Tap insertion, which shows that the membrane is overall more well structured with a protein and a suitable inner membrane model for transmembrane proteins. Which can also be reinforced by how the RMSD of PIM_2 with Tap is lower than DPPC with Tap, and how Tap is more stable in PIM_2 then in DPPC.

Conclusion

Is this work we performed the first simulations of PIM_2 bilayer as a model for *M. tuberculosis* IM. Our results showed that the behavior of our bilayer PIM_2 model at different temperatures was coherent for lipids in both gel and fluid phases, showing viability to study the temperature dependence of this membrane. This is important since many conditions can be simulated, specially between the natural body temperature and more extreme conditions similar temperatures above the phase transition. Also, a spontaneous aggregation process was observed, which shows the ability of the model to self-assemble in a bilayer, and allows studies concerning vesicular systems based on PIM_2 mixtures with other lipids as well as those related to the transient pore formation mechanism in the presence of other agents (anti-TB drugs, for example).

The behavior of the bilayer with the insertion of Tap protein also highlights it as a reliable IM model. The bilayer was even more stable with the insertion of the protein, even when compared to a DPPC bilayer with Tap insertion. The protein also reached stability faster in the PIM_2 bilayer than in a DPPC bilayer. Therefore, we conclude that this model can be used for studies using trans membrane proteins typical of membranes rich in PIM_2 lipids, including further analysis of Tap efflux pump. Molecular Dynamics studies using Tap has been published, and therefore a model that is adequate for insertion of this protein is an important step. Also, this model can be employed to study others trans membrane proteins, nanoparticle based drug delivery systems, and others process that occurs in the *M. tuberculosis* membrane.

Acknolodgement

The authors thank the support from the Brazilian Agencies CNPq, CAPES and FAPERGS. JLRS thanks the Coordenação de Aperfeiçoamento de Pessoal de Nível Superior (CAPES), Finance Code 001. Without the public funding this research would be impossible.

References

(1) World Health Organization, Global tuberculosis report 2020 ; 2020.

(2) Gygli, S. M.; Borrell, S.; Trauner, A.; Gagneux, S. Antimicrobial resistance in Mycobac-terium tuberculosis: mechanistic and evolutionary perspectives. FEMS microbiology reviews 2017, 41, 354-373.

(3) Bansal-Mutalik, R.; Nikaido, H. Mycobacterial outer membrane is a lipid bilayer and the inner membrane is unusually rich in diacyl phosphatidylinositol dimannosides. Pro-ceedings of the National Academy of Sciences of the United States of America 2014, 111, 4958-4963.

(4) Sartain, M. J.; Dick, D. L.; Rithner, C. D.; Crick, D. C.; Belisle, J. T. Lipidomic analyses of Mycobacterium tuberculosis based on accurate mass measurements and the novel Mtb LipidDB. Journal of Lipid Research 2011, 52, 861-872.

(5) Guerin, M. E.; Kordulakova, J.; Alzari, P. M.; Brennan, P. J.; Jackson, M. Molecu-
lar Basis of Phosphatidyl-myo-inositol Mannoside Biosynthesis and Regulation in My-cobacteria. The Journal of Biological Chemistry 2010, 285, 33577-33583.

(6) Sancho-Vaello, E.; Albesa-Jove, D.; Rodrigo-Unzueta, A.; Guerin, M. E. Structural basis of phosphatidyl-myo-inositol mannosides biosynthesis in mycobacteria. Biochimica Et Biophysica Acta. Molecular and Cell Biology of Lipids 2017, 1862, 1355-1367.

(7) Chatterjee, D.; Lowell, K.; Rivoire, B.; McNeil, M. R.; Brennan, P. J. Lipoarabinoman-nan of Mycobacterium tuberculosis. Capping with mannosyl residues in some strains. The Journal of Biological Chemistry 1992, 267, 6234-6239.

(8) Khoo, K. H.; Dell, A.; Morris, H. R.; Brennan, P. J.; Chatterjee, D. Structural de -nition of acylated phosphatidylinositol mannosides from Mycobacterium tuberculosis: de nition of a common anchor for lipomannan and lipoarabinomannan. Glycobiology 1995, 5, 117-127.

(9) Bovigny, C.; Tamo, G.; Lemmin, T.; Ma no, N.; Dal Peraro, M. LipidBuilder: A

Frame-work To Build Realistic Models for Biological Membranes. Journal of Chemical Infor-mation and Modeling 2015, 55, 2491-2499.

(10) Baumgart, T.; Hess, S. T.; Webb, W. W. Imaging coexisting uid domains in biomem-brane models coupling curvature and line tension. Nature 2003, 425, 821-824.

(11) de Vries, A. H.; Mark, A. E.; Marrink, S. J. Molecular Dynamics Simulation of the Spontaneous Formation of a Small DPPC Vesicle in Water in Atomistic Detail. Journal of the American Chemical Society 2004, 126, 4488-4489.

(12) Feller, S. E. Molecular dynamics simulations of lipid bilayers. Current Opinion in Col-loid & Interface Science 2000, 5, 217-223.

(13) Frigini, E. N.; Lopez Cascales, J. J.; Porasso, R. D. Molecular dynamics simulations of glyphosate in a DPPC lipid bilayer. Chemistry and Physics of Lipids 2018, 213, 111-117.

(14) Deserno, M.; Kremer, K.; Paulsen, H.; Peter, C.; Schmid, F. In From Single Molecules

to Nanoscopically Structured Materials; Basche, T., Mullen, K., Schmidt, M., Eds.; Springer International Publishing: Cham, 2014; pp 237-283.

(15) Sandhu, P.; Akhter, Y. The drug binding sites and transport mechanism of the RND pumps from Mycobacterium tuberculosis: Insights from molecular dynamics simula-tions. Archives of Biochemistry and Biophysics 2016, 592, 38-49.

(16) Cloete, R.; Kapp, E.; Joubert, J.; Christo els, A.; Malan, S. F. Molecular modelling and simulation studies of the Mycobacterium tuberculosis multidrug e ux pump protein Rv1258c. PLOS ONE 2018, 13, e0207605.

(17) Scaini, J. L. R.; Camargo, A. D.; Seus, V. R.; von Groll, A.; Werhli, A. V.; da Silva, P. E. A.; Machado, K. D. S. Molecular modelling and competitive inhibition of a Mycobac-terium tuberculosis multidrug-resistance e ux pump. Journal of Molecular Graphics & Modelling 2019, 87, 98-108.

(18) Sprott, G. D.; Dicaire, C. J.; Gurnani, K.; Sad, S.; Krishnan, L. Activation of Dendritic Cells by Liposomes Prepared from Phosphatidylinositol Mannosides from Mycobac-terium bovis Bacillus Calmette-Guerin and Adjuvant Activity In Vivo. Infection and Immunity 2004, 72, 5235-5246.

(19) Siewert J. Marrink, .; Erik Lindahl, ^.;a Olle Edholm, ^.;a ; Mark^Aa, A. E. Simulation of the Spontaneous Aggregation of Phospholipids into Bilayers. 2001; https://pubs. acs.org/doi/abs/10.1021/ja0159618.

(20) Siddiqi, N.; Das, R.; Pathak, N.; Banerjee, S.; Ahmed, N.; Katoch, V. M.; Hasnain, S. E. Mycobacterium tuberculosis isolate with a distinct genomic identity overexpresses a tap-like e ux pump. Infection 2004, 32, 109-111.

(21) Jiang, X.; Zhang, W.; Zhang, Y.; Gao, F.; Lu, C.; Zhang, X.; Wang, H. Assessment of e ux pump gene expression in a clinical isolate Mycobacterium tuberculosis by real-time reverse transcription PCR. Microbial Drug Resistance (Larchmont, N.Y.) 2008, 14, 7-11.

(22) Sud, M.; Fahy, E.; Cotter, D.; Brown, A.; Dennis, E. A.; Glass, C. K.; Merrill Jr, A. H.; Murphy, R. C.; Raetz, C. R.; Russell, D. W. et al. Lmsd: lipid maps structure database. Nucleic acids research 2006, 35, D527-D532.

(23) Hanwell, M. D.; Curtis, D. E.; Lonie, D. C.; Vandermeersch, T.; Zurek, E.; Hutchi-son, G. R. Avogadro: an advanced semantic chemical editor, visualization, and analysis platform. Journal of cheminformatics 2012, 4, 17.

(24) Koziara, K. B.; Stroet, M.; Malde, A. K.; Mark, A. E. Testing and validation of the Automated Topology Builder (ATB) version 2.0: prediction of hydration free enthalpies. Journal of computer-aided molecular design 2014, 28, 221-233.

(25) Berger, O.; Edholm, O.; Jahnig, F. Molecular dynamics simulations of a uid bilayer of dipalmitoylphosphatidylcholine at full hydration, constant pressure, and constant temperature. Biophysical Journal 1997, 72, 2002-2013.

(26) Oostenbrink, C.; Villa, A.; Mark, A. E.; Van Gunsteren, W. F. A biomolecular force eld based on the free enthalpy of hydration and solvation: the GROMOS force- eld parameter sets 53A5 and 53A6. Journal of computational chemistry 2004, 25, 1656- 1676.

(27) Pall, S.; Abraham, M. J.; Kutzner, C.; Hess, B.; Lindahl, E. Tackling exascale software challenges in molecular dynamics simulations with GROMACS. International Confer-ence on Exascale Applications and Software. 2014; pp 3-27.

(28) Abraham, M. J.; Murtola, T.; Schulz, R.; Pall, S.; Smith, J. C.; Hess, B.; Lindahl, E.

GROMACS: High performance molecular simulations through multi-level parallelism from laptops to supercomputers. SoftwareX 2015, 1, 19-25.

(29) A nsa, J. A.; Blokpoel, M. C. J.; Otal, I.; Young, D. B.; De Smet, K. A. L.; Mart n, C. Molecular Cloning and Characterization of Tap, a Putative Multidrug E ux Pump Present in Mycobacterium fortuitum and Mycobacterium tuberculosis. Journal of Bac-teriology 1998, 180, 5836-5843.

(30) De Rossi, E.; Arrigo, P.; Bellinzoni, M.; Silva, P. A. E.; Mart n, C.; A nsa, J. A.; Guglierame, P.; Riccardi, G. The multidrug transporters belonging to major facilitator superfamily in Mycobacterium tuberculosis. Molecular Medicine 2002, 8, 714-724.

(31) Peter Tieleman, State-of-the-art computational models of lipids and membrane pro-teins. 2015; http://wcm.ucalgary.ca/tieleman/downloads.

(32) Nagle, J. Area/lipid of bilayers from NMR. Biophysical journal 1993, 64, 1476-1481.

(33) Kandt, C.; Ash, W. L.; Peter Tieleman, D. Setting up and running molecular dynamics simulations of membrane proteins. Methods 2007, 41, 475-488.

(34) Justin Lemkul, KALP-15 in DPPC. 2015; http://www.bevanlab.biochem.vt.edu/Pages/Personal/justin/gmx-tutorials/membrane_protein/01_pdb2gmx.html.

(35) R Core Team, R: A language and environment for statistical computing; 2013.

(36) RStudio Team, RStudio: Integrated Development Environment for R; RStudio, Inc.: Boston, MA, 2015.

(37) Allen, W. J.; Lemkul, J. A.; Bevan, D. R. GridMAT-MD: a grid-based membrane analysis tool for use with molecular dynamics. Journal of Computational Chemistry 2009, 30, 1952-1958.

(38) Leonard, A.; Escrive, C.; Laguerre, M.; Pebay-Peyroula, E.; Neri, W.; Pott, T.; Katsaras, J.; Dufourc, E. J. Location of Cholesterol in DMPC Membranes. A Comparative
Study by Neutron Di raction and Molecular Mechanics Simulation. Langmuir 2001, 17, 2019-2030.

(39) Simon, S. A.; McIntosh, T. J. Methods in Enzymology; Biomembranes Part O: Protons and Water: Structure and Translocation; Academic Press, 1986; Vol. 127; pp 511-521.

(40) Kuklin, A.; Zabelskii, D.; Gordeliy, I.; Teixeira, J.; BrAzlet, A.; Chupin, V.; Cherezov, V.; Gordeliy, V. On the Origin of the Anomalous Behavior of Lipid Membrane Properties in the Vicinity of the Chain-Melting Phase Transition. Scienti c Reports 2020, 10 .

(41) Zhang, R.; Sun, W.; Tristram-Nagle, S.; Headrick, R. L.; Suter, R. M.; Nagle, J. F. Critical Fluctuations in Membranes. Physical Review Letters 1995, 74, 2832-2835, Publisher: American Physical Society.

(42) Moser, M.; Marsh, D.; Meier, P.; Wassmer, K. H.; Kothe, G. Chain con guration and exibility gradient in phospholipid membranes. Comparison between spin-label electron spin resonance and deuteron nuclear magnetic resonance, and identi cation of new conformations. Biophysical Journal 1989, 55, 111-123.

(43) Adhyapak, P.; Srivatsav, A. T.; Mishra, M.; Singh, A.; Narayan, R.; Kapoor, S. Dynamical Organization of Compositionally Distinct Inner and Outer Membrane Lipids of Mycobacteria. Biophysical Journal 2020, 118, 1279-1291.

(44) Shinoda, W. Permeability across lipid membranes. Biochimica et Biophysica Acta (BBA) - Biomembranes 2016, 1858, 2254-2265.

(45) Nagle, J. F.; Dilley, R. A. Models of localized energy coupling. Journal of Bioenergetics and Biomembranes 1986, 18, 55-64.

(46) Bordin, J. R.; Krott, L. B. Con nement e ects on the properties of Janus dimers.

Physical Chemistry Chemical Physics 2016, 18, 28740-28746.

(47) Grage, S. L.; Afonin, S.; Kara, S.; Buth, G.; Ulrich, A. S. Membrane Thinning and Thickening Induced by Membrane-Active Amphipathic Peptides. Frontiers in Cell and Developmental Biology 2016, 4, 65.

8 Manuscrito III

Mefloquine synergism with anti-tuberculosis drugs and correlation to membrane effects: biologic, spectroscopic and molecular dynamics simulations studies

Marinalva C. dos Santos, João L. R. Scaini, Márcio V. C. Lopes, Beatriz G. Rodrigues, Nichole O. Silva, Carla R. L. Borges, Sandra C. dos Santos, Karina S. Machado, Adriano V. Werhli, Pedro E. A. da Silva, Maria C. S. Lourenço, Emerson T. da Silva, Marcus V. N. de Souza, Vânia R. de Lima, Raoni S. B. Gonçalves

Figura 5: Resumo Gráfico do Artigo III

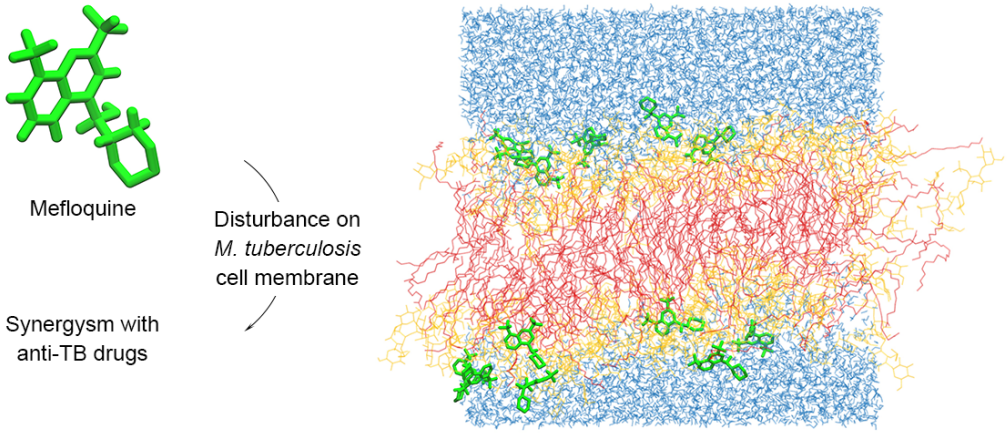

Imagem resume de forma gráfica a hipótese do artigo, de que a mefloquina promove sinergismo com antimicrobianos utilizados contra a TB através de distúrbios causados na membrana celular da *M. tuberculosis*. Essa hipótese foi testada utilizando o modelo de membrana de PIM2 para *M. tuberculosis* desenvolvida no Manuscrito II na Seção 7.

› Bioorg Chem. 2021 Mar 2;110:104786. doi: 10.1016/j.bioorg.2021.104786. Online ahead of print.

Mefloquine synergism with anti-tuberculosis drugs and correlation to membrane effects: Biologic, spectroscopic and molecular dynamics simulations studies

Marinalva Cardoso Dos Santos [1], João Luís Rheingantz Scaini [2], Márcio Vinicius Costa Lopes [3], Beatriz Gonçalves Rodrigues [1], Nichole Osti Silva [1], Carla Roberta Lopes Borges [1], Sandra Cruz Dos Santos [1], Karina Dos Santos Machado [4], Adriano Velasque Werhli [4], Pedro Eduardo Almeida da Silva [5], Maria C S Lourenço [6], Emerson T da Silva [7], Marcus V N de Souza [7], Vânia Rodrigues de Lima [8], Raoni Schroeder B Gonçalves [9]

Affiliations + expand

PMID: 33740676 DOI: 10.1016/j.bioorg.2021.104786

Abstract

Studies displaying the combination of mefloquine (MFL) with anti-tuberculosis (TB) substances are limited in the literature. In this work, the effect of MFL-association with two first-line anti-TB drugs and six fluoroquinolones was evaluated against Mycobacterium tuberculosis drug resistant strains. MFL showed synergistic interaction with isoniazid, pyrazinamide, and several fluoroquinolones, reaching fractional inhibitory concentration indexes (FICIs) ranging from 0.03 to 0.5. In order to better understand the observed results, two approaches have been explored: (i) spectroscopic responses attributed to the effect of MFL on physicochemical properties related to a liposomal membrane model composed by soybean asolectin; (ii) molecular dynamics (MD) simulation data regarding MFL interaction with a membrane model based on PIM_2, a lipid constituent of the mycobacterial cell wall. FTIR and NMR data showed that MFL affects expressively the region between the phosphate and the first methylene groups of soybean asolectin membranes, disordering these regions. MD simulations results detected high MFL density in the glycolipid interface and showed that the drug increases the membrane lateral diffusion, enhancing its permeability. The obtained results suggest that synergistic activities related to MFL are attributed to its effect of lipid disorder and membrane permeability enhancement.

Keywords: Drug repurposing; Fluoroquinolones; Mefloquine; Membrane interaction; Molecular dynamics; Tuberculosis.

Copyright © 2021 Elsevier Inc. All rights reserved.

O artigo foi aprovado pela revista “Bioorganic Chemistry”.

Mefloquine synergism with anti-tuberculosis drugs and correlation to membrane effects: biologic, spectroscopic and molecular dynamics simulations studies

Marinalva Cardoso dos Santos[2], João Luís Rheingantz Scaini[3,4], Márcio Vinicius Costa Lopes[1], Beatriz Gonçalves Rodrigues[2], Nichole Osti Silva[2], Carla Roberta Lopes Borges[2], Sandra Cruz dos Santos[2], Karina dos Santos Machado[3], Adriano Velasque Werhli[3], Pedro Eduardo Almeida da Silva[4], Maria C. S. Lourenço[6], Emerson T. da Silva[5], Marcus V. N. de Souza[5], Vânia Rodrigues de Lima[2]*, Raoni Schroeder B. Gonçalves[1]*

[1] Instituto de Química, Universidade Federal do Rio de Janeiro, Av. Athos da Silveira Ramos, 149 - Cidade Universitária, Rio de Janeiro – RJ, 21941-909 - Brazil.

[2] Grupo de Investigação de Interações Moleculares em Membranas, Escola de Química e Alimentos, Programa de Pós-Graduação em Química Tecnológica e Ambiental,

[3] COMBI-Lab, Grupo de Biologia Computacional, Centro de Ciências Computacionais, Universidade Federal do Rio Grande - FURG, Av. Itália, km 8, Campus Carreiros, 96203-900, Rio Grande, RS, Brazil.

[4] Faculdade de Medicina, Universidade Federal do Rio Grande - FURG, Av. Itália, km 8, Campus Carreiros, 96203-900, Rio Grande, RS, Brazil.

[5] FioCruz-Fundação Oswaldo Cruz, Instituto de Tecnologia em Fármacos-Far-Manguinhos, Rua Sizenando Nabuco, 100, Manguinhos, 21041-250 Rio de Janeiro, RJ, Brazil.

[6] Instituto de Pesquisas Clínica Evandro Chagas—IPEC, Av. Brasil, 4365, Manguinhos, Rio de Janeiro, Brazil.

Correspondent authors:
raoni.schroeder@ig.ufrj.br
vrlima23@hotmail.com, vanialima@furg.br

Abstract

In this work, the effect of mefloquine (MFL)-association with two first-line anti-TB drugs and six fluoroquinolones was evaluated against *Mycobacterium tuberculosis* drug resistant strains. MFL showed synergistic interaction with isoniazid, pyrazinamide, and several fluoroquinolones, reaching fractional inhibitory concentration indexes (FICIs) ranging from 0.03 to 0.5. Aiming to better understand the observed results, MFL physicochemical influence on lipid bilayers was analyzed by spectroscopic analyses using an ASO liposomes' model, and molecular dynamics (MD) simulation studies were performed using PIM_2 as a membrane model. FTIR and NMR data showed that MFL affects expressively the region between the phosphate and the first methylene groups of soybean asolectin membranes, disordering these regions. MD simulations results detected high MFL density in the glycolipid interface and showed that the drug increases the membrane lateral diffusion, enhancing its permeability. Both, spectroscopic and MD data indicates an enhancement of membrane permeability in the presence of MFL, which could be involved in the observed synergistic activities.

Keywords: mefloquine; fluoroquinolones; tuberculosis; drug repurposing; membrane interaction; molecular dynamics.

Introduction

Tuberculosis (TB) remains one of the top 10 causes of death worldwide and the leading cause among the infectious diseases [1]. According to the World Health Organization (WHO), around 10 million people developed TB in 2018 and more than 1.5 million deaths were caused by this disease. Particularly, the emergence of multidrug-resistant (MDR) TB (resistant to at least isoniazid and rifampicin) and extensively drug-resistant (XDR) TB (resistant to isoniazid, rifampicin, and at least one fluoroquinolone and an injectable agent) makes the TB epidemic an even greater problem. The treatment of these resistant forms is longer, requires the use of less

effective and more toxic drugs and the successful outcome is low, around 50% for MDR-TB and 30% for XDR-TB [2]. In this way, the discovery of more efficient treatment regimens is mandatory towards TB elimination.

During the last years, drug repurposing emerged as an important tool in the fight against TB [3–6]. This strategy is characterized by identifying new applications for approved drugs that are different from their initial scope, and it has the advantage that the pharmacological properties of the substance are known and the drug safety profile is already established [7–10]. In general, these characteristics make the development process faster, being particularly useful for the discovery of new antibiotics [11]. Among the different substances studied for drug repurposing against TB, mefloquine (MFL) has presented interesting results. Besides developed as an antimalarial agent, this substance displays a broad range activity against Gram-positive and Gram-negative bacteria [12–16] as well as against *Mycobacterium* spp [17,18]. Jayaprakash and coworkers [19] reported that MFL has a relatively high activity against nonreplicating persistent *Mycobacterium tuberculosis*. Bermudez and Meek [20] displayed the bactericidal activity of MFL against *M. tuberculosis* in acid and low oxygen media, to simulate the environments found in the phagocyte vacuole and in granulomas, respectively. The authors also demonstrated that MFL is significantly active against intracellular *M. tuberculosis* H37Rv in a macrophage infection model and it is not cytotoxic to the host cell. In a previous work published by our group, we demonstrated that MFL is active against the MDR-TB isolate T113, resistant to isoniazid, rifampicin, ethambutol and ofloxacin and the MIC was the same observed for the susceptible strain H37Rv [21]. Furthermore, it was active *in vivo*, in a murine model of TB after administration by the oral route and displayed an *in vitro* synergistic activity with isoniazid [22].

Herein, considering these encouraging results and the importance of the combination therapy in TB treatment [23,24], in the present study we evaluate the *in vitro* interaction profile of MFL with first-line anti-TB drugs and different

fluoroquinolones against the susceptible strain H37Rv and two resistant isolates of *M. tuberculosis*. Furthermore, based on published results demonstrating that MFL could affect the integrity of prokaryotic membranes [25], we hypothesized that the influence of MFL in the *Mycobacterium* membrane may be an important component in the observed synergistic activities. To further investigate this hypothesis, the interaction between MFL and *M. tuberculosis* membrane was evaluated spectroscopically using a simplified soybean asolectin (ASO)-based membrane model, as well as by molecular dynamics (MD) simulations, through a recently established Phosphatidyl-myo-inositol dimannoside (PIM_2) membrane model [26] following MD protocols for simulations on membrane previously applied on studies of *M. tuberculosis* [27].

Materials and methods

Chemicals

Soybean asolectin, Deuterium oxide (D_2O)/sodium 3-(trimethylsilyl)-[2,2,3,3-2H4]-1-propionate (TSP, 0.05%), tricine and salts were purchased from Sigma Aldrich (St. Louis, MO, USA). Lipid was used without further purification, and all other chemicals were of analytical grade. Gatifloxacin, moxifloxacin, ciprofloxacin, levofloxacin, ofloxacin and sparfloxacin were provided by Xiamen Mchem Pharma (Group). MFL was provided by Knoll-Abbott. Isoniazid and pyrazinamide were purchased from Tokyo Chemical Industry Company Limited. All active pharmaceutical ingredients were used without further purification.

Antimycobacterial Activity

Briefly, 200 µL of sterile deionized water was added in all outer-perimeter wells of sterile 96 well plates (falcon, 3072: Becton Dickinson, Lincoln Park, NJ) to minimize evaporation of the medium in the test wells during incubation. The 96 plates received

100µL of the Middlebrook 7H9 broth containing the mycobacterial cells (Difco laboratories, Detroit, MI, USA). The substances were tested alone and in combination in a 1:1 proportion (m/m). The final drug concentrations tested were 0.015 -100 µg/mL. Plates were covered and sealed with parafilm and incubated at 37ºC for five days. After this time, 25 µL of a freshly prepared 1:1 mixture of Alamar Blue (Accumed International, Westlake, Ohio) reagent and 10% Tween 80 was added to the plate and incubated for 24h. A blue color in the well was interpreted as absence of bacterial growth, and a pink color was scored as growth. The MIC (minimal inhibitory concentration) was defined as the lowest drug concentration, which prevented a color change from blue to pink.

Liposomes Preparation

Soybean asolectin (ASO) liposomes (as large multilamellar vesicles) were prepared by the reverse-phase evaporation method [28,29]. Accordingly, ASO (100mg/mL) was dissolved in chloroform and dispersed in water. This suspension was sonicated for 2 min, to obtain a homogeneous, opalescent dispersion of reverse micelles. Thus, the chloroform was rotary-evaporated, generating an organogel. Liposomes were then obtained by adding in tricine/ $MgCl_2$ buffer solution (10 mM, pH 7.4) to the organogel with vigorous shaking. Liposome samples consisted of pure ASO liposomes (control) and MFL-loaded liposomes. The MFL (10 mg/mL, MFL:ASO ratio equivalent to 0.1, m,m) was added in the solvent co-solubilisation step.

Liposomes´ Spectroscopic Characterization

Fourier Transform Infrared experiments

Horizontal Attenuated Total Reflectance-Fourier transform infrared (HATR-FTIR) experiments were performed at 21°C using a Shimadzu IR Prestige-21 spectrometer (Kyoto, JP), with 2 cm^{-1} resolution. ASO liposomes empty (ASO, 100 mg/mL) and

loaded with MFL (ASO+MFL, MFL:ASO ratio equivalent to 0.1, m,m) were deposited in a ZnSe crystal cell and immersed into a 10 mM tricine/$MgCl_2$ buffer (pH 7.4). Forty-five scans of HATR-FTIR interferograms were averaged and registered in a wavenumber range from 400 to 4000 cm^{-1}. Spectra were obtained by a Shimadzu IR solution software (version 1.5). These spectra were analyzed considering the changes induced by MFL in the ASO initial FTIR peak wavenumbers and bandwidths (at three-fourths of the peak height position) values. The analyzed ASO vibrational modes are listed as follows: phosphate antisymmetric stretching (ν_{as} PO_2^-), which appears in a wavenumber range from 1260 to 1220 cm^{-1} ; the choline antisymmetric stretchings, in the wavenumbers around 970 (ν_{as} $N^+(CH_3)_3$) and nearly 3005 cm^{-1} (ν_{as} NCH); the carbonyl vibrational mode (ν C=O), in a wavenumber ranging from 1725 to 1740 cm^{-1} ; the symmetric and antisymmetric stretchings of acyl chain methylenes, detected at wavenumbers around 2850 (ν_s CH_2) to 2920 cm^{-1} (ν_{as} CH_2), respectively [30,31].

Nuclear Magnetic Resonance Measurements

^{31}P-Nuclear Magnetic Resonance (NMR) spectra of ASO liposomes (100 mg/mL), both empty (control) or containing MFL (ASO+MFL, MFL:ASO ratio equivalent to 0.1, m,m) were obtained on a Bruker Avance DRX 400 NMR spectrometer at 161 MHz, with proton broadband decoupling, using 80:20 water: deuterated water (H_2O:D_2O, v,v) as external reference. The acquisition parameters were: recycling time: 4 s, delay: 0.2 s, acquisition time: 0.5111808 s and scans numbers: 2048. Line width measurements were obtained at three-fourth (75%) of the ^{31}P NMR peak height position [32]. ^{1}H NMR spin–lattice relaxation times (T_1) values were obtained at 400 MHz. With this aim, inversion recovery pulse sequences (180°–τ 90°) were performed at 25°C, with time delay (t) ranging from 0.4 to 12.8 s, also using H_2O:D_2O (80:20, v,v) as external reference. Chemical shifts were referenced to the TSP signal at 0 ppm. The T_1 values and relative intensities were calculated by fitting the exponential data to the TOPSPIN software.

Molecular Dynamics

MD is a computational method developed to analyze the physical movements of atoms and molecules. MD simulations can track rapid processes at atomic resolution and for this reason is used to study many biologically relevant systems [33]. In order to analyze the possible effects of MFL in the *M. tuberculosis* membrane, MD Simulations were performed using the GROMACS 2016.4 package, which is mainly designed for simulations of proteins, lipids and nucleic acids [34,35]. The model for this membrane - a PIM_2 bilayer - was proposed by Scaini et al., 2019 [26]. The PIM_2 molecule used in this model can be found at Lipid Maps [36] (LM ID: LMGP15010062). The MFL topology was obtained from Automated Topology Builder (ATB) ID: I1ZF [37] and adapted to the parameters of the "Berger lipids" [38] modification for GROMOS96 53a6 force field [39].

Two MD simulations were performed, PIM_2 membrane in water (PIM_2 system), and membrane in water with MFL molecules (PIM_2-MFL system). These systems consisted of lipid bilayers (128 PIM_2 molecules, 64 in each layer) perpendicular to the z-axis, and two water boxes at each side of the membrane, also perpendicular to the z-axis. The height of these water boxes was 0.6 nm on the PIM_2 system and 0.8 nm in the PIM_2-MFL system. Each water box of the PIM_2-system had 6 MFL molecules. The total number of 12 MFLs for 128 lipid molecules is close to the MFL:ASO ratio (equivalent to 0.1, m,m) used in liposomes´spectroscopic characterization, and were equally distributed for both water boxes. To neutralize the systems, 128 sodium ions were added to both systems (PIM_2 model has charge of -1, therefore we use one sodium ion for each PIM_2 molecule to neutralize the system), and 12 chloride ions were also added to PIM_2-MFL system (MFL has charge of +1, so we add one chloride ion for each MFL molecule).

For both PIM_2 and PIM_2-MFL solvated systems, we performed energy minimization (EM), equilibration and production MD simulations steps. The

equilibration was performed with restraints on lipid phosphorus in the z-axis, preventing them from moving vertically. The equilibration consisted of two steps. The first step was a 10 ns NVT simulation for temperature adjustment to 310 K using the velocity rescale thermostat. The second step was a 10 ns NPT simulation keeping the temperature fixed in 310 K or 328.15 K by the Nosè-Hoover thermostat and the pressure adjusted to 1 bar by the Parrinello-Rahman semi-isotropic barostat, which means the pressure in the z-direction was not fixed. Finally, the systems went to 100 ns NPT simulation for the production step. Here no restraints were applied, and the same temperature and pressure control from the equilibration step were used.

GROMACS provided the calculation for some analysis that were plotted using R 3.1.3 and R studio 0.99.491 softwares [40,41]. The production step was analyzed in each system. The Root-mean-square deviation (RMSD) was calculated at each 2 ps along the entire production step of MD simulations, to determine the stability of the bilayer in both systems. The mass density profile measures how mass is distributed along the membrane z-axis and was calculated for different atom groups (water, lipid head groups, acyl chains, and MFL, when present) to have an overview of this distribution. The deuterium order parameters of the acyl chains of the bilayer were calculated in order to determine how rigid the bilayer is. The lateral diffusion of the lipid bilayer was calculated to determine its fluidity which is related with the lateral movement of these molecules. The thickness is defined as the distances between the average positions of the lipid phosphate groups and was calculated for the final structure of the membrane using GridMAT-MD [42] and plotted using Matplotlib.

Results and Discussion

MFL drug interactions against *M. tuberculosis* strains

The *in vitro* interaction profile of MFL was evaluated in association to two first-line anti-TB drugs: isoniazid (INH) and pyrazinamide (PYR), and six fluoroquinolones: gatifloxacin (GAT), moxifloxacin (MOX), ciprofloxacin (CPX), levofloxacin (LVX), ofloxacin (OFX) and sparfloxacin (SPR). MFL was combined with the second drug in a 1:1 (m/m) proportion and the resulting combination was tested against the susceptible strain of *M. tuberculosis* H37Rv (ATCC 27294) and two clinical resistant isolates: T3609 (resistant to OFX, and streptomycin) and T113 (resistant to INH, rifampicin, ethambutol and OFX). The synergistic interactions were determined using the checkerboard assay. It is a well-established technique that determines the effect on potency of a combination of antibiotics with regard to their individual activities and is expressed through the fractional inhibitory concentration index (FICI) [43–48]. FICI ≤ 0.5 indicate synergistic activity, and FICI ≥ 4 indicate antagonism whereas values between that range indicate additivity. The resistant strains used in this work were isolated from clinical cases of pulmonary tuberculosis in the city of Rio de Janeiro (Brazil) and belong to the collection of the Laboratory of Biotechnology and Biotests of the Evandro Chagas Institute of Clinical Research of the Oswaldo Cruz Foundation. The susceptibility profiles were evaluated using the microplate alamar blue assay (MABA) [49], a non-toxic methodology that employs a thermally-stable reagent and shows good correlation with proportional and BACTEC radiometric methods [50,51]. The minimal inhibitory concentration (MIC) was defined as the lowest drug concentration that prevented a color change from blue to pink and was expressed in µg/mL.

The results are summarized in **Table 1**. An increase in the susceptibility to INH when combined with MFL was observed on the *M. tuberculosis* strain H37Rv and the isolate T3609 (entries 1 and 2). However, only an additive effect was observed against the isolate T113, which is resistant to INH (entry 3). With regard to PYR, a synergistic interaction with MFL was observed against the strain H37Rv (entry 4). The interactions of MFL with PYR could not be determined against the isolates T3609 and T113 since PYR was not active in the tested concentrations using MABA. It is

important to mention that PZA is thought to be more active at an acidic pH such as in the macrophage compartment.

Table 1: *In vitro* interactions of MFL combined with different substances against the *Mycobacterium tuberculosis* laboratory strain H37Rv and the resistant isolates T3609 and T113.

Entry	**Isolate**	**Combination**				**FICI**	**Outcome**
		MFL + INH					
		MFL		INH			
		MIC 1 (µg/mL)	MIC 2 (µg/mL)	MIC 1 (µg/mL)	MIC 2 (µg/mL)		
1	H37Rv	12.5	0.1	0.2	0.1	**0.5**	**Synergistic**
2	T3609	12.5	0.015	0.5	0.015	**0.03**	**Synergistic**
3	T113	12.5	3.12	6.25	3.12	0.7	Additive
		MFL + PYR					
		MFL		PYR			
		MIC 1 (µg/mL)	MIC 2 (µg/mL)	MIC 1 (µg/mL)	MIC 2 (µg/mL)		
4	H37Rv	12.5	3.12	100	3.12	**0.3**	**Synergistic**
5	T3609	12.5	0.62	>100	-	-	-
6	T113	12.5	0.62	>100	-	-	-
		MFL + GAT					
		MFL		GAT			
		MIC 1 (µg/mL)	MIC 2 (µg/mL)	MIC 1 (µg/mL)	MIC 2 (µg/mL)		
7	H37Rv	12.5	0.12	0.12	0.12	1.0	Additive
8	T3609	12.5	0.31	0.62	0.31	**0.5**	**Synergistic**
9	T113	12.5	0.15	0.12	0.15	1.3	Additive

		MFL + MOX					
		MFL		MOX			
		MIC 1 (µg/mL)	MIC 2 (µg/mL)	MIC 1 (µg/mL)	MIC 2 (µg/mL)		
10	H37Rv	12.5	0.15	0.25	0.15	0.6	Additive
11	T3609	12.5	0.62	1.25	0.62	**0.5**	**Synergistic**
12	T113	12.5	0.31	0.25	0.31	1.3	Additive
		MFL + CPX					
		MFL		CPX			
		MIC 1 (µg/mL)	MIC 2 (µg/mL)	MIC 1 (µg/mL)	MIC 2 (µg/mL)		
13	H37Rv	12.500	0.620	0.620	0.620	1.0	Additive
14	T3609	12.500	3.120	5.000	3.120	0.9	Additive
15	T113	12.500	0.310	0.620	0.310	**0.5**	**Synergistic**
		MFL + LVX					
		MIC 1 (µg/mL)	MIC 2 (µg/mL)	MIC 1 (µg/mL)	MIC 2 (µg/mL)		
16	H37Rv	12.5	0.62	0.62	0.62	1.0	Additive
17	T3609	12.5	2.5	2.5	2.5	1.2	Additive
18	T113	12.5	0.31	0.62	0.31	**0.5**	**Synergistic**
		MFL + OFX					
		MFL		OFX			
		MIC 1 (µg/mL)	MIC 2 (µg/mL)	MIC 1 (µg/mL)	MIC 2 (µg/mL)		
9	H37Rv	12.5	0.62	1.25	0.62	**0.5**	**Synergistic**
20	T3609	12.5	2.5	5.0	2.5	0.7	Additive
21	T113	12.5	0.62	1.25	0.62	**0.5**	**Synergistic**
		MFL + SPR					

		MFL		SPR			
		MIC 1 (µg/mL)	MIC 2 (µg/mL)	MIC 1 (µg/mL)	MIC 2 (µg/mL)		
22	H37Rv	12.5	0.12	0.12	0.12	1.0	Additive
23	T3609	12.5	0.62	1.25	0.62	**0.5**	**Synergistic**
24	T113	12.5	0.12	0.12	0.12	1.0	Additive

MFL= mefloquine; INH= isoniazid; PYR= pyrazinamide; GAT= gatifloxacin; MOX= moxifloxacin; CPX= ciprofloxacin; LVX= levofloxacin; OFX= ofloxacin; SPR= sparfloxacin; MIC 1= minimal inhibitory concentration of the substance tested alone; MIC 2= minimal inhibitory concentration of the substance tested in combination; FICI: fractional inhibitory concentration index.

The synergistic interaction of MFL with these first line anti-TB agents is a promising result, considering the specific role of each drug in the disease treatment. INH is a potent bactericidal drug, with a primordial role in the beginning of the treatment since it kills actively replicating bacteria and typically causes 1-log10-unit reduction in colony counts during the initial few days of therapy [52]. On the other hand, PYR is more active against dormant or semi-dormant microorganisms and it is important to accelerate the sterilizing effect of isoniazid and rifampicin [53].

With regard to the fluoroquinolones, all of them presented a synergistic interaction with MFL against at least one strain. GAT, MOX and SPR had an increase in their activity against the isolated T3609. CPX, LVX and SPR presented a synergistic interaction with MFL against the isolate T113 and the effect of OFX with MFL was synergic against the standard strain H37Rv and the isolate T113. Noticeably, no antagonist interactions were observed.

An interesting observation in these results is the synergistic interaction of MFL with antibiotics that acts through different mechanisms of action. The mechanism of action of MFL against the *M. tuberculosis* has not yet been defined. In an attempt to identify a possible cellular target and the mechanisms of resistance to MFL in mycobacteria, Danelishvili and coworkers used a genomic approach [12]. The authors

employed two different techniques, DNA microarray and green fluorescent protein (GFP), to examine the effect of MFL on the level of gene expression in *M. tuberculosis* and *M. avium*. The initial attempt to clone the resistant phenotype by identifying a resistant strain to MFL was unsuccessful and could indicate that the mutation of the target is lethal or MFL has more than a single target. Upon exposure to subinhibitory concentrations of MFL, *M. tuberculosis* and *M. avium* upregulated a number of genes, the major part belonging to metabolic pathways and cell wall synthesis. When *M. tuberculosis* was exposed to 4 x MIC, the bacterium upregulated the expression of genes coding for membrane proteins, many of them involved in transport mechanisms, what can suggest that either the target for MFL is on the cell wall or membrane or many of these proteins are associated with the transport of this compound. In another work, Martín-Galiano and coworkers determined that MFL inhibits the F0F1 bifunctional ATP synthase/ATPase of *S. pneumoniae* which is the same target of the diarylquinoline TMC207 in *M. tuberculosis* [54]. Considering the structural similarities between both substances, the F0F1 bifunctional ATP synthase/ATPase is also a possible target for MFL in *M. tuberculosis*.

Bioactive substances can interact in different ways to show a synergistic correlation. The most accepted models are: (*i*) the parallel pathway inhibition and (*ii*) the bioavailability model. In the first case, two drugs will be synergistic if they inhibit two proteins on parallel pathways that are essential for an observed phenotype. In the second case, the drugs will have a synergistic interaction if one drug's action helps another drug's availability in the target cells [55]. A common example of synergistic mechanism in the bioavailability model is a positive modulation of drug transport or permeation, with enhancement of drug absorption via destabilization of transport barrier or inhibition of drug efflux [55].

Despite the possibility that MFL may present more than one mode of action, the synergism with substances that inhibits *M. tuberculosis* growth through different mechanisms probably indicates a non-specific interaction and the bioavailability model seems more logical to explain the observed results. Herein, based on previous

evidences of MFL-membrane interactions in *P. falciparum* and *E.coli*, [25,56] we wonder whether the presence of MFL could affect the *M. tuberculosis* cell membrane, facilitating the transport and increasing the level of antibiotics uptake.

To explore this hypothesis, the MFL physical and physico-chemical influences on lipid bilayers were monitored by spectroscopic analyses, using an ASO liposomes´ model, as well as by MD simulations studies, using PIM_2 as membrane model.

Liposomes´ spectroscopic characterization: MFL interactions and effects on lipids physico-chemical properties

HATR-FTIR spectra related to MFL-loaded liposomes and control (empty liposomes), as well as the MFL-induced variations on the wavenumber and bandwidth of ASO groups stretching (v) peaks are shown in Figure 1. The wavenumber and bandwidth assignments related to the v vibrations of specific ASO liposomes´ groups are listed in Table 2.

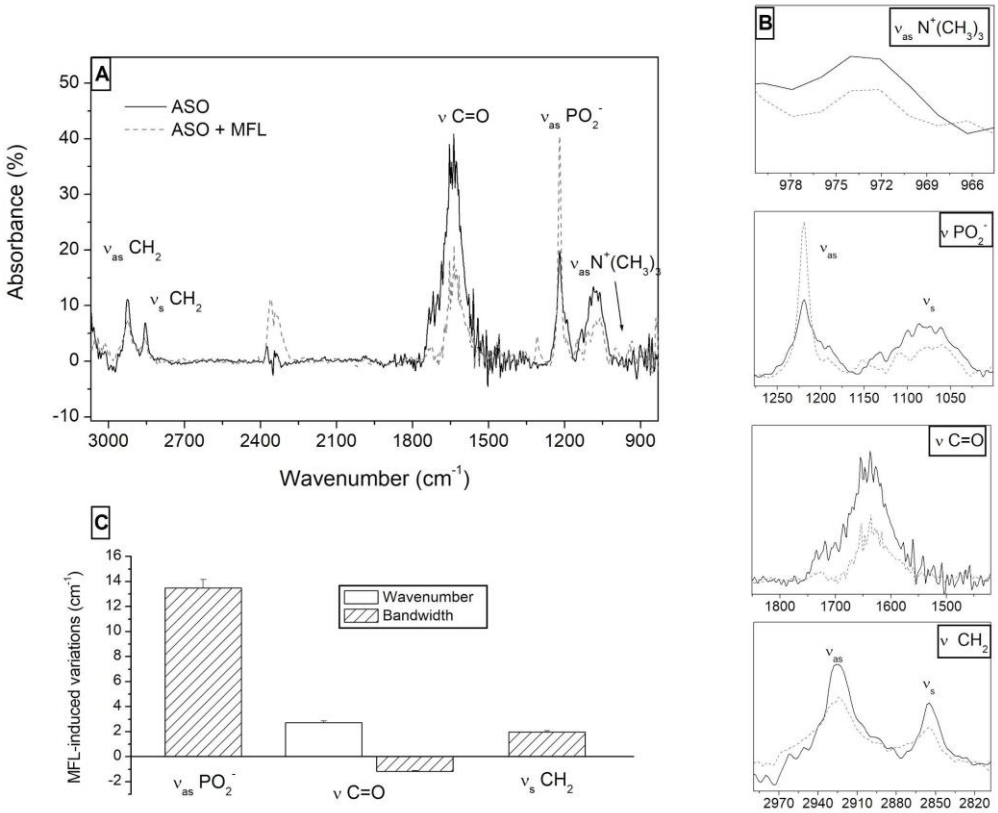

Figure 1- (A) HATR- FTIR spectra of empty soybean asolectin liposomes (ASO, control) and MFL-loaded liposomes (ASO + MFL). (B) Zooms related to spectra showed in (A), at specific lipid stretching peaks regions. (C) MFL- induced variations in wavenumbers and bandwidths related to ASO liposomes´ FTIR peaks. Significant wavenumber variations are considered above the equipment resolution (2 cm^{-1}) and bandwidths above 0.9 cm^{-1}. Interferograms were obtained from the average of 45 scans, with a resolution of 2 cm^{-1}, in a wavenumber range from 400 to 4000 cm^{-1}.

Table 2- Empty soybean asolectin liposomes (ASO, control) HATR-FTIR stretching (ν) peaks parameters.

ASO peaks attribution *

Lipid stretching mode	Wavenumber (cm^{-1})	Bandwidth (cm^{-1})
$v_{as}\ N^{+}(CH_3)_3$	973.32	3.25
$v_{as}\ PO_2^-$	1219.79	11.24
$v_s\ PO_2^-$	1077.57	53.19
v C=O	1641.62	42.10
$v_s\ CH_2$	2855.64	9.87
$v_{as}\ CH_2$	2925.48	17.76

* From these parameters, Figure 1C values were calculated.

Wavenumber variations of an IR lipid peak may reflect changes on the nature of the vibrational mode caused by different motions, such as rotational, translational and collisional ones [57]. Figure 1A-C shows no significant changes in FTIR ASO $v_{as}\ PO_2^-$, provoked by MFL. This indicates that MFL did not affect the phosphate hydration degree [58,59]. With respect to the interfacial region, the MFL-induced increase of 2.71 cm^{-1}, observed to lipid v C=O wavenumber, indicates that the drug reduced the lipid carbonyl hydration degree. This is due to the fact of the v C=O band being sensitive to environmental hydrogen bonding or polarity [60]. No significant variations induced by MFL in the v CH_2 peaks wavenumber were observed, and this shows no *trans-gauche* isomerization in the lipid acyl chains [61]. Bandwidth variations related to lipid v peaks are sensitive to rotational, translational and collisional parameters. The bandwidth analyses allow the study of motion freedom of lipid groups considering the

amplitudes and rates of motion within its environment, as well as the main thermal transition and then, the methylene *trans/gauche* conformers proportion. Besides the changes in *gauche* conformers quantities, bandwidth alteration also reflects librational and torsional motion of lipid chains [57].

Figure 1C showed that MFL changed significantly [62] the bandwidth of $\nu_s PO_2^-$, ν C=O and $\nu_s CH_2$. The increase in $\nu_s PO_2^-$ bandwidth, equivalent to 13.48 cm^{-1}, reflected the MFL-induced motional freedom enhancement of phosphate lipid group, while the decrease of ν C=O bandwidth, which corresponded to 1.17 cm^{-1}, indicated a restricted lipid carbonyl motion. As cited before, the increase in $\nu_s CH_2$ bandwidth suggest that by MFL promoted one of these two events: (i) a disordering effect in the ASO acyl chain methylene region due to the increase of trans-gauche isomerization; or (ii) the increase of librational and torsional motion of ASO lipid chains. Considering non-significant changes promoted by MFL in νCH_2 wavenumber, it is probable that the observed bandwidth increase is related to the second event (ii).

As MFL-induced changes in the FTIR parameters are also related to lipid groups rotation [57], NMR experiments were performed in order to investigate MFL effects in the ASO liposomes phosphate, choline and methylene bonds rotation. Also, to obtain information related to MFL influence on lipid phase-of-state and chemical shift anisotropy (CSA) [63–66]. ^{31}P nucleus chemical shift anisotropy (CSA) values give information concerning changes in fluidity and rotation rate of lipid polar heads. The CSA is related to the distance (in ppm) between the σ_{II} and $\sigma_{\perp}$ chemical shielding tensors components [67]. Thus, measurement of ^{31}P NMR peak linewidth gives important information related to conformation and molecular motion [65]. Figure 2 shows the ^{31}P NMR spectra related to MFL-loaded liposomes.

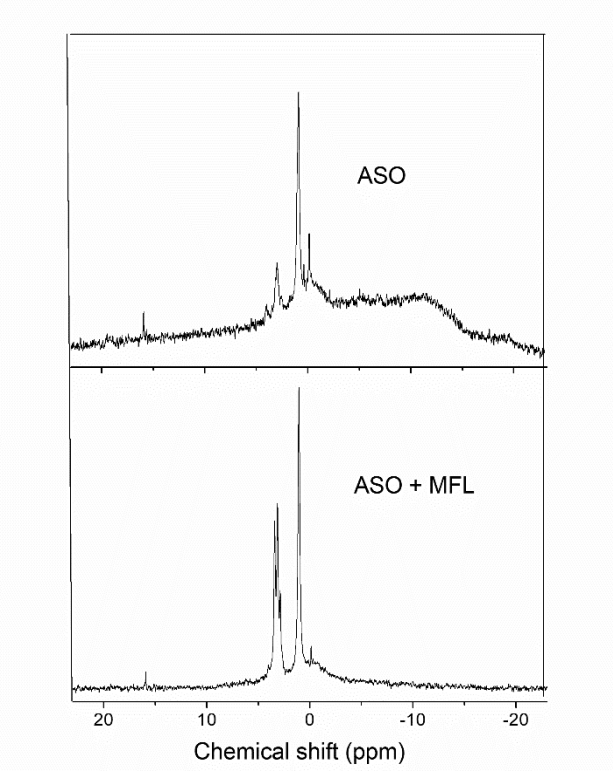

Figure 2- ^{31}P NMR spectra of empty soybean asolectin liposomes (ASO, control) and MFL-loaded liposomes (ASO + MFL). ^{31}P NMR measurements were recorded at 161 MHz, using water: deuterated water (H_2O:D_2O, 80:20, v/v) as solvent the reference. DS=4 and NS=2048.

From Figure 2, MFL reduced the ASO ^{31}P NMR linewidth by approximately 85% (from 15.9 ppm to 2.7 ppm, a variation equivalent to 13.2 ppm). The narrowing of the ^{31}P NMR resonance indicates an enhancement in the ASO phosphate motion freedom [66,68]. The ^{31}P NMR data suggest that the MFL-promoted the increase of phosphate rotation motion. This result is in agreement to FTIR bandwidth v PO_2^- data, suggesting that rotation plays an important role in MFL-induced increase in ASO phosphate mobility. ASO ^{31}P NMR peak shape analysis shows a broad shoulder at the high field (corresponding to the chemical shielding tensor σ_{II} component) and a narrow peak at the low field (corresponding to the chemical shielding tensor $\sigma_{\perp}$ component), typical of

the inverted hexagonal (H_{II}) phase. This phase is attributed to the phosphatidylethanolamine content (around 25%) [66,69]. Results indicated that, despite the increase in ^{31}P rotation motion, MFL did not change the lipid phase-of-state.

MFL-induced changes in choline and methylene bond rotation were monitored by ^{1}H NMR T_1 [63,64]. Figure 3 shows the ^{1}H FID signal recoveries related to ASO choline (3.2 ppm) and methylene (1-2 ppm) groups, in MFL-loaded liposomes. From these data, the ^{1}H NMR T_1 values were calculated. MFL decreased the choline ^{1}H T_1 in 1.063 s (from 1.316 to 0.253 s) and methylene ^{1}H T_1 in 1.007 s (from 1.268 s to 0.261 s). For the tested liposomes, the decrease in ^{1}H T_1 values implies in the decrease of correlation time, which has an inverse relationship to the rotation rate [70,71]. This result then indicates that MFL increased the lipid choline and methylene rotation rate in approximately 80%.

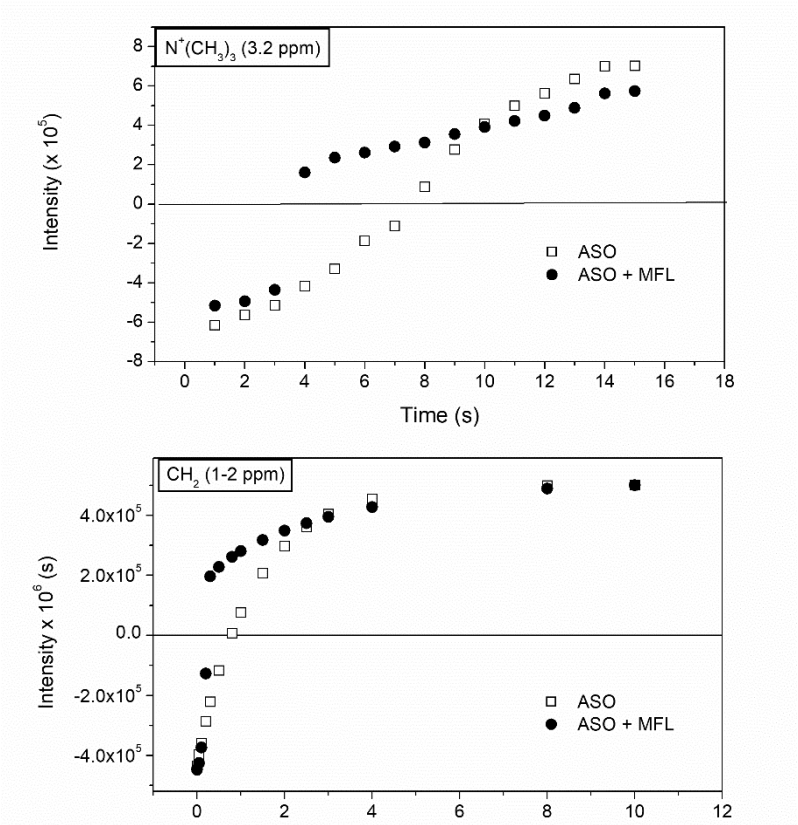

Figure 3- Recovery of asolectin choline ($N^+(CH_3)_3$, 3.2 ppm) and methylene (CH_2, 1-2 ppm) ^1H FID signal, for empty liposomes (ASO, control) and for those loaded with MFL (ASO+MFL) after several inversion pulses. From these curves, the ^1H T_1 values were obtained.

The increase in the lipid phosphorus and choline hydrogens rotation motion complements FTIR data, which shows that MFL affects ASO´s polar region. This is probable due to the dipolar interaction between phosphate and MFL quinolyl and piperidine nitrogen, and ASO choline groups to trifluoromethyl and hydroxyl substituents. These polar dipolar interactions may interfere in the electrostatic attraction forces between the ASO phosphate group and neighboring lipid choline group [72], increasing the fluidity in this region. It is important to note that carbonyl lipid groups may also interact by dipolar forces to MFL nitrogen but, as seen by FTIR results, they not seem to affect the ester region as the phosphate one (it can be seen by a difference of approximately 12 cm^{-1} in the MFL-induced wavenumber variation of v_s PO_2^- and v C=O). It is then possible that the ASO carbonyl group interaction to quinolyl and piperidine nitrogen interaction only reflected a discreet decrease on its water hydrogen bonds (as seen by MLF-induced FTIR v C=O peak wavenumber variation). The correlation times associated with methylene ^1H T_1 values are related to chain rotation about the diffusion tensor axis, reorientation of this axis, as well as trans-gauche isomerization [73]. As FTIR data showed no *trans-gauche* isomerism in methylene stretching analyses, MFL may then affect other lipid parameters besides rotational isomerism, such as segmental motion, overall angular fluctuations and rotations about the long axis of lipid molecules [74].

Liposomes-related spectroscopy characterization data may bring evidence concerning the molecular interaction role in the MFL effect on the permeability of *M. tuberculosis* membrane models. To reinforce these evidences, PIMs permeability were then investigated by MD studies, as follows.

PIM_2 -MFL MD simulations

The effect of MFL on the permeability of *M. tuberculosis* related PIM_2 membrane model was investigated with MD simulations. Two systems were studied: one is the membrane in water (PIM_2 system) and the other is the membrane in water with MFL molecules (PIM_2-MFL system). To evaluate the effect of MFL on PIM_2 we analyzed the 100 ns MD production phase step of both systems considering the final conformations (Figure 4), RMSD (Figure 5), mass density (Figure 6), lateral diffusion (Figure 7), thickness (Figure 8) and deuterium (Figure 9).

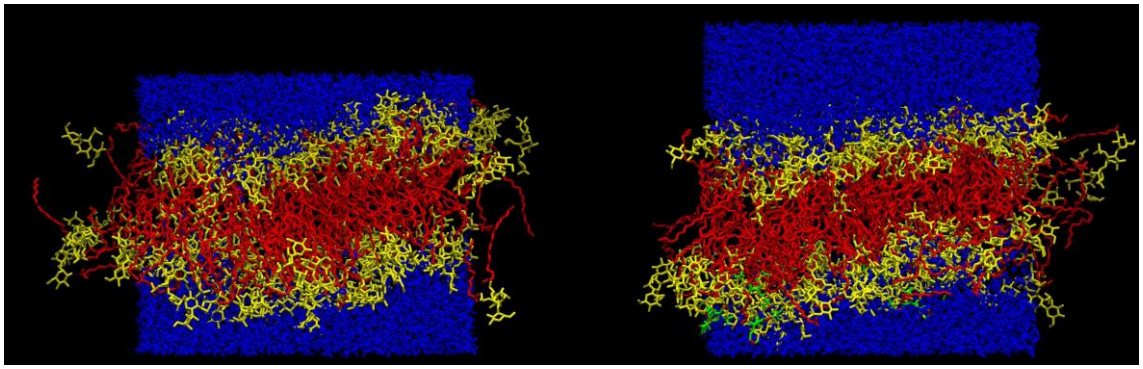

Figure 4. Final conformation of MD simulations. On left the PIM_2 system and on right the PIM_2-MFL system. In blue, the water box. In yellow the lipid headgroups and red the lipid acyl chains. MFLs are in green. This figure was generated using VMD (Humphrey et al., 1996).

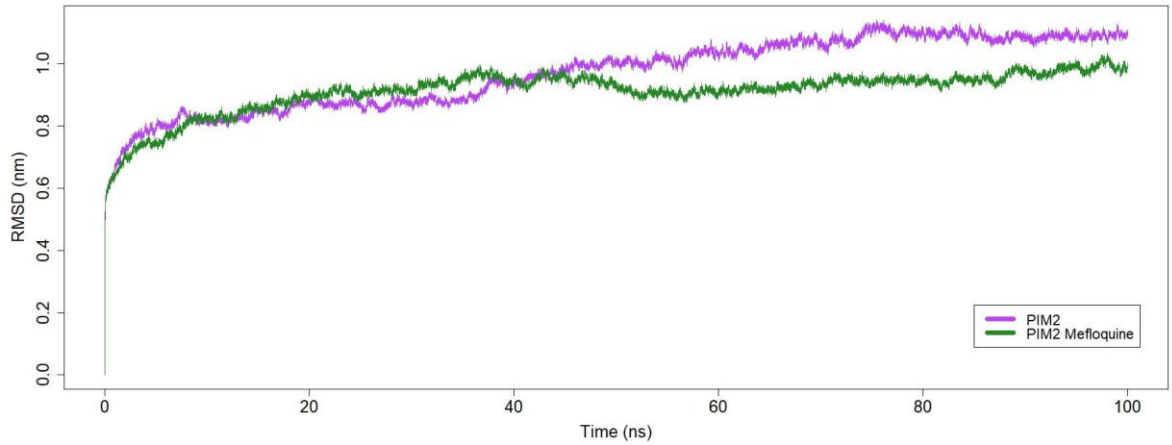

Figure 5. Root mean square deviation (RMSD) of the PIM_2 bilayer in the PIM_2 system (magenta) and in the PIM_2-MFL system (green) systems during the 100 ns production phase step.

The root mean square deviation (RMSD) was calculated to analyze the stability of both the PIM2 system and the PIM_2-MFL system. PIM_2 bilayer on the PIM_2-MFL system stabilized starting at 20 ns at around 0.9 nm, while still fluctuating around 0.87 and 1 ns. PIM_2 bilayer at the PIM_2 system stabilized starting at 60 ns, at around 1 and 1.1 ns, and also showed a higher RMSD, and therefore, more instability.

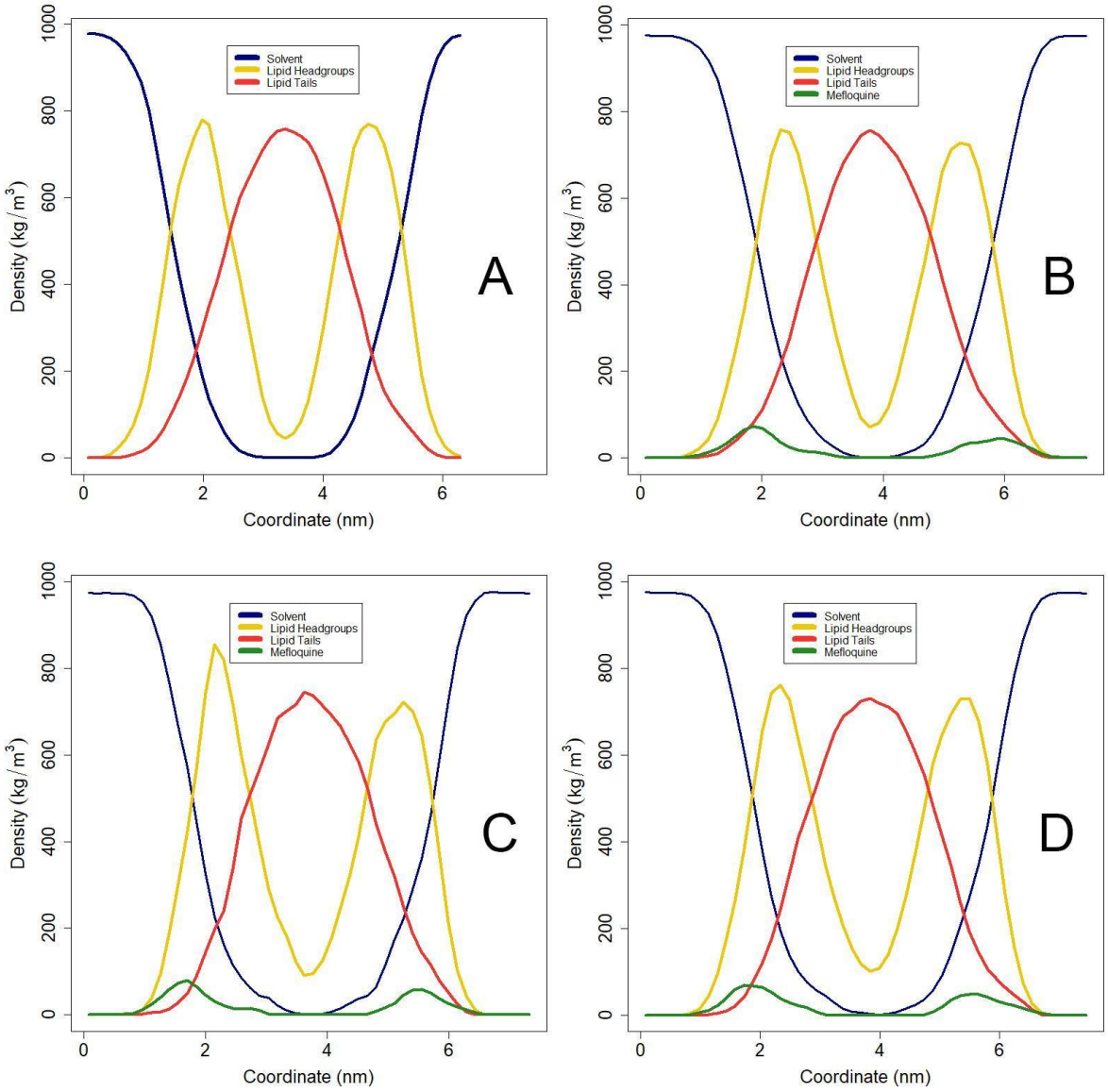

Figure 6. Density of PIM_2 system (A), and PIM_2-MFL system from 0 to 40 ns (B), from 40 to 50 ns (C), from 50 to 100 ns (D).

The partial density was calculated to analyze the distribution of different atom groups - lipid head groups, lipid acyl chains, solvent (water) and MFL - in the PIM_2 system and PIM_2-MFL system. The PIM_2 system showed the expected behaviour, where water remained in the extremes of the z-axis and did not penetrate toward the

hydrophobic acyl chains - water molecules interact with the hydrophilic lipid head groups, and the acyl chains are located at the membrane's hydrophobic center. The PIM_2-MFL system showed similar density profiles through the first 40 ns (Figure 6B), and also from 50 to 100 ns (Figure 6D). Between 40 to 50 ns (Figure 6C), however, it was observed a difference in the density of both lipid headgroups. MFL is concentrated closer to the lipid interface before 40 ns, then it gets further away between 40 and 50 ns, and maintains the distance until the end of the simulation. This may indicate that contacts between MFL and PIM_2 may have happened mainly on the first 40 ns of the simulation.

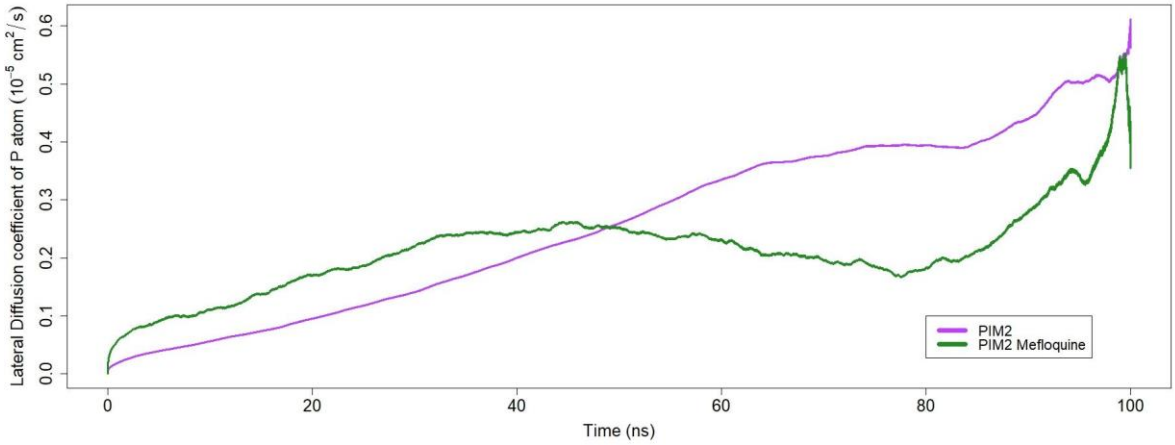

Figure 7. Lateral diffusion of the P atoms of the PIM_2 bilayer at PIM_2 (magenta) and PIM_2-MFL (green) systems during the 100 ns production step.

The mean square displacement (MSD) of the lateral diffusion coefficient of the PIM_2 P atoms was calculated to analyze the lateral diffusion in the PIM_2 system and PIM_2-MLF system. The lateral diffusion coefficient in the PIM_2-MFL system raised throughout the first 35 ns, from 35 to 42 ns it stabilized at around 0.24 x 10^{-5} cm^2/s, then raised to around 0.26 x 10^{-5} cm^2/s at 46 ns, falling back to 0.24 x 10^{-5} cm^2/s at 53 ns when it keeps decreasing to around 0.17 x 10^{-5} cm^2/s at 77 ns, and raised again at

the end, reaching over 0.5 x 10^{-5} cm^2/s. The lateral diffusion coefficient in the PIM_2 system raised until the end of the simulation, reaching 0.6 x 10^{-5} cm^2/s.

The MFL density was concentrated closer to the lipidic interface until around 40 ns, when the lateral diffusion is higher in the presence of MFL. Considering this information, and since the MSD analysis of an interval of the MD is used in related work [75], we consider the lateral diffusion until this point as the most representative. This higher lateral diffusion indicates higher flexibility in the membrane in the presence of MFL, which may indicate a higher permeability. Here, it is important to note that the higher MFL density closer to the lipid interface, as well as the drug-induced increase in the membrane lateral diffusion are in agreement to the MFL location and perturbation effects suggested by spectroscopic FTIR and NMR data, i.e., a proposed location between the polar region and the first hydrophobic tails´methylenes and a disordering effect on the lipid groups.

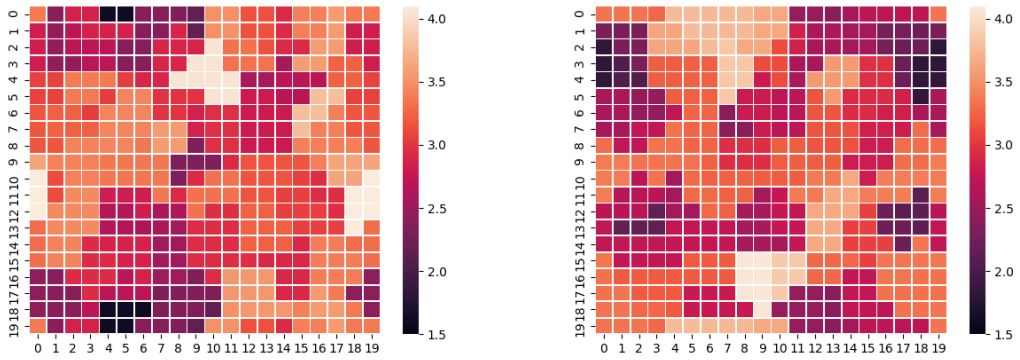

Figure 8. Thickness of the PIM_2 (left) and PIM_2-MFL (right) systems on the last conformation (100 ns) for both systems. The x and y axes are grid points representing the x and y axes of the system, respectively, and the z axis represents the thickness.

The thickness of the PIM_2 bilayer with and without MFL was evaluated to analyze the influence of MFL in the membrane thickness. Figure 8 shows the thickness according to the region, where the x and y axes represent the x and y axes of the membrane. The bilayer in the PIM_2 system had 46.25% of its thickness under 3 nm,

while the bilayer in the PIM_2-MFL system had 48.25% of its thickness under 3 nm. Thus, we can observe that there are more thinner regions in the presence of MFL. This may indicate that the membrane is thinner, which matches with the density results and reinforces that MFL decreases this membrane package, and causes disorder.

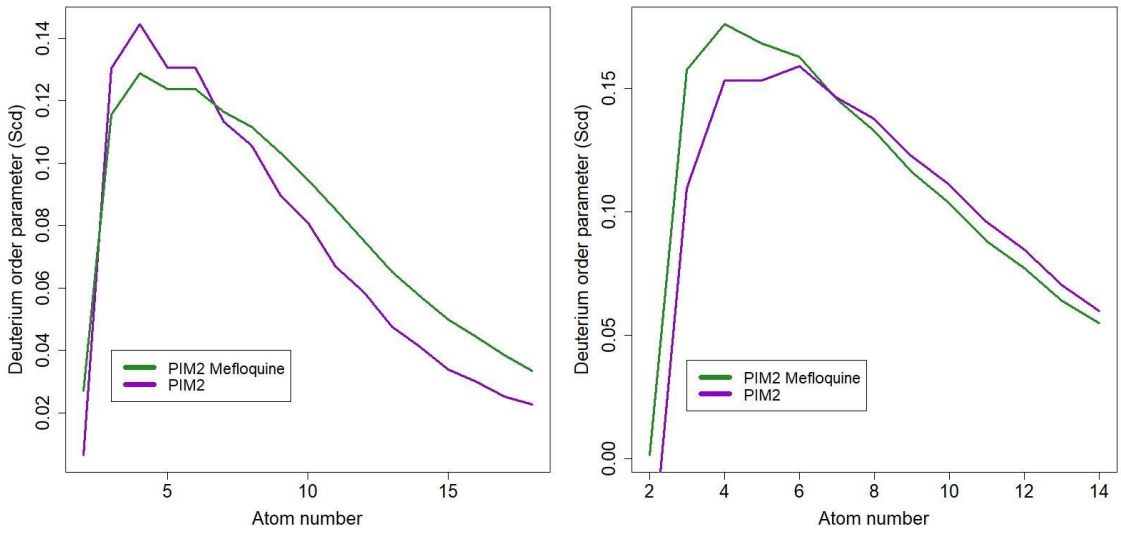

Figure 9. Deuterium order of acyl chains 1 (left) and 2 (right) for both PIM_2 and PIM_2-MFL systems

Deuterium order parameters were calculated to analyze how ordered were the acyl chains of the PIM_2 bilayer in both PIM_2 and PIM_2-MFL systems. Acyl chain 1 is more ordered in the PIM_2 system closer to the headgroups, and more ordered in the PIM_2-MFL system further away from the headgroups. Acyl chain 2 is more ordered in the PIM_2-MFL system closer from the headgroups, and more ordered in the PIM_2 system further away from the headgroups.

Conclusions

In conclusion, we have demonstrated that MFL presents a synergistic activity with the first line anti-TB agents INH and PYR and different fluoroquinolones against the susceptible strain of *M. tuberculosis* H37Rv (ATCC 27294) and two clinical

resistant isolates (T3609 and T113). Considering that the synergism was observed between MFL and substances that act through different mechanisms, it was proposed that these drugs present a non-specific interaction: MFL could disturb the *M. tuberculosis* cell membrane and therefore facilitate the availability of the other drugs in the target cell. To support this hypothesis, the MFL physicochemical influence on lipid bilayers was analyzed by spectroscopic analyses, using an ASO liposomes' model. Furthermore, MD simulation studies were performed using PIM_2 as a membrane model.

FTIR bandwidth and NMR data evidenced that the disordering effect in these ASO groups is due to a "spacer" effect related to MFL aromatic rings located between phosphate and the first chain methylenes. This may reduce the lipid intermolecular communication in all lipid regions, disordering the membrane and increasing its permeability. These consequences were also evidenced and reinforced by PIM_2 MD simulations, in which the lateral diffusion coefficient MSD of the PIM_2 was higher at the presence of MFL while the MFL molecules were closer to the membrane interface (at the first 40 ns). Both results are in agreement with an increased membrane permeability and a decrease of lipid package in the presence of MFL.

Acknowledgements

We acknowledge financial support from CAPES, CNPq and FAPERJ.

References

[1] World Health Organization, Global tuberculosis report 2019, Geneva, 2019.
[2] J. Hafkin, N. Hittel, A. Martin, R. Gupta, Early outcomes in MDR-TB and XDR-TB patients treated with delamanid under compassionate use, The European Respiratory Journal. 50 (2017) 10–13. https://doi.org/10.1183/13993003.00311-2017.
[3] A. Maitra, S. Bates, T. Kolvekar, P.V. Devarajan, J.D. Guzman, S. Bhakta, Repurposing-a ray of hope in tackling extensively drug resistance in tuberculosis,

International Journal of Infectious Diseases. 32 (2015) 50–55. https://doi.org/10.1016/j.ijid.2014.12.031.
[4] J.C. Palomino, A. Martin, Is repositioning of drugs a viable alternative in the treatment of tuberculosis?, Journal of Antimicrobial Chemotherapy. 68 (2013) 275–283. https://doi.org/10.1093/jac/dks405.
[5] D.R. Silva, M. Dalcolmo, S. Tiberi, M.A. Arbex, M. Munoz-Torrico, R. Duarte, L. D'Ambrosio, D. Visca, A. Rendon, M. Gaga, A. Zumla, G.B. Migliori, New and repurposed drugs to treat multidrug- and extensively drug-resistant tuberculosis, Jornal Brasileiro de Pneumologia. 44 (2018) 153–160. https://doi.org/10.1590/s1806-37562017000000436.
[6] I. Vitro, I. Vivo, crossm, (2019) 1–12.
[7] V. Parvathaneni, N.S. Kulkarni, A. Muth, V. Gupta, Drug repurposing: a promising tool to accelerate the drug discovery process, Drug Discovery Today. 24 (2019) 2076–2085. https://doi.org/10.1016/j.drudis.2019.06.014.
[8] S. Pushpakom, F. Iorio, P.A. Eyers, K.J. Escott, S. Hopper, A. Wells, A. Doig, T. Guilliams, J. Latimer, C. McNamee, A. Norris, P. Sanseau, D. Cavalla, M. Pirmohamed, Drug repurposing: Progress, challenges and recommendations, Nature Reviews Drug Discovery. 18 (2018) 41–58. https://doi.org/10.1038/nrd.2018.168.
[9] S. Rasheed, S.S. Sánchez, S. Yousuf, S.M. Honoré, M.I. Choudhary, Drug repurposing: In-vitro anti-glycation properties of 18 common drugs, PLoS ONE. 13 (2018) 1–9. https://doi.org/10.1371/journal.pone.0190509.
[10] A. Talevi, C.L. Bellera, Challenges and opportunities with drug repurposing: finding strategies to find alternative uses of therapeutics, Expert Opinion on Drug Discovery. 15 (2020) 397–401. https://doi.org/10.1080/17460441.2020.1704729.
[11] V.L. Simpkin, M.J. Renwick, R. Kelly, E. Mossialos, Incentivising innovation in antibiotic drug discovery and development: Progress, challenges and next steps, Journal of Antibiotics. 70 (2017) 1087–1096. https://doi.org/10.1038/ja.2017.124.
[12] L. Danelishvili, M. Wu, L.S. Young, L.E. Bermudez, Genomic approach to identifying the putative target of and mechanisms of resistance to mefloquine in mycobacteria, Antimicrobial Agents and Chemotherapy. 49 (2005) 3707–3714. https://doi.org/10.1128/AAC.49.9.3707-3714.2005.
[13] C.M. Kunin, W.Y. Ellis, Antimicrobial activities of mefloquine and a series of related compounds, Antimicrobial Agents and Chemotherapy. 44 (2000) 848–852. https://doi.org/10.1128/AAC.44.4.848-852.2000.
[14] E. Nissani, H. Ginsburg, Protonophoric effects of antimalarial drugs and alkylamines in Escherichia coli membranes, BBA - Biomembranes. 978 (1989) 293–298. https://doi.org/10.1016/0005-2736(89)90127-2.
[15] P.B. Tarigan, 済無No Title No Title, Journal of Chemical Information and Modeling. 53 (2013) 1689–1699. https://doi.org/10.1017/CBO9781107415324.004.
[16] D. Zannoni, Mefloquine: an antimalarial drug interacting with the b/c region of bacterial respiratory chains, FEBS Letters. 183 (1985) 340–344.

https://doi.org/10.1016/0014-5793(85)80806-1.
[17] L.E. Bermudez, P. Kolonoski, M. Wu, P.A. Aralar, C.B. Inderlied, L.S. Young, Mefloquine is active in vitro and in vivo against Mycobacterium avium complex, Antimicrobial Agents and Chemotherapy. 43 (1999) 1870–1874. https://doi.org/10.1128/AAC.43.8.1870.
[18] L.E. Bermudez, P. Kolonoski, L.E. Seitz, M. Petrofsky, R. Reynolds, M. Wu, L.S. Young, SRI-286, a thiosemicarbazole, in combination with mefloquine and moxifloxacin for treatment of murine Mycobacterium avium complex disease, Antimicrobial Agents and Chemotherapy. 48 (2004) 3556–3558. https://doi.org/10.1128/AAC.48.9.3556-3558.2004.
[19] S. Jayaprakash, Y. Iso, B. Wan, S.G. Franzblau, A.P. Kozikowski, Design, synthesis, and SAR studies of mefloquine-based ligands as potential antituberculosis agents, ChemMedChem. 1 (2006) 593–597. https://doi.org/10.1002/cmdc.200600010.
[20] L.E. Bermudez, L. Meek, Mefloquine and Its Enantiomers Are Active against Mycobacterium tuberculosis In Vitro and in Macrophages, Tuberculosis Research and Treatment. 2014 (2014) 1–5. https://doi.org/10.1155/2014/530815.
[21] R.S.B. Gonalves, C.R. Kaiser, M.C.S. Loureno, F.A.F.M. Bezerra, M.V.N. De Souza, J.L. Wardell, S.M.S.V. Wardell, M.D.G.M.D.O. Henriques, T. Costa, Mefloquine-oxazolidine derivatives, derived from mefloquine and arenecarbaldehydes: In vitro activity including against the multidrug-resistant tuberculosis strain T113, Bioorganic and Medicinal Chemistry. 20 (2012) 243–248. https://doi.org/10.1016/j.bmc.2011.11.006.
[22] V.S. Rodrigues-Junior, A.D. Villela, R.S.B. Gonçalves, B.L. Abbadi, R.V. Trindade, A. López-Gavín, G. Tudó, J. González-Martín, L.A. Basso, M.V.N. de Souza, M.M. Campos, D.S. Santos, Mefloquine and its oxazolidine derivative compound are active against drug-resistant Mycobacterium tuberculosis strains and in a murine model of tuberculosis infection, International Journal of Antimicrobial Agents. 48 (2016) 203–207. https://doi.org/10.1016/j.ijantimicag.2016.04.029.
[23] J. Costa-Gouveia, E. Pancani, S. Jouny, A. Machelart, V. Delorme, G. Salzano, R. Iantomasi, C. Piveteau, C.J. Queval, O.R. Song, M. Flipo, B. Deprez, J.P. Saint-André, J. Hureaux, L. Majlessi, N. Willand, A. Baulard, P. Brodin, R. Gref, Combination therapy for tuberculosis treatment: Pulmonary administration of ethionamide and booster co-loaded nanoparticles, Scientific Reports. 7 (2017) 1–14. https://doi.org/10.1038/s41598-017-05453-3.
[24] G. Sotgiu, R. Centis, L. D'Ambrosio, G. Battista Migliori, Tuberculosis treatment and drug regimens, Cold Spring Harbor Perspectives in Medicine. 5 (2015). https://doi.org/10.1101/cshperspect.a017822.
[25] R.E. Brown, F.A. Stancato, A.D. Wolfe, THE EFFECTS OF MEFLOQUINE ON ESCHERICHIA COLI, Vol . (1979) 8.
[26] J.L.R. Scaini, A.V. Werhli, V.R. de Lima, P.E.A. da Silva, J.R. Bordin, K.S. Machado, All-atom Molecular Dynamics model for mycobacterial plasma

membrane, BioRxiv. (2019) 788299. https://doi.org/10.1101/788299.
[27] J.L.R. Scaini, A.D. Camargo, V.R. Seus, A. von Groll, A.V. Werhli, P.E.A. da Silva, K.D.S. Machado, Molecular modelling and competitive inhibition of a Mycobacterium tuberculosis multidrug-resistance efflux pump, J. Mol. Graph. Model. 87 (2019) 98–108. https://doi.org/10.1016/j.jmgm.2018.11.016.
[28] F. Szoka, D. Papahadjopoulos, Procedure for preparation of liposomes with large internal aqueous space and high capture by reverse-phase evaporation., Proceedings of the National Academy of Sciences. 75 (1978) 4194–4198. https://doi.org/10.1073/pnas.75.9.4194.
[29] O. Mertins, M. Sebben, A.R. Pohlmann, N.P. da Silveira, Production of soybean phosphatidylcholine–chitosan nanovesicles by reverse phase evaporation: a step by step study, Chemistry and Physics of Lipids. 138 (2005) 29–37. https://doi.org/10.1016/j.chemphyslip.2005.07.004.
[30] M.M. Moreno, P. Garidel, M. Suwalsky, J. Howe, K. Brandenburg, The membrane-activity of Ibuprofen, Diclofenac, and Naproxen: A physico-chemical study with lecithin phospholipids, Biochimica et Biophysica Acta (BBA) - Biomembranes. 1788 (2009) 1296–1303. https://doi.org/10.1016/j.bbamem.2009.01.016.
[31] C.R.L. de Azambuja Borges, N.O. Silva, M.R. Rodrigues, M.A. Germani Marinho, F.S. de Oliveira, M. Cassiana, A.P. Horn, A.L. Parize, D.C. Flores, R.M. Clementin, V.R. de Lima, Dimiristoylphosphatidylcholine/genistein molecular interactions: A physico-chemical approach to anti-glioma drug delivery systems, Chemistry and Physics of Lipids. 225 (2019) 104828. https://doi.org/10.1016/j.chemphyslip.2019.104828.
[32] W. Niederberger, J. Seelig, Phosphorus-31 chemical shift anisotropy in unsonicated phospholipid bilayers, J. Am. Chem. Soc. 98 (1976) 3704–3706. https://doi.org/10.1021/ja00428a053.
[33] D.W. Borhani, D.E. Shaw, The future of molecular dynamics simulations in drug discovery, Journal of Computer-Aided Molecular Design. 26 (2012) 15–26.
[34] M.J. Abraham, T. Murtola, R. Schulz, S. Páll, J.C. Smith, B. Hess, E. Lindahl, GROMACS: High performance molecular simulations through multi-level parallelism from laptops to supercomputers, SoftwareX. 1 (2015) 19–25.
[35] S. Pall, M.J. Abraham, C. Kutzner, B. Hess, E. Lindahl, Tackling exascale software challenges in molecular dynamics simulations with GROMACS, in: International Conference on Exascale Applications and Software, Springer, 2014: pp. 3–27.
[36] M. Sud, E. Fahy, D. Cotter, A. Brown, E.A. Dennis, C.K. Glass, A.H. Merrill Jr, R.C. Murphy, C.R. Raetz, D.W. Russell, others, Lmsd: lipid maps structure database, Nucleic Acids Research. 35 (2006) D527–D532.
[37] K.B. Koziara, M. Stroet, A.K. Malde, A.E. Mark, Testing and validation of the Automated Topology Builder (ATB) version 2.0: prediction of hydration free enthalpies, Journal of Computer-Aided Molecular Design. 28 (2014) 221–233.
[38] O. Berger, O. Edholm, F. Jähnig, Molecular dynamics simulations of a fluid bilayer

of dipalmitoylphosphatidylcholine at full hydration, constant pressure, and constant temperature, Biophys. J. 72 (1997) 2002–2013. https://doi.org/10.1016/S0006-3495(97)78845-3.
[39] C. Oostenbrink, A. Villa, A.E. Mark, W.F. Van Gunsteren, A biomolecular force field based on the free enthalpy of hydration and solvation: the GROMOS force-field parameter sets 53A5 and 53A6, Journal of Computational Chemistry. 25 (2004) 1656–1676.
[40] R Core Team, R: A language and environment for statistical computing, Vienna, Austria, 2013.
[41] RStudio Team, RStudio: Integrated Development Environment for R, RStudio, Inc., Boston, MA, 2015. http://www.rstudio.com/.
[42] W.J. Allen, J.A. Lemkul, D.R. Bevan, GridMAT-MD: a grid-based membrane analysis tool for use with molecular dynamics, J Comput Chem. 30 (2009) 1952–1958. https://doi.org/10.1002/jcc.21172.
[43] F. Ge, F. Zeng, S. Liu, N. Guo, H. Ye, Y. Song, J. Fan, X. Wu, X. Wang, X. Deng, Q. Jin, L. Yu, In vitro synergistic interactions of oleanolic acid in combination with isoniazid, rifampicin or ethambutol against Mycobacterium tuberculosis, Journal of Medical Microbiology. 59 (2010) 567–572. https://doi.org/10.1099/jmm.0.014837-0.
[44] S. Ramón-García, C. Ng, H. Anderson, J.D. Chao, X. Zheng, T. Pfeifer, Y. Av-Gay, M. Roberge, C.J. Thompson, Synergistic drug combinations for tuberculosis therapy identified by a novel high-throughput screen, Antimicrobial Agents and Chemotherapy. 55 (2011) 3861–3869. https://doi.org/10.1128/AAC.00474-11.
[45] E. Rey-Jurado, G. Tudó, J.A. Martínez, J. González-Martín, Synergistic effect of two combinations of antituberculous drugs against Mycobacterium tuberculosis, Tuberculosis. 92 (2012) 260–263. https://doi.org/10.1016/j.tube.2012.01.005.
[46] Z. Zhang, T. Li, G. Qu, Y. Pang, Y. Zhao, In vitro synergistic activity of clofazimine and other antituberculous drugs against multidrug-resistant Mycobacterium tuberculosis isolates, International Journal of Antimicrobial Agents. 45 (2015) 71–75. https://doi.org/10.1016/j.ijantimicag.2014.09.012.
[47] W. Zhao, M. Zheng, B. Wang, X. Mu, P. Li, L. Fu, S. Liu, Z. Guo, Interactions of linezolid and second-line anti-tuberculosis agents against multidrug-resistant Mycobacterium tuberculosis in vitro and in vivo, International Journal of Infectious Diseases. 52 (2016) 23–28. https://doi.org/10.1016/j.ijid.2016.08.027.
[48] L. Zou, M. Liu, Y. Wang, J. Lu, Y. Pang, Determination of in vitro synergy between linezolid and other antimicrobial agents against Mycobacterium tuberculosis isolates, Tuberculosis. 95 (2015) 839–842. https://doi.org/10.1016/j.tube.2015.07.003.
[49] S.G. Franzblau, R.S. Witzig, J.C. Mclaughlin, P. Torres, G. Madico, A. Hernandez, M.T. Degnan, M.B. Cook, V.K. Quenzer, R.M. Ferguson, R.H. Gilman, Rapid, low-technology MIC determination with clinical Mycobacterium tuberculosis isolates by using the microplate Alamar Blue assay, Journal of Clinical Microbiology. 36 (1998) 362–366. https://doi.org/10.1128/jcm.36.2.362-

366.1998.
[50] R.S. Reis, I. Neves, S.L.S. Lourenc, M.C.S. Lourenc, Comparison of Flow Cytometric and Alamar Blue Tests with the Proportional Method for Testing Susceptibility of, Society. 42 (2004) 2247–2248. https://doi.org/10.1128/JCM.42.5.2247.
[51] J.D. Vanitha, C.N. Paramasivan, Evaluation of microplate Alamar blue assay for drug susceptibility testing of Mycobacterium avium complex isolates, Diagnostic Microbiology and Infectious Disease. 49 (2004) 179–182. https://doi.org/10.1016/j.diagmicrobio.2004.04.003.
[52] C. Craik, 基因的改变NIH Public Access, Bone. 23 (2008) 1–7. https://doi.org/10.1038/jid.2014.371.
[53] Y. Zhang, W. Shi, W. Zhang, D. Mitchison, Mechanisms of Pyrazinamide Action and Resistance, Molecular Genetics of Mycobacteria. 2 (2015) 479–491. https://doi.org/10.1128/9781555818845.ch24.
[54] A.J. Martín-Galiano, B. Gorgojo, C.M. Kunin, A.G. De la Campa, Mefloquine and new related compounds target the F0 complex of the F0F1 H+-ATPase of Streptococcus pneumoniae, Antimicrobial Agents and Chemotherapy. 46 (2002) 1680–1687. https://doi.org/10.1128/AAC.46.6.1680-1687.2002.
[55] M. Cokol, H.N. Chua, M. Tasan, B. Mutlu, Z.B. Weinstein, Y. Suzuki, M.E. Nergiz, M. Costanzo, A. Baryshnikova, G. Giaever, C. Nislow, C.L. Myers, B.J. Andrews, C. Boone, F.P. Roth, Systematic exploration of synergistic drug pairs, Molecular Systems Biology. 7 (2011) 1–9. https://doi.org/10.1038/msb.2011.71.
[56] L.H. Schmidt, R. Crosby, J. Rasco, D. Vaughan, Antimalarial Activities of Various 4-Quinolinemethanols with Special Attention to WR-142,490 (Mefloquine)t, ANTIMICROB. AGENTS CHEMOTHER. 13 (1978) 20.
[57] H.L. Casal, D.G. Cameron, I.C. Smith, H.H. Mantsch, Acholeplasma laidlawii membranes: a Fourier transform infrared study of the influence of protein on lipid organization and dynamics, Biochemistry. 19 (1980) 444–451. https://doi.org/10.1021/bi00544a007.
[58] F. López-García, V. Micol, J. Villalaín, J.C. Gómez-Fernández, Infrared spectroscopic study of the interaction of diacylglycerol with phosphatidylserine in the presence of calcium, Biochim. Biophys. Acta. 1169 (1993) 264–272. https://doi.org/10.1016/0005-2760(93)90250-d.
[59] B. Moreno, A. Vivas, R. Nogales, E. Benitez, Solvent tolerance acquired by Brevibacillus brevis during an olive-waste vermicomposting process, Ecotoxicology and Environmental Safety. 72 (2009) 2109–2114. https://doi.org/10.1016/j.ecoenv.2009.06.011.
[60] W. Hübner, A. Blume, Interactions at the lipid–water interface, Chemistry and Physics of Lipids. 96 (1998) 99–123. https://doi.org/10.1016/S0009-3084(98)00083-8.
[61] M. Hereć, A. Islamov, A. Kuklin, M. Gagoś, W.I. Gruszecki, Effect of antibiotic amphotericin B on structural and dynamic properties of lipid membranes formed with egg yolk phosphatidylcholine, Chemistry and Physics of Lipids. 147 (2007)

78–86. https://doi.org/10.1016/j.chemphyslip.2007.03.007.
[62] Z. Arsov, L. Quaroni, Detection of lipid phase coexistence and lipid interactions in sphingomyelin/cholesterol membranes by ATR-FTIR spectroscopy, Biochimica et Biophysica Acta (BBA) - Biomembranes. 1778 (2008) 880–889. https://doi.org/10.1016/j.bbamem.2007.12.012.
[63] M. Bloom, J. Thewalt, Spectroscopic determination of lipid dynamics in membranes, Chemistry and Physics of Lipids. 73 (1994) 27–38. https://doi.org/10.1016/0009-3084(94)90172-4.
[64] M.F. Brown, Theory of spin-lattice relaxation in lipid bilayers and biological membranes. Dipolar relaxation, The Journal of Chemical Physics. 80 (1984) 2808–2831. https://doi.org/10.1063/1.447030.
[65] B.A. Cornell, J.B. Davenport, F. Separovic, Low-frequency motion in membranes. The effect of cholesterol and proteins, Biochimica et Biophysica Acta (BBA) - Biomembranes. 689 (1982) 337–345. https://doi.org/10.1016/0005-2736(82)90267-X.
[66] S. Villasmil-Sánchez, A.M. Rabasco, M.L. González-Rodríguez, Thermal and 31P-NMR studies to elucidate sumatriptan succinate entrapment behavior in Phosphatidylcholine/Cholesterol liposomes. Comparative 31P-NMR analysis on negatively and positively-charged liposomes, Colloids and Surfaces B: Biointerfaces. 105 (2013) 14–23. https://doi.org/10.1016/j.colsurfb.2012.12.019.
[67] C. Moreau, M. Le Floch, J. Segalen, G. Leray, L. Metzinger, J.D. de Certaines, E. Le Rumeur, Static and magic angle spinning ^{31} P NMR spectroscopy of two natural plasma membranes, FEBS Letters. 461 (1999) 258–262. https://doi.org/10.1016/S0014-5793(99)01461-1.
[68] J.C. Debouzy, S. Aous, V. Dabouis, Y. Neveux, E. Gentilhomme, Phospholipid matrix as a target for sulfur mustard (HD): NMR study in model membrane systems, Cell Biol. Toxicol. 18 (2002) 397–408. https://doi.org/10.1023/a:1020815723009.
[69] D. Lasic, Novel applications of liposomes, Trends in Biotechnology. 16 (1998) 307–321. https://doi.org/10.1016/S0167-7799(98)01220-7.
[70] E.J. Dufourc, Solid-State NMR in Biomembranes, in: B. Larijani, Colin.A. Rosser, R. Woscholski (Eds.), Chemical Biology, John Wiley & Sons, Ltd, Chichester, UK, 2006: pp. 113–131. https://doi.org/10.1002/9780470319253.ch8.
[71] R. Ghosh, Phosphorus-31 and deuterium NMR studies of structure and motion in bilayers of phosphatidylcholine and phosphatidylethanolamine, Biochemistry. 27 (1988) 7750–7758. https://doi.org/10.1021/bi00420a025.
[72] A.V. Popova, D.K. Hincha, Intermolecular Interactions in Dry and Rehydrated Pure and Mixed Bilayers of Phosphatidylcholine and Digalactosyldiacylglycerol: A Fourier Transform Infrared Spectroscopy Study, Biophysical Journal. 85 (2003) 1682–1690. https://doi.org/10.1016/S0006-3495(03)74598-6.
[73] M. Moser, D. Marsh, P. Meier, K.H. Wassmer, G. Kothe, Chain configuration and flexibility gradient in phospholipid membranes. Comparison between spin-label electron spin resonance and deuteron nuclear magnetic resonance, and

identification of new conformations., Biophys J. 55 (1989) 111–123. https://doi.org/10.1016/S0006-3495(89)82784-5.
[74] D. Chapman, Phospholipid bilayers physical principles and models., Cell Biochem. Funct. 6 (1987) 442. https://doi.org/10.1002/cbf.290060221.
[75] M. Jan Akhunzada, F. D'Autilia, B. Chandramouli, N. Bhattacharjee, A. Catte, R. Di Rienzo, F. Cardarelli, G. Brancato, Interplay between lipid lateral diffusion, dye concentration and membrane permeability unveiled by a combined spectroscopic and computational study of a model lipid bilayer, Scientific Reports. 9 (2019) 1508. https://doi.org/10.1038/s41598-018-37814-x.

9 Conclusões

As técnicas de bioinformática estrutural permitem um estudo com detalhes químicos e físicos que complementam de forma crítica os estudos experimentais, especialmente para o estudo racional de fármacos. Este trabalho desenvolveu modelos atomísticos das estruturas de membrana de PIM2 e da bomba de efluxo Tap de *M tuberculosis*, como alvos no estudo racional de antimicrobianos.

As técnicas de modelagem molecular de proteínas permitiram a construção de vários modelos moleculares da bomba de efluxo Tap. As técnicas de validação permitiram a eleição de um modelo, aliado às simulações de DM em membrana de dilpamitoil fosfatidil colina. Os estudos de docking molecular mostrou que a Tap pode realizar a extrusão de RIF, OFLO e até BDQ, e pode ser inibida por VERA e pela molécula sintetizada NUNL02. Este modelo pode ser utilizado em diversas aplicações práticas, como este estudo de afinidade.

Como as bombas de efluxo são proteínas transmembrana, um modelo adequado da complexa MI de *M. tuberculosis* é essencial para este estudo e diversas aplicações práticas. O modelo atomístico da membrana de PIM2 foi criada por este ser um lipídio extremamente abundante na MI, e essencial para formação da PC. Os resultados deste trabalho mostram que este modelo reage as diversas condições a qual foi exposta de forma coerente, e assim pode servir para diversos estudos de membrana, incluindo de bombas de efluxo na membrana.

Este modelo da membrana de PIM2 foi utilizado para testar a influência da mefloquina na membrana, que mostrou alterações que concordam com resultados experimentais. Além de isso ter aplicações práticas para o possível uso da mefloquina no tratamento para TB, estes resultados mostram o uso do modelo da membrana de PIM2 de *M. tuberculosis*, como representativo de seu envelope, reforçado por concordar com resultados experimentais

Finalmente, de forma geral, esta tese gerou trabalhos que descrevem o desenvolvimento destes dois importantes modelos atomísticos computacionais, da bomba de efluxo Tap e da PIM2, cujas funções se complementam, e também resultados práticos relevantes para a as ciências da saúde, que refletem a potencialidade destes modelos para o estudo racional de fármacos.

10 Considerações Finais e Perspectivas

Este trabalho mostra um método que permite a modelagem de outras bombas de efluxo, de forma a se ter uma representação mais completa do sistema de efluxo. Este modelo da Tap permite uma gama de outros trabalhos que tenham como interesse a própria Tap ou o efluxo em micobactérias. Da mesma forma, este trabalho abre o caminho para a criação de um modelo que represente a ME de *M. tuberculosis*, que junto com o modelo de MI desta tese, e com uma camada de peptidoglicano-arabinogalactano, pode se criar um modelo para todo o envelope celular. Assim como foi realizado com a mefloquina, este modelo de membrana permite que diversos trabalhos sejam realizados com outros fármacos cujo efeito na membrana de *M. tuberculosis* é de interesse. Além disso, os modelos podem ser estudados em campos de força diferentes. Outras análises podem ser aplicadas para se ter uma visão mais profunda dos modelos, como o RMSD 2D. Por fim, este trabalho abre o caminho para mais estudos focando as ações das bombas de efluxo em seu ambiente natural, a MI, e com a DM é possível fazer diversas análises sobre o mecanismo de extrusão destas proteínas.